Aus dem

Department für Anatomie Tübingen

Institut für Neuroanatomie und Entwicklungsbiologie

Olfactory placode organoids from human induced pluripotent stem cells

Inaugural-Dissertation
zur Erlangung des Doktorgrades
der Medizin

der Medizinischen Fakultät
der Eberhard Karls Universität
zu Tübingen

vorgelegt von

Frey, Karl Georg Simon

2023

Dekan: Professor Dr. B. Pichler

1. Berichterstatter: Professor Dr. S. Liebau
2. Berichterstatter: Professorin Dr. M. Avci-Adali

Tag der Disputation: 02.05.2023

Dedicated to the loving memory of

Dr. Hans-Jürgen Wilfried Haußmann

my godfather and idol, who always saw the scientist in me.

Table of contents

Table of figures 6

Table of lists 8

List of abbreviations 9

1 Summary 15

2 Zusammenfassung 17

3 Introduction 19

3.1 Spotlight on olfaction – the next great frontier? 19

3.2 Anatomy and function of the human olfactory system 20

3.2.1 Macroscopy – from the nose to the brain 20

3.2.2 Microscopy – from the air to the neuron 22

3.3 Early human development 25

3.3.1 Implantation & the bilaminar embryo 25

3.3.2 Gastrulation 25

3.3.3 Ectodermal patterning 26

3.3.4 Neurulation 28

3.4 Special olfactory development 30

3.4.1 Neural border & pre-placodal region 30

3.4.2 The PPR as a multipotent progenitor 31

3.4.3 Sub-specification of the pre-placodal region 31

3.4.4 The olfactory placode 34

3.5 Development of the central nervous system 36

3.6 Signaling pathways in the craniofacial development 38

3.7 Human induced pluripotent stem cells 41

3.8 2D vs. 3D – the rise of organoids 44

3.8.1 Brain organoids 46

3.8.2 Organoids in PPR-derived tissues 47

3.9 Aim of the thesis 49

4 Material 50

4.1 Cell lines 50

4.2 Media 50
4.2.1 Basal media 50
4.2.2 Media supplements 51
4.2.3 Starting media for differentiations 52
4.2.4 Differentiation media 53
4.3 Chemicals, enzymes, and additives 55
4.4 Buffer and solutions 56
4.5 Kits and assays 57
4.6 TaqMan™ probes 57
4.7 Antibodies 58
4.7.1 Primary 58
4.7.2 Secondary 59
4.8 Consumables 60
4.9 Laboratory equipment 62
4.10 Software 64
5 Methods 65
5.1 Ethics 65
5.2 Cell culture 65
5.3 hiPSC culture 65
5.3.1 Culture & passage 65
5.3.2 Freezing iPSC 66
5.3.3 Thawing iPSC 66
5.4 DOPEoid differentiation 67
5.4.1 SFEBq – EB formation 67
5.4.2 Differentiation 67
5.4.2.1 Classical protocol 67
5.4.2.2 Modified protocol 68
5.5 DOPEoid analysis – protein level 70
5.5.1 DOPEoid fixation 70
5.5.2 DOPEoid embedding 70
5.5.2.1 One-sample block 70

5.5.2.2 Four-sample block 71
5.5.3 DOPEoid cryosectioning 72
5.5.4 DOPEoid immunofluorescence staining 72
5.5.5 Picture acquisition 73
5.6 DOPEoid analysis – RNA level 73
5.6.1 DOPEoid selection & RNA isolation 73
5.6.2 RT-qPCR – Biomark™ Fludigm 74
6 Results 76
6.1 DOPEoids generation & definition 76
6.2 DOPEoids timeline 78
6.2.1 DOPEoids timeline – day 4 & day 8 79
6.2.2 DOPEoids timeline – day 10 80
6.2.3 DOPEoids timeline – day 13 81
6.2.4 Summary: DOPEoids timeline day 4 – day 13 82
6.2.5 DOPEoids timeline – day 16 83
6.2.6 DOPEoids timeline – day 25 84
6.2.7 DOPEoids timeline – day 31 86
6.2.8 Summary: DOPEoids timeline day 16 – day 31 88
6.3 DOPEoids characterization 90
6.3.1 DOPEoids characterization A 91
6.3.2 DOPEoids characterization B 93
6.3.3 DOPEoids characterization C 95
6.3.4 DOPEoids characterization D 97
6.3.5 DOPEoids characterization E & F 100
6.3.6 DOPEoids characterization G 102
6.3.7 DOPEoids characterization summary 103
6.4 RNA data 104
6.4.1 DOPEoids RNA expression timeline – epithelial markers 105
6.4.2 DOPEoids RNA expression timeline – PPR markers 107
6.4.3 DOPEoids RNA expression timeline – forebrain markers 109
6.4.4 DOPEoids RNA expression timeline – placodal & mesenchymal markers 111

6.5 DOPEoids protocol adaption – outlook 113
6.5.1 DOPEoids outlook – maturation & mesenchyme 114
6.5.2 DOPEoids outlook – definite olfactory progenitors 116
7 Discussion 118
7.1 Culture methods 118
7.1.1 Starting media 118
7.1.2 Starting conditions 118
7.1.3 Early TGFβ & WNT inhibition 118
7.1.4 BMP4 and Phenanthroline 120
7.1.5 Maturation 121
7.1.6 Hypoxia and ECM – key differences to other protocols 121
7.1.7 Summary – pushing towards an OP 123
7.2 NNE-like surface epithelium, PPR & Placodal patches 123
7.2.1 Surface epithelium – induction 123
7.2.2 Surface epithelium – PPR-like cells 124
7.2.3 Placodal patches 125
7.2.3.1 Anterior placodal region 126
7.2.3.2 Olfactory placode 127
7.2.4 RNA level – surface epithelium, PPR & placodal patches 129
7.2.5 Exclusion of other placodes 133
7.2.6 Surface epithelium, PPR & placodal patches – conclusion 134
7.3 Neural tubuli 135
7.3.1 Neural tubuli - morphology 135
7.3.2 Neural tubuli – protein data 136
7.3.3 Neural tubuli – morphology & protein data: summary 138
7.3.4 Neural tubuli – RNA data 138
7.3.5 Neural tubuli – summary 139
7.4 Mesenchyme 140
7.4.1 Mesenchyme – morphology & protein data 140
7.4.2 Mesenchyme – RNA data 141
7.4.3 Mesenchyme – summary 141

7.5 DOPEoids – a functional organoid model? 142
7.6 Outlook data 142
7.7 Conclusion & prospects 144
8 Supplemental information 146
8.1 DOPEoids vs. non-DOPEoids 146
8.2 DOPEoids outlook – basement membrane & SIX3 expression 148
9 References 154
Erklärung zum Eigenanteil 169
Acknowledgements 170

Table of figures

Figure 1: Architecture of the adult human olfactory epithelium……13
Figure 2: Markers of different cell types of the adult human OE……..24
Figure 3: Blastocyst & bilaminar embryo……..25
Figure 4: Gastrulation……..26
Figure 5: The pre-placodal region *in situ*……..28
Figure 6: Neurulation……...29
Figure 7: Neural border formation……31
Figure 8: Cranial placodes……..32
Figure 9: Sub-specification of the pre-placodal region……...33
Figure 10: Morphological development of the olfactory placode……..35
Figure 11: Regions of the forebrain……...38
Figure 12: Signaling pathways in placode development……40
Figure 13: Comparison of classical vs. modified differentiation protocol……70
Figure 14: Live cell comparison of DOPEoid & non-DOPEoid……74
Figure 15: Defining features of DOPEoids……..……77
Figure 16: DOPEoids timeline – day 4 & day 8……...79
Figure 17: DOPEoids timeline – day 10……80
Figure 18: DOPEoids timeline – day 13……81
Figure 19: DOPEoids timeline – day 16……83
Figure 20: DOPEoids timeline – day 25……84
Figure 21: DOPEoids timeline – day 25 closeup……85
Figure 22: DOPEoids timeline – day 31……86
Figure 23: DOPEoids timeline – day 31 closeup……87
Figure 24: Timeline & hallmarks of DOPEoid development……..89
Figure 25: DOPEoids characterization A – day 31……91
Figure 26: DOPEoids characterization B – day 31……93
Figure 27: DOPEoids characterization C – day 19……95
Figure 28: DOPEoids characterization D – day 22……97
Figure 29: DOPEoids characterization D – day 22 closeup……..98
Figure 30: DOPEoids characterization E – day 28……...100
Figure 31: DOPEoids characterization F – day 21……...101

Figure 32: DOPEoids characterization G – day 22……..102
Figure 33: Compartmental protein expression in DOPEoids……..103
Figure 34: DOPEoids RNA expression timeline – epithelial markers……105
Figure 35: DOPEoids RNA expression timeline – PPR markers……107
Figure 36: DOPEoids RNA expression timeline – forebrain markers……109
Figure 37: DOPEoids RNA expression timeline – placodal & mesenchymal markers……111
Figure 38: DOPEoids outlook: maturation & mesenchyme – d40……..114
Figure 39: DOPEoids outlook: definite olfactory progenitors – d40……...116
Figure 40: Canonical WNT pathway inhibitors……..120
Supplemental Figure S1: DOPEoids vs. non-DOPEoids – morphology & protein data……..146
Supplemental Figure S2: DOPEoids vs. non-DOPEoids – gene expression...147
Supplemental Figure S3: DOPEoids outlook: basement membrane & SIX3 expression……...148
Supplemental Figure S4: BioRender.com – publication licenses #1……149
Supplemental Figure S5: BioRender.com – publication licenses #2……150
Supplemental Figure S6: BioRender.com – publication licenses #3……151
Supplemental Figure S7: BioRender.com – publication licenses #4……152
Supplemental Figure S8: BioRender.com – publication licenses #5……153

Table of lists

Table 1: Cell line used for differentiation……..50
Table 2: List of basal media used……..50
Table 3: List of media supplements used……51
Table 4: Growth-factor free chemically defined medium (gfCDM) composition.52
Table 5: DOPEoid maturation medium (DMM) composition……53
Table 6: List of differentiation media used for the differentiation protocols…….53
Table 7: List of chemicals, enzymes & additives used……...55
Table 8: List of buffers & solutions used……..56
Table 9: List of kits & assays used……57
Table 10: List of TaqMan™ probes used……57
Table 11: List of primary antibodies used……58
Table 12: List of secondary antibodies used……59
Table 13: List of consumables used……..60
Table 14: List of laboratory equipment used……62
Table 15: List of software used……..64
Table 16: DOPEoids differentiation – classical protocol……68
Table 17: DOPEoids differentiation – modified protocol……69
Table 18: cDNA synthesis & pre-amplification cycler settings……..75

List of abbreviations

Abbreviation	Meaning
%	Percentage
(m)RNA	(Messenger) ribonucleic acid
°C	Degrees Celsius
2D	2-Dimensional
3D	3-Dimensional
3R	Replace, reduce, refine
A/V	Surface-area-to-volume ratio
AD	Alzheimer´s disease
ANOS1	Anosmin 1
A-P	Anterior-Posterior
ASCL1	Achaete-scute homolog 1
BDNF	Brain-derived neurotrophic factor
BMP	Bone morphogenetic protein
BSL-2	Biosafety level 2
ca.	*circa*
Ca^{2+}	Calcium(-ion)
cAMP	Cyclic adenosine monophosphate
Cl^-	Chloride(-ion)
c-Myc	Myc proto-oncogene
CNG	Cyclic nucleotide-gated
CNS	Central nervous system
CO_2	Carbon dioxide
CP	Cranial placode(s)
CPZ	Cortical plate
CRISPR	Clustered regularly interspaced short palindromic repeats
CRISPRa	CRISPR activation
CS	Carnegie stage
ct	Cycle threshold

DACH1	Dachshund homolog 1
DAPI	4′,6-diamidino-2-phenylindole
dCas9	Deactivated CRISPR associated protein 9
DLX3/5	Distal-less homeobox 3/5
DOPEoids	Differentiation of olfactory placode and epithelium (DOPE) organoids
dSMADi	Dual SMAD inhibition
D-V	Dorsal-Ventral
EB	Embryoid body/(bodies)
EBF2	Early B-cell factor-2
EBV	Epstein-Barr virus
E-CADHERIN	Epithelial cadherin
ECM	Extracellular matrix
EGFR	Epidermal growth factor receptor
EMT	Epithelial-to-mesenchymal-transition
EMX2	Empty spiracles homeobox 2
ENS	Enteric nervous system
ERNI	Early response to neural induction
ESC	Embryonic stem cell(s)
EYA1/2/3/4	Eyes absent homolog 1/2/3/4
FGF2/8	Fibroblast growth factor 2/8
FLRT3	Fibronectin leucine rich transmembrane protein 3
FOXD3	Forkhead box D3
FOXG1	Forkhead box G1
FOXI1/3	Forkhead box I1/I3
g	Gravitational acceleration (~ 9.81 $\frac{\mathrm{m}}{\mathrm{s}^2}$)
GAPDH	Glyceraldehyde 3-phosphate dehydrogenase
GATA2/3	GATA binding protein 2/3
GBC	Globose basal cell(s)
GBX2	Gastrulation brain homeobox 2
GDNF	Glial cell line-derived neurotrophic factor

GEMINI	Gem nuclear organelle associated protein
GFAP	Glial fibrillary acidic protein
gfCDM	Growth-factor free chemically defined medium
GNG13	Guanine nucleotide-binding protein G(I)/G(S)/G(O) subunit gamma-13
GNG8	Guanine nucleotide-binding protein G(I)/G(S)/G(O) subunit gamma-8
GnRH-1	Gonadotropin releasing hormone 1
G_{olf}	Guanine nucleotide-binding protein G(olf) subunit alpha
GSH2	Genetic-screened homeobox 2
h	Hours
HBC	Horizontal basal cell(s)
hCS	Human cortical spheroids
HES1/6	Hes family bHLH transcription factor 1/6
hESC	Human embryonic stem cell(s)
HESX1	Homeobox expressed in ES cells 1
hiPSC	Human induced pluripotent stem cell(s)
hPSC	Human pluripotent stem cell(s)
IP	Intermediate progenitor
iPSC	Induced pluripotent stem cell(s)
IRX1/2/3	Iroquois-class homeodomain protein 1/2/3
ISVZ	Inner sub-ventricular zone
IZ	Intermediate zone
Ki67	Marker of proliferation Ki-67
Klf4	Kruppel like factor 4
KOSR	KnockOut™ Serum Replacement
KRT5/17/18	Keratin 5/17/18
LGE	Lateral ganglionic eminence
LHX2	LIM homeobox 2
Lif	Leukemia inhibitory factor
m	Meter

mEpiSC	Murine epiblast-derived stem cells
mESC	Murine embryonic stem cell(s)
MGE	Medial ganglionic eminence
min	Minute
miPSC	Murine induced pluripotent stem cell(s)
ms	Millisecond
MSX1	Msh homeobox 1
MZ	Marginal zone
Na^+	Natrium(-ion)
NANOG	Nanog homeobox
NB	Neural border
NC	Neural crest
NCAM	Neural cell adhesion molecule
NEUROD1	Neurogenic differentiation 1
NEUROG1	Neurogenin-1
ng, µg, mg, g	Nanogram, microgram, milligram, gram
NKX2.1	NK2 homeobox 1
nl, µl, ml, l	Nanoliter, Microliter, Milliliter, Liter
NNE	Non-neural ectoderm
NOTCH1	Neurogenic locus notch homolog protein 1
NP	Neural plate
NPY	Neuropeptide Y
NT	Neural tube
NT-ESC	Nuclear transfer embryonic stem cell(s)
O_2	Oxygen
OB	Olfactory bulb
OCT3/4	Octamer-binding transcription factor 3/4
OE	Olfactory epithelium
OEC	Olfactory ensheathing cell(s)
OMP	Olfactory marker protein
OP	Olfactory placode
OR	Olfactory receptor(s)

oRG	Outer radial glia
ORN	Olfactory receptor neuron(s)
OSVZ	Outer sub-ventricular zone
OTX2	Orthodenticle homeobox 2
p63	Tumor protein p63
p75NGFR	p75 neurotrophin receptor
PAX2/3/6/7/8	Paired box 2/3/6/7/8
PBS$^{-/-}$	Phosphate buffered saline without Magnesium and Calcium
pc	*Post conceptionem*
PD	Parkinson´s disease
PFA	Paraformaldehyde
PGC	Primordial germ cells
PITX1/2/3	Paired-like homeodomain 1/2/3
PNS	Peripheral nervous system
PPR	Pre-placodal region
PSC	Pluripotent stem cell(s)
r	Radius
RAX	Retina and anterior neural fold homeobox
RG	Radial glia
ROCK	Rho associated coiled-coil containing protein kinase 1
rpm	Revolutions per minute
RT	Room temperature
RT-qPCR	Reverse transcription quantitative real-time polymerase chain reaction
RX	Retinal homeobox protein Rx
s	Second
S100B	S100 calcium binding protein B
S2	Safety level 2 (see BSL-2)
SAG	Smoothened agonist
SCID	Severe combined immunodeficiency
SCNT	Somatic cell nuclear transfer

SFEB	Serum-free, floating culture of embryoid body-like aggregates
SFEBq	Serum-free, floating culture of embryoid body-like aggregates, quick aggregation
SHH	Sonic hedgehog
SIX1/2/3/4/6	Sine oculis homeobox homolog 1/2/3/4/6
SMAD	Small worm phenotype + mothers against decapenta-plegic
SNAIL2	Snail family transcriptional repressor 2
SOX2/9/10	Sex determining region Y box transcription factor 2/9/10
SOXB1	*SOX* gene family comprising of *SOX1/2/3*
SPZ	Sub-plate zone
SSEA3/4	Stage-specific embryonic antigen 3/4
Stat3	Signal transducer and activator of transcription 3
SVZ	Sub-ventricular zone
T	T-box transcription factor T / Brachyury
TFAP2A	Transcription factor AP-2 alpha
TGFβ	Transforming growth factor beta
TRA-1-60	Podocalyxin
TRA-1-81	Podocalyxin
TRA-2-49/6E	Alkaline phosphatase
TUBB3	Class III β-tubulin
UCHL1	Ubiquitin carboxy-terminal hydrolase L1
VZ	Ventricular zone
WNT	Wingless-type family
WNTa	Wingless-type family antagonists
XaXi	X-inactivation
Zic1	Zic family member 1
ZO1	Tight junction protein 1
π	Pi

1 Summary

The olfactory sense is one of the oldest and most fundamental senses we have, serving a multitude of purposes like partner choice and risk avoidance. Additionally, olfactory decompensation is an early symptom of many neurodegenerative diseases and the olfactory epithelium – as a potential entry point to the central nervous system for unknown agents – is possibly even at the center of their pathophysiology. The olfactory epithelium is also one of the few tissues capable of adult neurogenesis and neuroregeneration, poorly understood processes with great therapeutic potential in an aging and chronically ill population. Nevertheless, olfaction has long remained in the offsite of biomedical research and profound interest in its function and development only arose over the last couple of decades.

The developmental mechanisms of the human olfactory epithelium are poorly understood, and any insight is mostly based on model organism research like mice and *xenopus laevis*. To study the development of the human olfactory epithelium, as well as to generate a three-dimensional model system for neurodegenerative disease and drug testing, I have established a differentiation protocol of human induced pluripotent stem cell derived olfactory placode organoids.

In this thesis, I describe and characterize the differentiation of human olfactory placode organoids. For this purpose, I have first established a developmental timeline of the organoid development from day 4 to day 31 of the differentiation, using morphology and immunofluorescence staining of key markers of ectoderm and olfactory development SIX1, TFAP2A and E-CADHERIN. The olfactory placode organoids are composed of a non-neural surface ectoderm containing placodal patches on the outside, neural tubuli representing the developing forebrain on the inside and a head mesenchyme in between, mimicking the developmental situation *in vivo*. I have further characterized the discovered features on a protein level and analyzed bulk RNA data from whole olfactory placode organoids. To improve maturation of the organoids and their distinctive features, the differentiation protocol was adapted based on brain organoid and other organoid techniques. The preliminary result of the modified protocol shows a high level of

maturation and organization, but further efforts are needed to generate a mature human olfactory epithelium *in vitro*.

This work shows for the first time the generation of an olfactory placode organoid derived from human induced pluripotent stem cells, exhibiting patches of developing olfactory tissue in a three-dimensional *in vitro* system. Furthermore, these olfactory placode organoids show an outside-out orientation incorporating at least four different tissues. The surface epithelium as well as the neural tubuli are anchored on their own basement membrane providing stability and orientation. These features of high-level organization closely resemble the embryonic head and have – to my best knowledge – not been achieved in a three-dimensional organoid model before.

This thesis sets the groundwork for the generation of a fully functional human olfactory epithelium model in a three-dimensional *in vitro* organoid and gives first insight on human olfactory development. In the future, the obtained results could contribute to the generation of a powerful model system for neuroscience and developmental biology.

2 Zusammenfassung

Der Geruchssinn erfüllt als einer unserer ältesten und grundlegendsten Sinne eine Vielzahl von Funktionen, wie der Partnerwahl und Risikovermeidung. Zusätzlich ist die Dekompensation des Geruchssinns ein Frühsymptom vieler neurodegenerativer Erkrankungen und das olfaktorische Epithel steht als potenzielle Eintrittspforte für unbekannte Auslöser ins zentrale Nervensystem möglicherweise im Zentrum ihrer Pathophysiologie. Das olfaktorische Epithel ist drüber hinaus eins der wenigen Gewebe, in denen adulte Neurogenese und Neuroregeneration – zwei eingeschränkt verstandene Prozesse – möglich sind. Diese Vorgänge bergen ein großes therapeutisches Potential in einer alternden und chronisch kranken Bevölkerung. Nichtsdestotrotz war die Olfaktion lange im Abseits der biomedizinischen Forschung und ein tiefgreifendes Interesse für Ihre Funktion und Entwicklung entstand erst in den letzten Jahrzehnten.

Die Mechanismen der Entwicklung des humanen olfaktorischen Epithels sind bis dato schlecht verstanden und vorhandenes Wissen basiert meist auf der Erforschung von Modelorganismen wie Mäusen oder *Xenopus laevis*. Um die Entwicklung des humanen olfaktorischen Epithels zu untersuchen, wie auch um ein dreidimensionales Modelsystem für neurodegenerative Erkrankungen und pharmakologische Tests zu etablieren, habe ich ein Differenzierungsprotokoll für humane induziert pluripotente Stammzellen zu Organoiden der olfaktorischen Plakode entwickelt.

In dieser Arbeit beschreibe und charakterisiere ich die Differenzierung dieser humanen olfaktorischen Plakoden Organoide. Zu diesem Zweck habe ich zunächst einen Entwicklungszeitstrahl der Organoidentwicklung von Tag 4 bis Tag 31 der Differenzierung etabliert. Hierzu habe ich die Morphologie, wie auch Immunfluoreszenzfärbungen von Schlüsselmarkern des Ektoderms und der olfaktorischen Entwicklung, namentlich SIX1, TFAP2A und E-CADHERIN analysiert. Die olfaktorischen Plakoden Organoide bestehen aus einem nicht-neuralen Oberflächenektoderm mit plakodalen Verdickungen auf der Außenseite und neuralen Tubuli, die das sich entwickelnde Prosencephalon darstellen, auf der Innenseite. Zwischen diesen beiden Strukturen liegt ein Kopf Mesenchym. Diese Architektur

ahmt die Entwicklung *in vivo* recht genau nach. Im Folgenden habe ich die beschriebenen Strukturen der Organoide auf Proteinebene charakterisiert und RNA Analysen von ganzen olfaktorischen Plakoden Organoiden durchgeführt. Um die Ausreifung der Organoide und den darin enthaltenen Strukturen zu verbessen, habe ich das Differenzierungsprotokoll basierend auf Erkenntnissen von Gehirn Organoiden und anderen Organoiden modifiziert. Die vorläufigen Ergebnisse dieses Protokolls zeigen ein hohes Level an Ausreifung und Organisation, wenn auch weitere Anstrengungen von Nöten sind, um ein reifes humanes olfaktorisches Epithel *in vitro* zu generieren.

Diese Arbeit beschreibt zum ersten Mal die Differenzierung von humanen olfaktorischen plakodalen Organoiden *in vitro* aus humanen induziert pluripotenten Stammzellen. Diese dreidimensionalen Organoide beinhalten Verdickungen mit sich entwickelndem olfaktorischen Gewebe. Des Weiteren enthalten sie mindestens vier verschiedene Gewebe und weisen eine physiologische Orientierung mit der Außenseite nach Außen auf. Sowohl das Oberflächen Ektoderm wie auch die neuralen Tubuli sind auf ihrer eigenen Basalmembran verankert, die Stabilität und apiko-basale Orientierung liefert. Diese Charakteristika an stark ausgeprägter Organisation sind den Verhältnissen im sich entwickelnden embryonalen Kopf sehr ähnlich und wurden – meinem Wissen nach – noch nicht in einem dreidimensionalen Organoid Modell beschrieben.

Diese Arbeit bildet die Grundlage für die Entwicklung eines voll funktionsfähigen humanen olfaktorischen Epithel-Models in einem dreidimensionalen Organoid und liefert erste Erkenntnisse über die humane olfaktorische Entwicklung. Die Ergebnisse dieser Arbeit können in der Zukunft einen Teil zur Etablierung eines vielseitigen Modellsystems für Neurowissenschaften und die Entwicklungsbiologie beitragen.

3 Introduction

3.1 Spotlight on olfaction – the next great frontier?

In the past, our understanding of chronic neurologic diseases such as Parkinson´s (PD) or Alzheimer´s (AD) disease, as well as Multiple Sclerosis (MS) has been poor, especially when it comes to their causes. Over the last 20 years, there has been a profound paradigm shift in neurology and psychiatry, with compiling evidence that many of these diseases might be due to genetic mutations or external causes – not “idiopathic”. Recently, an excellent longitudinal study of > 10 million individuals has uncovered that the Epstein-Barr virus (EBV) is most likely the leading cause of MS (1).

Braak´s theory poses a similar hypothesis for PD: A neurotrophic factor enters the central nervous system (CNS) through the olfactory epithelium (OE) as well as the *nucleus dorsalis nervi vagi* and induces the formation of α-synuclein aggregates (Lewi-bodies) (2). From these first affected areas, the α-synuclein burden then spreads through the CNS, causing the clinical manifestations of PD (3). This theory is backed by a multitude of *in vitro* and *in vivo* evidence (4). In PD and AD, olfactory deficits precede classical symptoms for years and can be used as early markers for the disease (5,6). Furthermore, Lewi-bodies can be found early in the OE and olfactory bulbs (OB) of patients with PD (3,7). The OE with its bipolar neurons – being in contact with the CNS and the outside world – is an intriguing entry site for possible pathogens (8).

Yet, the olfactory system is one of the least studied sensory systems in humans. The development of the human OE remains largely uncharted territory, since most studies examine model organisms as mouse or *xenopus laevis* (9).

Human induced pluripotent stem cells (hiPSC) and novel three-dimensional (3D) cell culture techniques called “organoids” pose the potential to not only illuminate the human developmental processes, but also to create a model system of the OE to study neurodegenerative diseases *in vitro* and act as steppingstones for future therapies. Moreover, an *in vitro* model system of the OE would enable

research on a key feature of the OE – lifelong neurogenesis – the holy grail of neuroscience (10).

This thesis will take the first steps in the development of such a much-needed tool for neuroscience.

3.2 Anatomy and function of the human olfactory system

Olfaction is an intricate sense and serves a multitude of functions below our level of aware consciousness, since it is the only sensory system not integrating information through the *thalamus dorsalis* (11). If impaired, the loss of olfactory function does not lead to debilitating conditions such as hearing loss or blindness, long putting it in the offsite of biomedical research. Yet, this long standing neglect of olfaction is short sighted and in recent years interest in the olfactory system has grown substantially (11). The perception of smell is not only important for orientation, the detection of harmful substances, environmental hazards or spoiled food, but also partner choice and memory are closely tied to olfaction (12,13). This is only made possible by the olfactory systems unique ability to sense volatile substances in the air and transduce this information into patterns of action potentials in the brain.

3.2.1 Macroscopy – from the nose to the brain

As air is inhaled, it enters the nose through the bilateral nostrils (*nares*) and moves through the *vestibulum nasi* into the *cavitas nasi propria.* On the roof of the *cavitas nasi propria* resides the primary sensory olfactory organ, the OE. It spans cranially over the nasal part of the *lamina cribrosa ossis ethmoidalis*, laterally over the *concha nasalis superior ossis ethmoidalis* and medially over the *lamina perpendicularis ossis ethmoidalis* of the nasal septum (14).

To generate the perception of smell, the inhaled air with its odors must come in contact with the OE. However, only around 14 % of the inhaled air reaches the olfactory mucosa (15). This percentage can be increased by “sniffing” with multiple short and shallow inhalations (14). Now, inspired air is moving upward, predominantly ventral to the nasal *conchae* in the so called “sniffing-groove”, directly to the olfactory region (14).

The axons of the primary sensory neurons in the OE penetrate the basement membrane of the OE and pass the *lamina propria* and *submucosa* (14). Within the *lamina propria* the axons are surrounded by olfactory ensheathing cells (OEC) and penetrate the *lamina cribrosa ossis ethmoidalis* as nerve bundles (*fila olfactoria*), making up the 1st cranial nerve (*nervus olfactorius*) (14,16). The *fila olfactoria* enter the OB and the axons form synapses with projecting- and inter-neurons (14). The olfactory information is then projected to multiple brain regions like the *area pre-piriformis*, the septum region, the hippocampus / limbic system and the hypothalamus (14). Many brain regions closely interact in the integration of olfactory information as the olfactory system is the only sensory system not reliant on thalamic representation (14).

3.2.2 Microscopy – from the air to the neuron

The OE is a pseudostratified columnar epithelium made up of five different cell types: (I) olfactory receptor neurons (ORN), (II) microvillar cells, (III) supporting cells, (IV) basal cells and (V) Bowman's gland ductal cells (10)(**Fig. 1**).

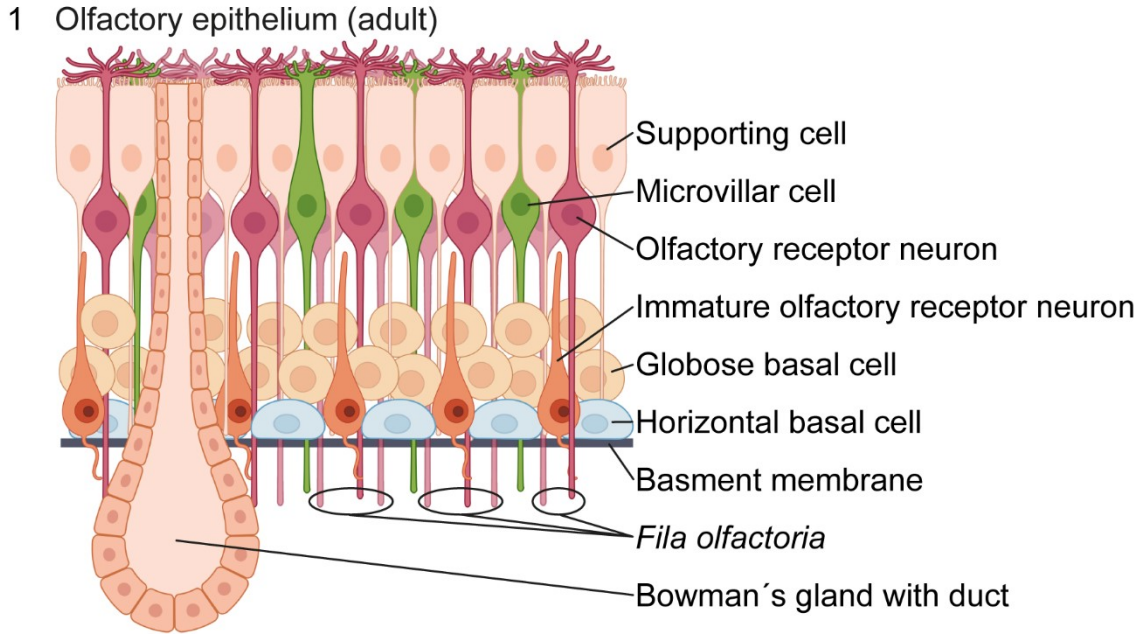

Figure 1: Architecture of the adult human olfactory epithelium

The human OE incorporates many different cell types spanning the pseudostratified epithelium. Horizontal basal cells (light blue), globose basal cells (yellow) and immature ORN (orange) are located more basal, whilst microvillar cells (green) and ORN (red) are located more apical with their cilia and microvilli extended into the nasal lumen (top). The axons of the ORN penetrate the basement membrane and make up the *fila olfactoria*, the anatomical correlate for the 1st cranial nerve. Supporting cells span the whole epithelium and are anchored on the basement membrane (grey). Their microvilli also reach the nasal cavity. Bowman´s glands lie underneath the epithelium with their ductuli passing through it. Figure created with BioRender.com.

ORN are true bipolar, primary sensory neurons that sense odorants and project their action-potentials into the OB (10,14). They have a single dendrite, which bears 5-30 sensory cilia extending into the nasal lumen, where olfactory receptors (OR) in its membrane sense odorants (10). Upon binding of an odorant, the α-subunit of G_{olf} activates an adenylate cyclase, producing cAMP (17). CAMP binds to CNG cation channels, allowing Na^+ and Ca^{2+} influx, which further activates Cl^--channels and creates an action potential (17,18).

OR are encoded by a superfamily of 851 genes of which more than 50 % are non-functional pseudogenes due to frame-reading mutations (19). Scattered

across the genome, OR genes make up ~ 3 % of all genes which makes them the biggest human gene family (20,21). Mature ORN generally express only one OR but immature ORN can express multiple OR (22,23). Immature ORN can be characterized by their expression of UCHL1, TUBB3, G_{olf}, NCAM, GNG8 and LHX2, whilst mature ORN express UCHL1, OMP, G_{olf}, NCAM and GNG13 (24,25).

Microvillar cells are located apically in the OE, extend microvilli into the nasal lumen, and have a single unmyelinated axon (10). Whilst their exact function remains unclear, they seem to play a role in the orchestration of ORN regeneration (10,26). They are marked by the expression of NPY (26).

Supporting cells span the epithelium and extend microvilli into the nasal lumen whilst anchoring on the basement membrane (10). They give structural support, perform phagocytosis, and express metabolic enzymes for xenobiotics, giving them a glial-like role in the OE (10). Supporting cells are labeled by HES1, E-CADHERIN, PAX6, KRT18, EGFR and SOX2 (24,27).

Bowman´s gland ductal cells form the *ductuli* connecting the submucosal Bowman´s glands with the nasal lumen (10). The Bowman´s glands produce most of the mucus and secretion of the OE and express high levels of metabolic enzymes. The ductal cells can be marked by SOX9, E-CADHERIN, PAX6, KRT18 (10).

Basal cells are the somatic stem cells of the OE responsible for regeneration and neurogenesis throughout adulthood, rendering the OE a rare site of life long neurogenesis (10). There are two types of morphologically and functionally distinct types of basal cells in rodents: horizontal and globose basal cells (HBC & GBC, respectively) (28). In humans, these functionally distinct cell types both share a round morphology, similar to GBC in rodents, but can be distinguished morphologically via electron microscopy (24,25,28). GBC are the actively dividing tissue stem cell population for neuronal and non-neuronal cell types, whilst HBC are reserve stem cells only activated through severe tissue damage (27). HBC are abundant and can be marked by their expression of KRT5, KRT17, P63, SOX2, PAX6, EGFR and p75NGFR, whilst GBC express SOX2, ASCL1, Ki67, NOTCH1,

HES6, p75NGFR, NEUROG1 and NEUROD1, but resemble a more heterogeneous population (24,25,27,29,30).

Another important cell type in the olfactory mucosa is the OEC. They do not reside in the OE but surround the axons of the ORN in the *lamina propria* and *submucosa* until they reach the OB and are characterized by their expression of GFAP, p75NGFR and S100B (10,25,30).

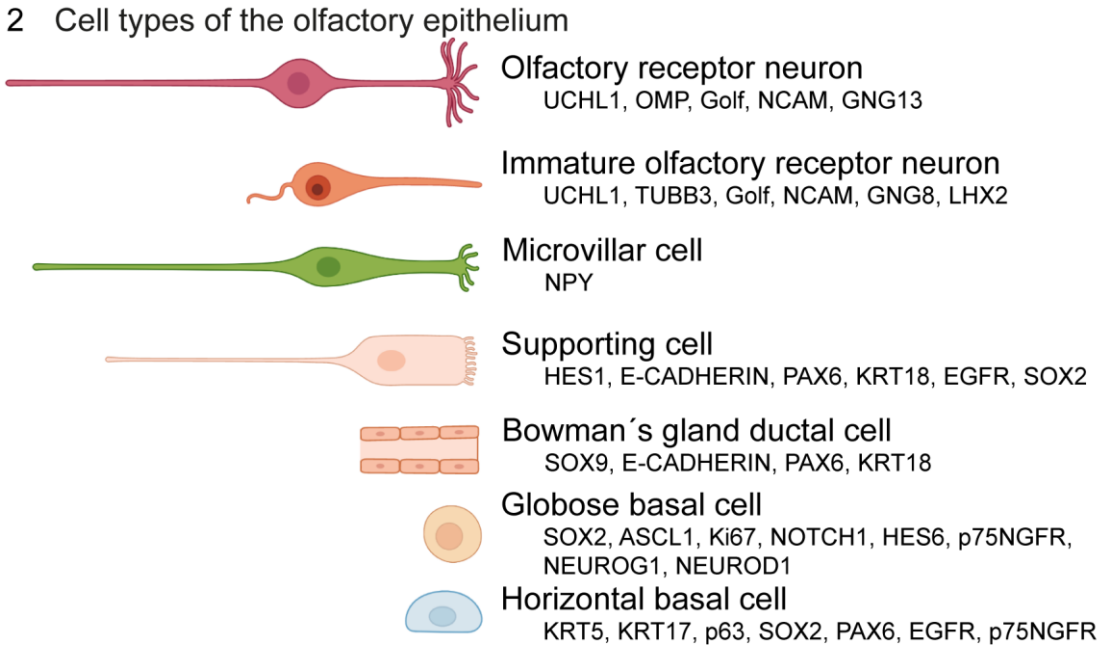

Figure 2: Markers of different cell types of the adult human OE

Schematic drawing of the seven cell types of the adult human OE (left) with their annotated marker expression (right). Figure created with BioRender.com.

These cell types and their markers are highly conserved among rodents and humans (24). Nevertheless, the murine OE shows a high-level laminar organization and different morphology in basal cells, highlighting limiting differences between humans and model species (30).

3.3 Early human development

The olfactory sense is phylogenetically the first specialized sense in animals, and develops early during embryogenesis (10). Because the anlage for the olfactory system arises early in ontogenesis and key patterns of this are reproduced in a 3D organoid model *in vitro* in this study, our comprehension of early human development is of great importance.

3.3.1 Implantation & the bilaminar embryo

6-8 days *post conceptionem (pc)* the blastocyst, consisting of the embryoblast and the trophoblast, nidates in the endometrium (14). Cells of the embryoblast, oriented towards the trophoblast, form the epiblast and the lining of the amniotic cavity, whilst cells oriented towards the blastocyst cavity form the hypoblast and the yolk sac (14). The bilaminar embryo, consisting of the epiblast and the hypoblast, has formed (**Fig. 3**).

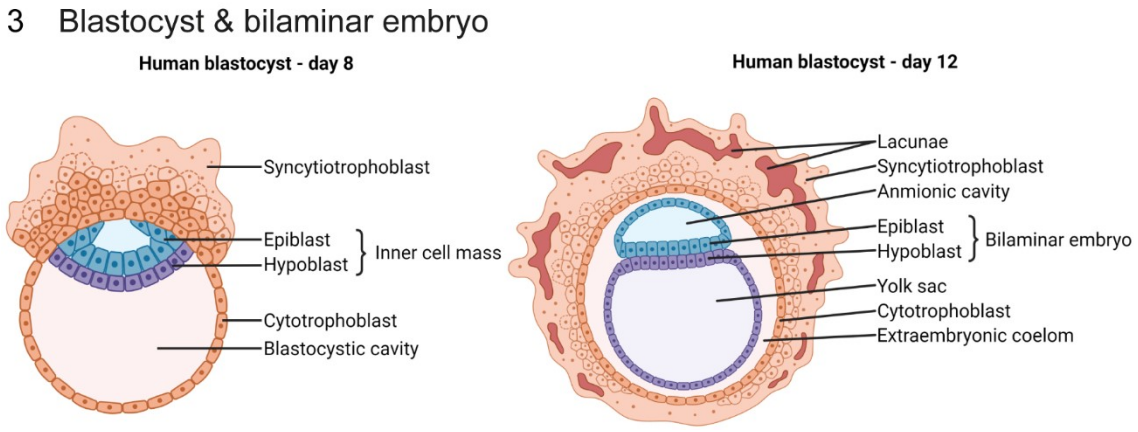

Figure 3: Blastocyst & bilaminar embryo

Schematic drawing of a human blastocyst on day 8 (left) and day 12 (right) *pc*. Epiblast cells (blue) forming the lining of the amnionic cavity and hypoblast cells (purple) forming the lining of the yolk sac. Cytotrophoblast and syncytiotrophoblast in orange and light orange, respectively. Figure created with BioRender.com.

3.3.2 Gastrulation

In the 3rd week *pc*, starting at day 15 (Carnegie Stage [CS] 7-8), the process of gastrulation occurs (14,31). Here, the pluripotent epiblast of the bilaminar embryo, gives rise to the trilaminar embryo (14). Beginning caudally, the primitive streak extends cranially in the epiblast until forming the primitive node at its

cranial end (at half the length of the embryo) (14). The primitive streak forms the primitive groove, from which epiblast cells delaminate and migrate between the hypo- and the epiblast in a process called “epithelial-to-mesenchymal-transition” (EMT), forming the new intraembryonic mesoderm (14,32). Cells from the cranial part of the primitive groove migrate into the hypoblast and displace the hypoblast cells to form the new endoderm (14). Furthermore, a cell mass migrating cranially from the primitive node forms the chordal process which invaginates and delaminates from the endoderm deriving the *corda dorsalis* (14). This *corda dorsalis* (also called notochord) plays a pivotal role in the further patterning of the embryo (14). Under the influence of morphogenic cues from the new mesoderm and endoderm, the remaining epiblast cells make up the new ectoderm (14)(**Fig.4**).

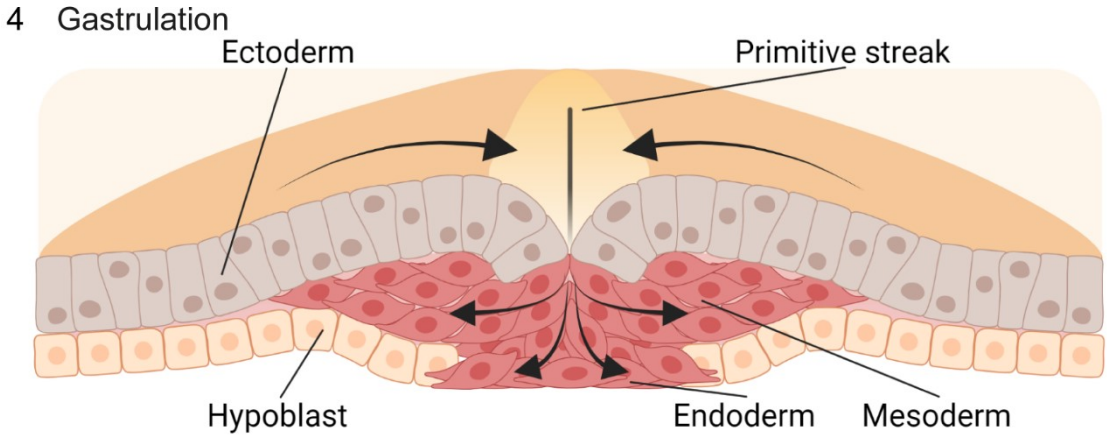

Figure 4: Gastrulation

Schematic drawing of a horizontal section during gastrulation in the 3rd week *pc*. Epiblast / ectoderm (brown), mesoderm and young endoderm (red), hypoblast (yellow). Cell movements annotated with arrows. Figure created with BioRender.com.

3.3.3 Ectodermal patterning

This primitive ectoderm later gives rise to various structures namely the epidermis, the CNS, the neural crest (NC) with its derivatives like peripheral and enteric nervous system (PNS & ENS), and the cranial sensory placodes (CP) (33). This patterning occurs along a dorso-ventral (D-V) axis in vertebrates, with the primitive node and the *chorda dorsalis* acting as organizers (14,34–36). These underlying structures secrete Nogging and other inhibitors of the bone morphogenic proteins (BMPs) close to the midline, which induces the formation of the columnar

neural plate (NP) in the ectoderm (37). Furthermore, inhibition of the canonical WNT pathway is required to induce neural fates, whilst also providing strong induction cues towards anteriorization (38).

During gastrula stages, as the ectoderm is divided into the NP – later giving rise to the CNS – and the non-neural ectoderm (NNE), which will give rise to the epidermis of the skin, a third ectodermal structure forms between these two tissues (9). In response to direct interaction between the NP and the NNE, as well as due to morphogenic cues from underlying tissues, a specialized “neural border zone” (NB) forms within the NNE around the NP (9,39). From this NB, the NC, and the pre-placodal region (PPR) arise, which later sub-specifies and breaks down into the CP (40).

CP are focal thickenings in the head ectoderm of vertebrates, sometimes with a partly interrupted basement membrane (9,41). These CP later give rise to the anterior pituitary gland, the OE, the lens, large neurons of the cranial sensory ganglia (trigeminal, facial, glossopharyngeal and vagal cranial nerves), the otic and vestibular sensory organs (39). In fish and amphibians, the PPR also gives rise to the CP of the lateral line, a sensory organ detecting water movements and electric fields, and the hypobranchial ganglia of yet unknown function (9,42).

The NC is a purely migratory and multipotent cell population and as such gives rise to various cell types as craniofacial cartilage and bone, pigmented cells, and the neurons and glia of the ENS and PNS (9,43). Whilst the NC is induced laterally to the whole NP, the PPR is only formed around the anterior NP in a horseshoe-shaped manner, partly lateral to the NC (9) (**Fig. 5**).

5 Pre-placodal region

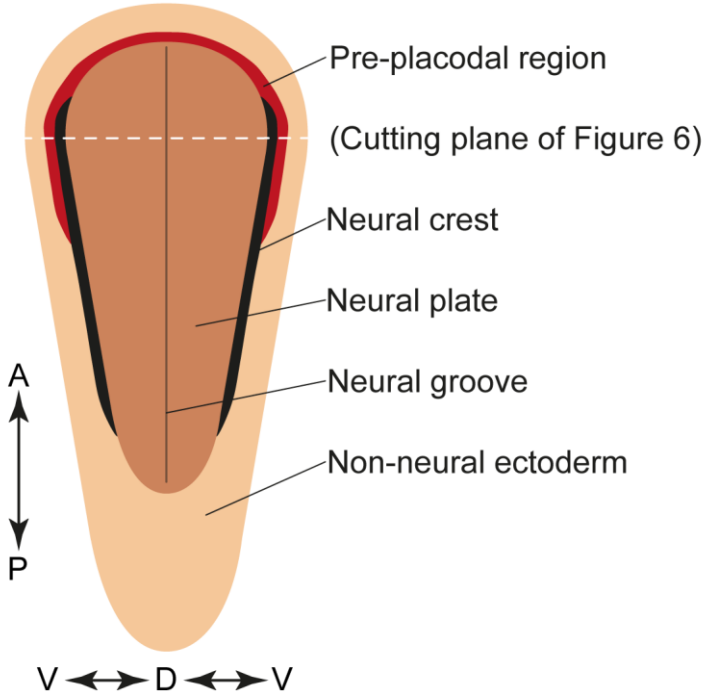

Figure 5: The pre-placodal region in situ

Schematic drawing of a dorsal view of an embryo in the early 4th week pc. The PPR (red) forms in a horseshoe-shaped manner around the anterior NP (brown), laterally to the NC (black). Whilst the PPR forms only around the anterior NP, the NC forms laterally to the whole NP, except the anterior pole. White dashed line annotates section plain of ***(Fig.6)****. Anterior (A), posterior (P), ventral (V), dorsal (D).*

As the NP forms the neural tube (NT) during neurulation, the NC is displaced from the ectoderm and the PPR breaks down into distinct CP (9,14,44). Both, the NC and the CP with their derivatives are likely key factors for the evolutionary success of vertebrates (40).

3.3.4 Neurulation

In the 4th week *pc* starting on day 18-19 (CS 10-13) the process of neurulation occurs. Here, the NP – which extends from the buccopharyngeal membrane to the primitive node – forms the so-called neural groove under the influence of the *chorda dorsalis* (14). Laterally to the neural groove the so-called neural folds form, which also comprise the NB with the NC and PPR (14). Starting on day 20, the neural folds approximate and begin to fuse on somite level four propagating cranially and caudally, forming the NT (14,31). During this closure of the NT, the PPR acquires an anterior-posterior (A-P) identity and becomes regionalized (39).

The remaining openings, the *neuroporus cranialis* and *neuroporus caudalis*, close on day 24 and 26, respectively (14). The NC is displaced laterally to the now formed NT and, as a highly migratory and multipotent cell lineage, give rise to various different cell types (14) (**Fig.6**).

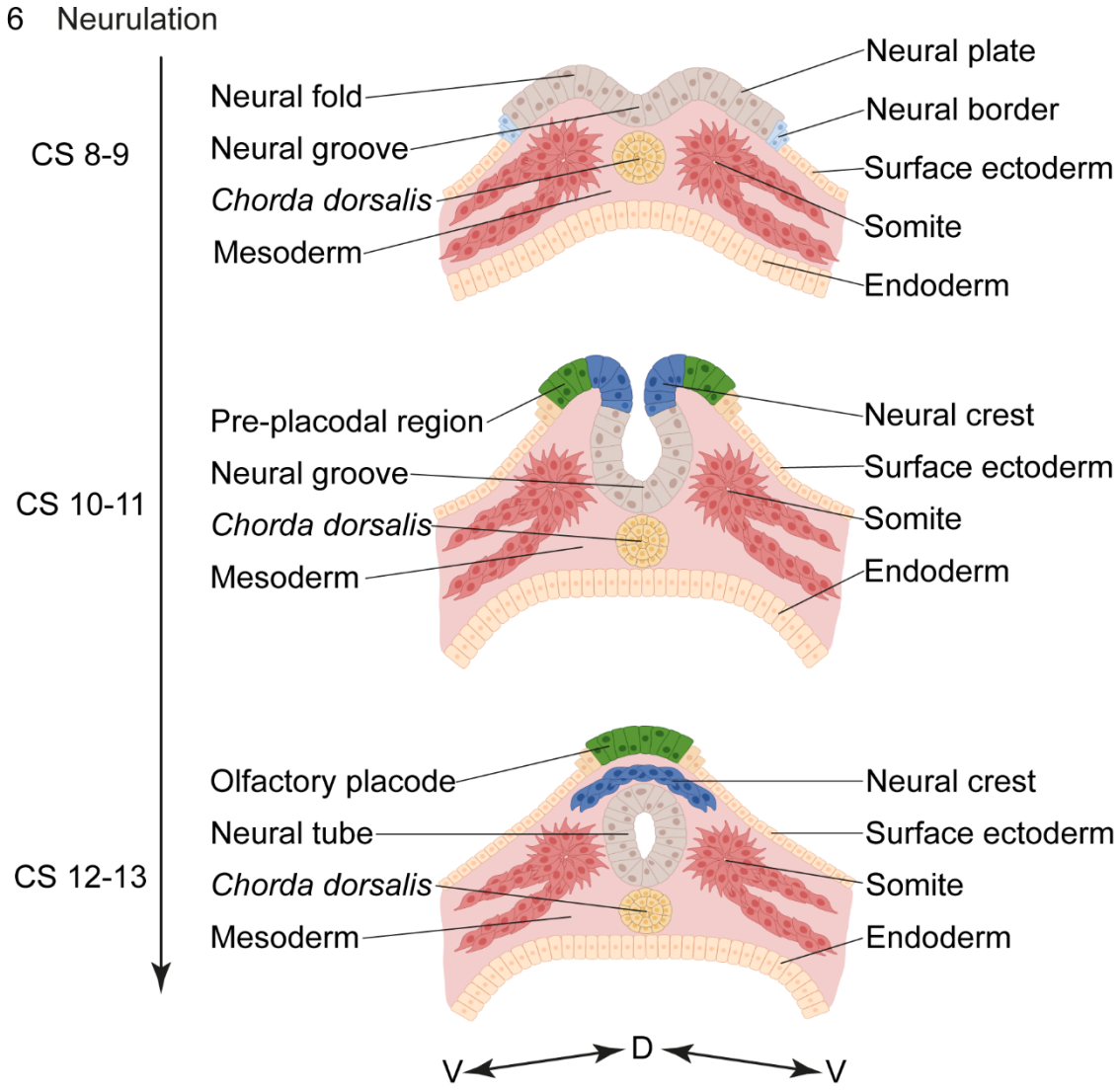

Figure 6: Neurulation

Schematic drawing of a cross section view of an embryo undergoing neurulation starting in the 4th week *pc*. Timeline annotated in CS from top to bottom. Section plane annotated in **(Fig. 5)**. NP / NT (brown), NB (light blue), NNE (yellow, cuboid), chorda dorsalis (yellow, cell strand), mesoderm & somites (red), endoderm (yellow, columnar), NC (dark blue), PPR & olfactory placode (green). Dorsal (D), ventral (V). Figure created with BioRender.com.

3.4 Special olfactory development

The formation of a NB between the NP and the definite NNE, the development of the NC and the PPR, as well as the rise of specific placodes like the olfactory placode (OP) (and subsequently the OE) is a highly conserved process along vertebrates (45). This being the case, significant interspecies differences can be observed comparing model organisms (zebrafish, xenopus, chick, mouse) regarding gene expression (39). Expression patterns and timelines in model organisms can be strong clues to elucidate the human olfactory development – on which there is not a lot of data – but interpretations should always be made with caution and respect to remaining uncertainty. The knowledge of the olfactory development is largely based on these model organisms.

3.4.1 Neural border & pre-placodal region

The NB is initially specified by the overlap of the expression of pre-neural genes (*SoxB1*, *Zic*, Otx2, ERNI, Gemini) with non-neural genes (Tfap2a, Gata2/3, Msx1, Foxi1/3, *Dlx*) (39,46). These genes – called “NB-specifying” genes – then orchestrate the specification and further sub-division of the NB into the NC and PPR (39,46). The borders between the NP, NC, PPR and NNE are defined and maintained by the expression of key regulators, which activate further downstream commitment and repress expansion of adjacent territories (46). The NC and its borders are marked by the expression of Msx1, Pax3/7, FoxD3, Sox9/10, *Dlx*-genes, Tfap2a, and Snail2 (39,46). The PPR can be exclusively marked by their expression of *Six*- and *Eya*-family genes, with Six1/2/4 and Eya1/2/3/4 being expressed in the whole PPR, albeit with some interspecies differences (9,45). Additional gene-products also mark the PPR (Tfap2a, Gata2/3, Dlx3/5), but are also expressed in other locations, so that PPR definition using these genes needs “combinational codes” (9,45,47).

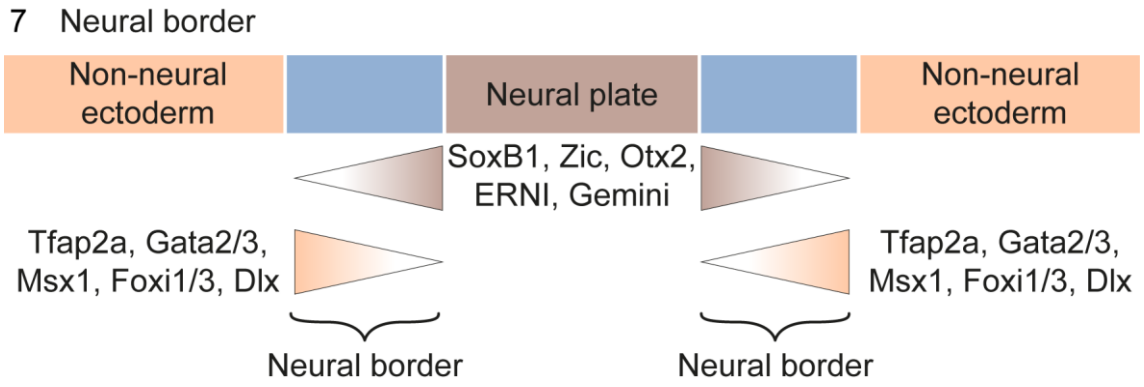

Figure 7: Neural border formation

The expression patterns of the NP (brown) and the NNE (orange) overlap in a region defined as the NB (blue).

3.4.2 The PPR as a multipotent progenitor

Initially, the PPR is a multipotent region, in which all cells can form all placodes due to their shared molecular patterning, and distinct placodes arise later due to external cues (45,46).

Prove for this idea was first demonstrated by Jacobson in amphibians. Here, he showed that the early PPR could be re-grafted anywhere within the PPR and give rise to the appropriate placode according to its new position, whilst the later PPR gave rise to the placode from its original location (48).

Furthermore, the PPR is a necessary step in the induction of placodes, since only the PPR reacts to morphogen exposure with the development of placodes (49). This is also true for hESC based differentiations, where PPR genes TFAP2A, GATA, and DLX genes must be expressed before cells can acquire CP markers (50).

3.4.3 Sub-specification of the pre-placodal region

As mentioned earlier, the PPR acquires an A-P identity during neuralization (39). During this process, the PPR breaks down into an anterior (anterior pituitary, olfactory, lens), intermediate (trigeminal) and posterior (otic, lateral line, epi/hypobranchial) placodal field, each later giving rise to specific placodes (39) (**Fig.8**).

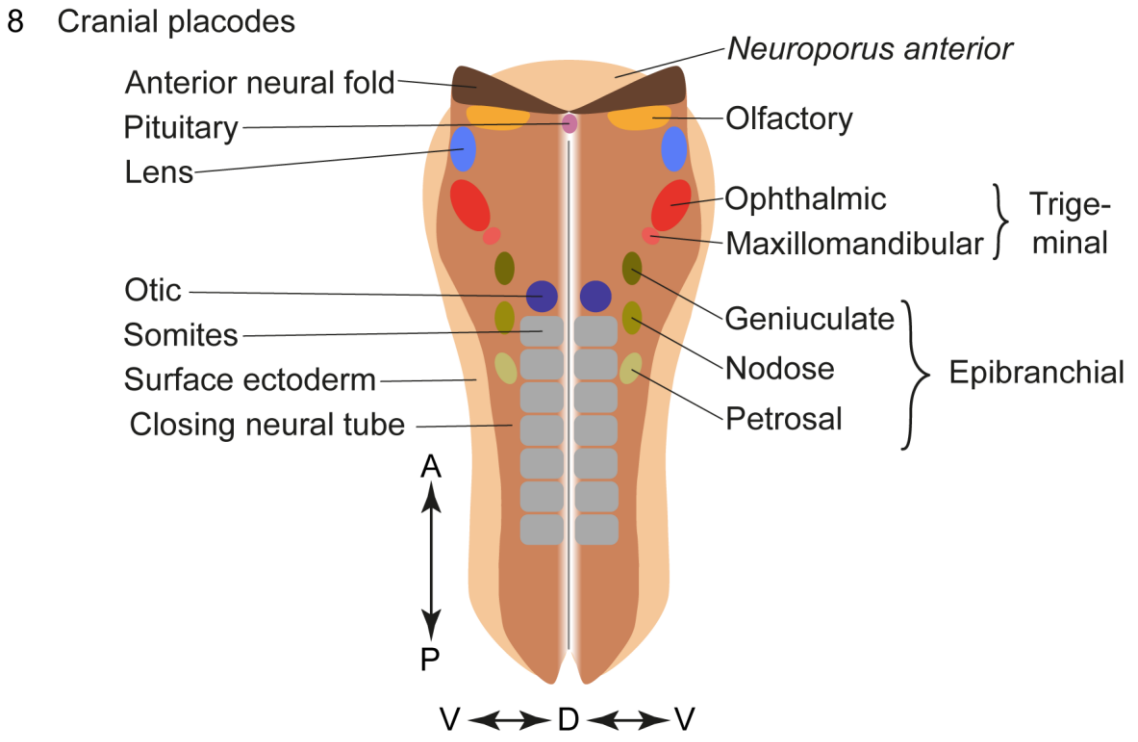

Figure 8: Cranial placodes

Schematic drawing of a dorsal view of an embryo after breakdown of the PPR into CP during neurulation. NT (brown), anterior neural fold (dark brown), pituitary placode (magenta), OP (yellow), lens placodes (light blue). The ophthalmic (red) and maxillomandibular (light red) placodes make up the trigeminal placodes. The geniculate (dark green), nodose (green) and petrosal (light green) placodes make up the epibranchial placodes. Otic placodes (dark blue), somites (grey), anterior (A), posterior (P), ventral (V), dorsal (D). Adapted after (51,52).

Spatial and temporal signals from the NP, NNE and mesenchyme are inducing these changes in the PPR (9). Similar to the situation in the adjacent neural tube, Otx2 and Gbx2 play important roles as initial patterning factors for this process, with Otx2 being expressed anterior and Gbx2 being expressed posterior (39).

Genes of the *Six* and *Eya* family lie in the center of the regulatory pathway, being broadly expressed in the PPR (9,46). When binding to Six, Eya can translocate to the nucleus, where it can act as a co-factor for Six and change the function of other co-factors (Dach) from co-repressors to co-activators (9,53,54). These changes in transcription uphold PPR potential, repress NP, NC and NNE genes, and induce downstream genes for sub-specification (46,55).

One of the most important gene family for the spatial identity of placodal fields are the *Pax* genes (9). They are activated downstream of the Six / Eya network

and pattern the PPR into the anterior (Pax6), intermediate (Pax3) and posterior (Pax2/8) placodal regions (46). They not only activate further downstream pathways for fate commitment, but also define placodal fields by co-repression (39,56).

During this breakdown of the PPR, molecular markers become more distinct and restricted to specific placodal fields and later placodes (9,39,45). The anterior field is expressing Otx2, Pax6, Six3/6, and Pitx1/2, the intermediate zone is expressing Otx2, Pax3, and Irx1/2/3, and the posterior field is expressing Gbx2, Pax2/8, Irx1/2/3, Foxi3 (9,45).

The anterior placodal field subsequently breaks down into the placodes of the anterior pituitary, the lens, and the OE, whilst the posterior placodal field gives rise to the epibranchial and otic placodes (9).

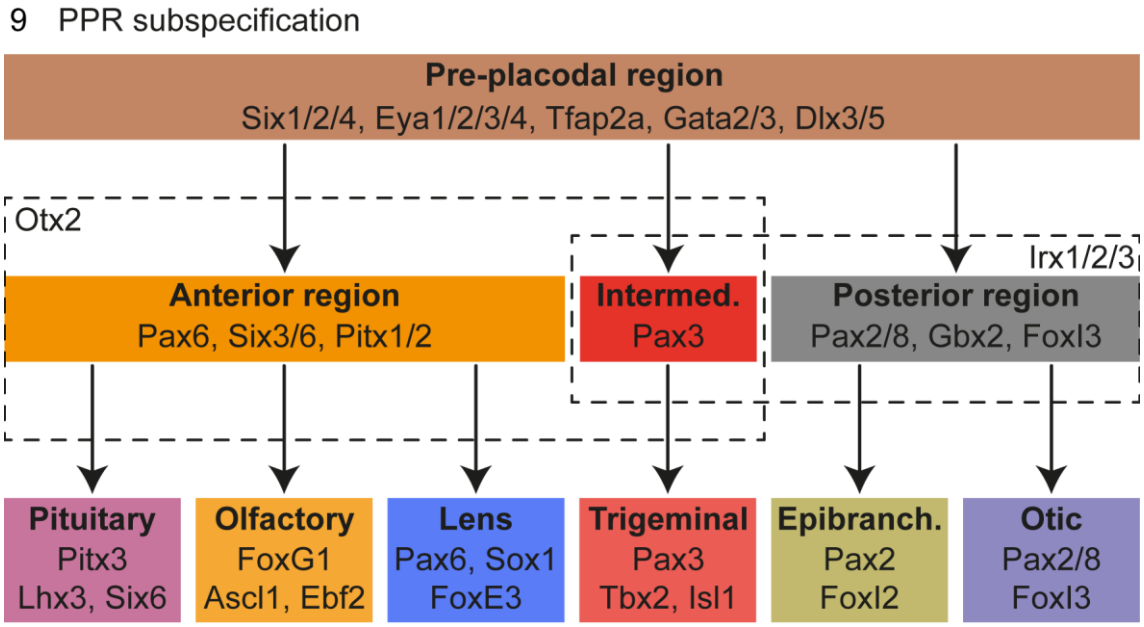

Figure 9: Sub-specification of the pre-placodal region

Schematic drawing the of the PPR sub-specification into the placodal fields and later the CP. Regions and CP characterized with their specific marker expression. Overlapping expression for Otx2 and Irx1/2/3 indicated by dashed lines. Adapted after (45).

3.4.4 The olfactory placode

The further sub-specialization of the anterior placodal field is again mediated by signals from adjacent and underlying tissues (45). For example, signals from the anterior neural fold (Fgf8) induce the OP in the anterior placodal region, but the cranial mesenchyme also plays a vital role in this process (45,47). The OP also demarks and specializes with the expression of transcription factors necessary for neural fate (9,57). Consequently, the OP expresses markers associated with the capacity to generate neurons, such as Six1, Eya2, Sox2 and Foxg1, as well as markers indicating early ORN lineage such as Ascl1 and Ebf2 (39,45,57).

The OP is the only neurogenic placode of the anterior placodal field and as such gives rise to the OE with its ORN (39). Also, GnRH1^{+}-neurons originate from the OP and migrate along the olfactory and terminal nerve, through the anterior forebrain and into the hypothalamus (29,58,59). Here, GnRH1^{+}-neurons play an important role for fertility and mating functions in the hypothalamic-pituitary-gonadal axis (60,61). Within the OP, which likely integrates PPR and NC cells to some degree, the GnRH1^{+}-neurons are partly of NC origin (62).

Starting day 26 *pc* (CS 11), the OP can be seen as so-called “nasal plate” laterally to the *neuroporus cranialis* (63). In stages 12 / 13 the OP thickens and a mesenchyme appears between the forebrain and the OP (63). In stage 14 the OP forms the nasal groove and starts to invaginate into the mesenchyme in stage 15, forming the nasal pit (63). This mesenchyme – product of the NC – expresses Pax7 upon invagination in mice on E10.5 (~ CS 13 / 14) (39,64). In CS 16, the mesenchyme further proliferates and the central olfactory structures as the anlagen of the OB and olfactory tuberosity become clearly visible (63). Finally, in stage 17, the nasal pit closes, forming the nasal sac and the OB with axons from the OP / OE are more prominent (63) (**Fig.10**).

As the development of the OE from the OP and PPR are complex in nature and dependent on multiple cross-tissue interactions, this work seeks to model the situation *in vivo*, by juxtaposing multiple tissues within 3D organoids *in vitro*. One structure, which seems to play a pivotal part in olfactory development is the fetal brain.

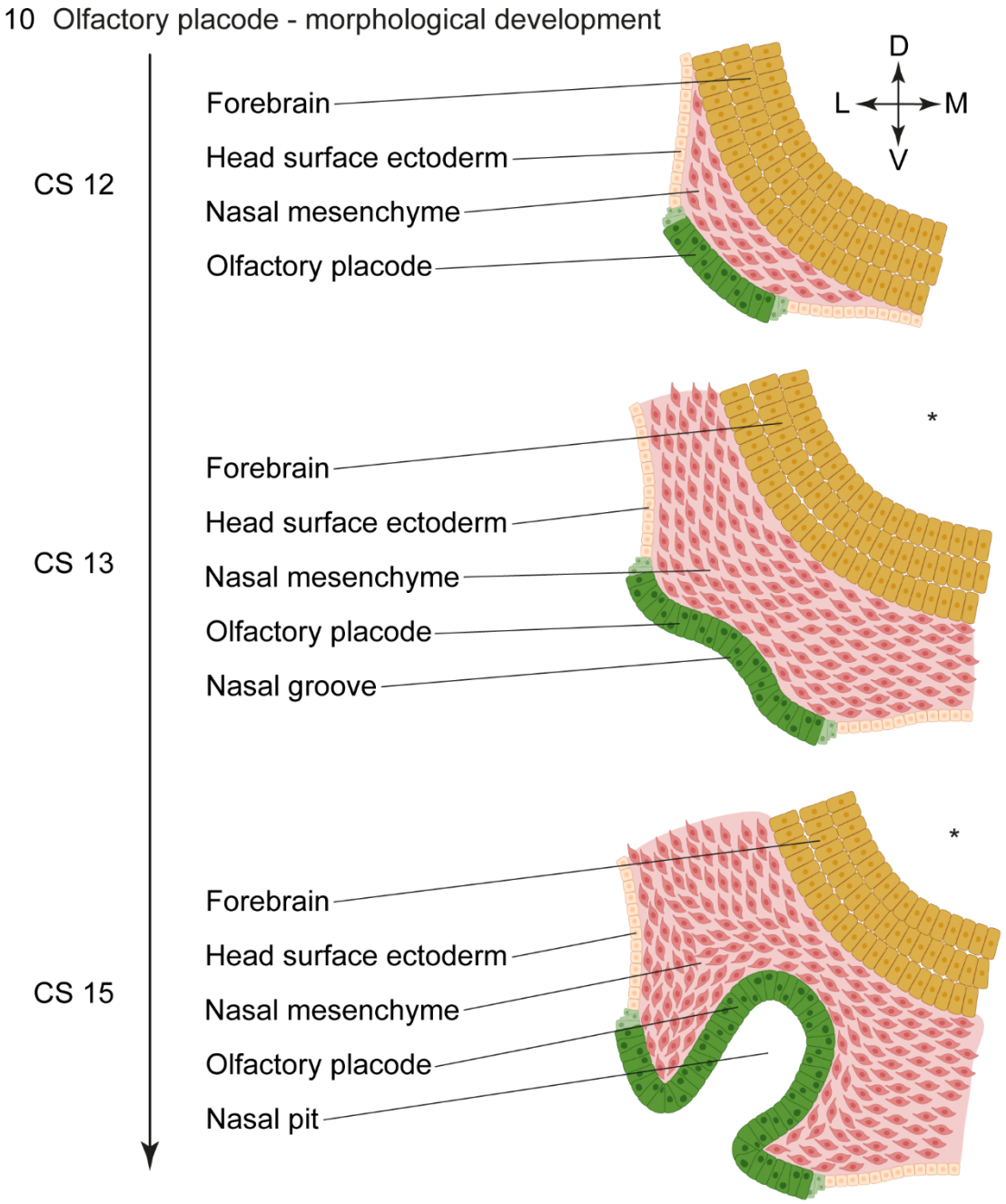

Figure 10: Morphological development of the olfactory placode

Schematic drawing of a cross section view of an embryo head from CS 12 to CS 15 showing invagination of OP into a growing head mesenchyme directly adjacent to the developing forebrain. Timeline annotated in CS from top to bottom. Forebrain (yellow, columnar / stratified), head mesenchyme (red), OP / nasal groove / nasal pit (green), head NNE (yellow, simple cuboidal). Ventricle of forebrain annotated withs asterisk. Dorsal (D), ventral (V), lateral (L), medial (M). Figure created with BioRender.com.

3.5 Development of the central nervous system

The evolutionary success of the large-brained mammals like humans is unprecedented. The brain with its computational power and reason has given humans the ability to conquer and change the world like no other animal has before – for better or worse. The OE and the brain are not only in close proximity, but also directly influence each other's development, rendering them closely interconnected (65).

The CNS, comprised of the brain rostrally and the spinal cord posterior, develops from the NT. As the NT starts to fuse in the 4th week *pc* and the early brain is divided into the three primary vesicles, the *prosencephalon* (forebrain), the *mesencephalon* (midbrain), and the *rhombencephalon* (hindbrain) (66). In the 5th week *pc*, as the brain anlage further grows, the three primary vesicles mature to form the five secondary vesicles. These include the (I) *telencephalon* and (II) *diencephalon* from the *prosencephalon*, the (III) *mesencephalon*, as well as the (IV) *metencephalon* and (V) *myelencephalon* from the *rhombencephalon* (66).

The NT and the brain vesicles are patterned by the *chorda dorsalis* into a thin floor plate ventrally and roof plate dorsally (66). Between these D-V poles, the bilateral basal plates and alar plates develop ventrally and dorsally, respectively (66). Later, the basal plate gives rise to somatomotoric neurons, the alar plate produces the somatosensory neurons, whilst the visceromotoric and -sensory neurons are derived in between (66). As this is the case in more "rudimentary" regions of the CNS like the spinal cord, the neurons of the *telencephalon* and *diencephalon* derive solely from the alar plate (66).

From the progenitor cells in the neural tube all major CNS cell lineages, namely neurons, astrocytes and oligodendrocytes develop (66). Endothelial cells, microglia and the meninges (except the *leptomeninx*) are not of ectodermal, but of mesodermal descent (66).

As the neural tube in the prospective forebrain area thickens during development due to neurogenesis, a characteristic layered structure emerges. Faced towards the lumen of the neural tube lies the ventricular zone (VZ), which is home to the progenitor stem cells, the radial glia (RG) (67). The RG also form the inner and

outer limiting glial membrane and guide migrating cells (66). Outside of the VZ lies the sub-ventricular zone (SVZ), which is (only in humans) divided by an inner fiber layer into the outer and inner sub-ventricular zone (OSVZ & ISVZ) (68). Outside of the SVZ first lie the intermediate zone (IZ), subplate zone (SPZ) and the cranial plate (CPZ), followed by the outermost marginal zone (MZ) (66).

Mitotic cell divisions of the RG in the VZ – the earliest zone of the NT – give rise to the cells making up the outer regions (66). Through asymmetrical cell division, they generate neurons, which migrate ventriculofugally into the IZ and CP (66). Neurons migrating to the CPZ do so in an outside-in fashion, with the later born neurons on the outside (69). The RG also give rise to intermediate progenitors (IP), another neural stem cell population, inhabiting the whole SVZ (66). Another human specific stem cell population inhabit the OSVZ, called outer radial glia (oRG) (70,71).

The MZ later give rise to layer I of the neocortex, whilst the SPZ and CPZ give rise to layers II-VI (66). This complex makeup of the brain vesicles with its human specific features allowed for the rapid expansion in brain size and neuronal output (69,72).

Before the closure of the NT, the forebrain divides into the anterior *telencephalon* ($FOXG1^+$) and the more posterior *diencephalon* ($OTX2^+$) (73,74). As the *telencephalon* enlarges to the anterior, two diverticula are formed from its lateral alar plates, quickly growing in size (66). These two diverticula give rise to the hemispheres and their NT-lumen become the 1^{st} & 2^{nd} ventricles (66). Through rapid expansion and a characteristic counterclockwise rotation of the newly formed hemispheres, the telencephalon acquires its characteristic shape. The dorsal *telencephalon* (pallium, future neocortex) expresses PAX6 and EMX2, whilst it expresses NKX2.1 and GSH2 in its ventral sub-pallium (75). This ventral sub-pallium gives rise to the basal ganglia, incorporating the lateral ($GSH2^+/FOXG1^+$) and medial ($NKX2.1^+/FOXG1^+$) ganglionic eminence (LGE & MGE), important sources of telencephalic neurons and interneurons (66,76–78). Both the MGE and especially the LGE have close ties to the OB and olfactory system (66,79).

11 Forebrain regions

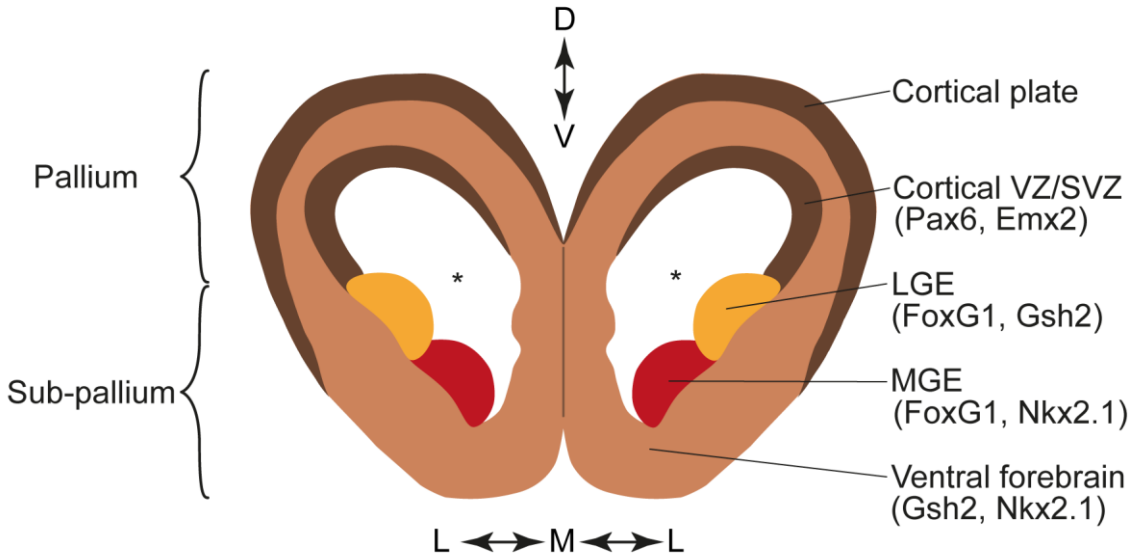

Figure 11: Regions of the forebrain

Schematic drawing of a coronary section of an embryonic forebrain during gestational week 18-20. Pallium containing the CPZ and cortical VZ/SVZ dorsally (brown), subpallium containing the ventral forebrain (light brown), as well as the MGE (red) and LGE (yellow) ventrally. Developing brain ventricles marked by asterisks. Dorsal (D), ventral (V), medial (M), lateral (L). Adapted after (75).

The primary olfactory lobe is formed by the antero-medial and ventral floor of the hemispheres, whilst the remaining floor gives rise to the striatum and the amygdaloid complex (66). The rest of the hemispheres (media, lateral, dorsal and caudal regions) form the majority of the *telencephalon* with its gyrated cortex and white matter (66). Here, the OB is an extension of the medial pallium (80).

3.6 Signaling pathways in the craniofacial development

The development of the OE as well as the CNS relies on the spatial and temporal interaction of a multiple signaling pathways, modulated by a multitude of tissues (61,81). Here, the BMP, WNT, FGF, TGFβ pathways orchestrate the developmental processes (**Fig.12**). The development of the NP in the primitive ectoderm relies on the inhibition of WNT and BMP signaling, as well as the activation of FGF signaling in the midline (45). Pluripotent stem cells (PSC) can also be differentiated towards neural fates using these principles. The dual SMAD inhibition (dSMADi) method uses recombinant Noggin (a BMP antagonist) and the small molecule SB431542 (a TGFβ antagonist) to induce anterior CNS precursors (82).

Likewise, TGFβ and WNT antagonism have been used to create telencephalic precursors from PSC (83).

Initially these CNS precursors adopt the fate of the anterior CNS (forebrain) (84), but can later be posteriorized under the influence of dorsalizing agents such as WNT (38) and retinoic acid (85). Likewise, anterior CNS fates are promoted by the inhibition of WNT (38) and activation of FGF8 (86,87). In the developing forebrain, Sonic Hedgehog (SHH) is a well-known ventralizing agent (88). In accordance, SHH signaling has been used to induce ventral forebrain in brain organoids (76) and hypothalamic like tissues in pituitary organoids (89).

In the specification of the NB between the NP and the NNE and its breakdown into NC and PPR, these signaling pathways are also involved (45). As mentioned earlier, the NP relies on WNT and BMP inhibition and FGF activation. In contrast to that, the induction of NNE relies on WNT and BMP signals (90) and epidermal fate can be blocked by FGF signaling (46). The NB lies between these two zones and it is generally accepted, that an initial BMP exposure is needed for NB specification (91). For the breakdown of the NB, the PPR later is promoted by low BMP signaling (91) and blocked by WNT signaling (81). The NC on the other hand is promoted by intermediate levels of BMP as well as WNT signaling originating from the neural fold (92). Due high expression of WNT antagonists in the anterior *telencephalon*, the anterior NB only gives rise to PPR and not NC, which is reliant on WNT signaling (38,45,93). This has been recapitulated in PSC derived tissues, where an initial exposure to BMP followed by low BMP, low WNT and high FGF levels where necessary to promote PPR and CP fate (94,95).

The specific role of FGF signaling in PPR induction is debated, since contradicting results in different model organisms suggest cross species variability (45). Nevertheless, FGFs play an important part in the induction of the PPR, with the head mesoderm as their secretion source (81). TGFβ inhibition using SB431542 was able to produce NNE *in vitro* (96).

12 Signaling pathways in placode development

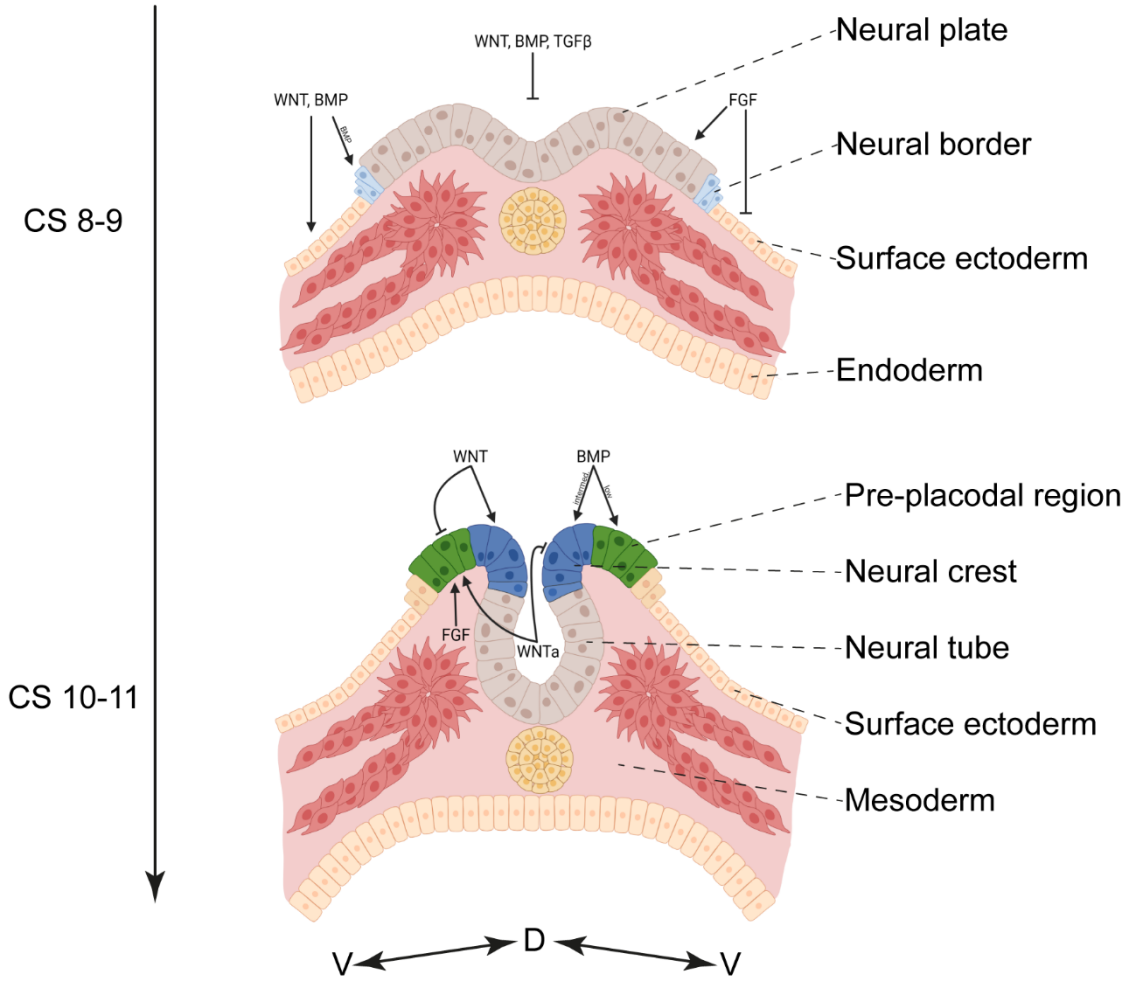

Figure 12: Signaling pathways in placode development

Schematic drawing of a cross section view of an embryo undergoing neurulation starting in the 4th week *pc*. Influence of key signaling pathways on tissue differentiation annotated with arrows (activation) and blunt arrows (inhibition). Timeline annotated in CS from top to bottom. Section plane annotated in **(Fig. 5)**. WNT-antagonists (WNTa), NP / NT (brown), NB (light blue), NNE (yellow, cuboid), chorda dorsalis (yellow, cell strand), mesoderm (red), endoderm (yellow, columnar), NC (dark blue), PPR (green). Dorsal (D), ventral (V). Figure created with BioRender.com.

During the breakdown of the PPR into different placodal fields and CP, patterning factors along the A-P axis are important. The anterior placodal region seems to be the default state, giving rise to the lens placode if not subject to morphogens (47). WNT signaling is a strong caudalizing factor, as WNT activation is necessary for the posterior otic placodes to develop (97) and WNT inhibition also blocks the formation of trigeminal placodes (98). Likewise, retinoic acid is a potent posteriorizing factor, not only in the CNS but also in PPR breakdown (99). In the

anterior placodal field, Fgf8 plays a pivotal role inducing olfactory and suppressing lens fate (47), whilst prolonged BMP signaling enhances the lens placode (45,92). Different spatiotemporal FGF signals are important for the formation of all CP from the PPR primordium (45). The casualizing effects of WNT in a permissive FGF environment and low BMP conditions have previously been recapitulated in the development of otic organoids (96). Likewise, the anteriorizing effect of WNT inhibition in PSC derived CP has been shown by the expansion of $PAX6^+$ anterior placodal cells at the expense of $PAX3^+$ intermediate placodal cells (94). This study also showed the importance of FGF signaling to induce CP in PSC derived differentiations (94).

SHH is a potent factor promoting the anterior pituitary placode formation in the oral ectoderm (100). Here, SHH signaling blocks lens / olfactory and promotes pituitary fate (101). In a PSC based organoid model, the induction of the anterior pituitary placode by SHH agonist SAG has been described (89).

As these signaling pathways have been shown to be important in CP formation, their careful modulation in a morphogen based, 3D organoid differentiation protocol is an important part of this thesis. Furthermore, the interaction of multiple tissues within one PSC derived organoid is pivotal, also relying on these pathways. At the basis of this morphogen and interaction-based differentiation protocol are human PSC which are a key technology for this thesis.

3.7 Human induced pluripotent stem cells

The isolation of PSC from the inner blastocyst cell mass and their cultivation can be regarded as a milestone in the field of developmental biology (102,103). These cells can self-renew indefinitely and have the ability to differentiate into cells of all three germ layers (ecto-, meso- and endoderm) (104). They can subsequently give rise to any somatic tissue, granting them unprecedented potential for the use in regenerative- and personalized medicine (104). PSC can be utilized for developmental studies, disease modeling, drug testing and toxicity screens, as for the development of cell (replacement) therapies (105).

Their pluripotency is characterized by (I) the ability to form teratoma in SCID mice (106), (II) the ability to form whole chimeras when injected into a donor pre-

implantation blastocyst (104), (III) the ability to form embryoid bodies (EB), which give rise to cells of all three germ layers *in vitro* (107), and (IV) the expression of pluripotency markers (OCT3/4, SOX2, NANOG, SSEA3, SSEA4, TRA-1-60, TRA-1-81 and TRA-2-49/6E [alkaline phosphatase]) (104,108).

The first PSC to be isolated and maintained in culture were murine embryonic stem cells (mESC) (102,103). Human embryonic stem cells (hESC) were only isolated and cultured much later (109). Whilst human and murine ESC both show pluripotency, their maintenance and pathway dependence of the self-renewing state differs. Murine ESC are dependent on Lif and the Stat3 pathway, whilst human ESC rely on FGF2 and TGFb/Activin/Nodal signaling (110,111).

HESC share great similarities with murine epiblast stem cells (mEpiSC) which have – in contrast to mESC – (I) undergone X-chromosome inactivation (XaXi) (112), (II) easily differentiate into primordial germ cells (PGC) (113), (III) have an impaired ability to form chimeras (114), (IV) are sensitive to single cell passaging (114), (V) show a flat morphology in 2D cell culture (114), and have (VI) significant epigenetic and gene expression differences to mESC (115). For mEpiSC and mESC the terms primed and naïve pluripotency were coined, respectively (116). This nomenclature can be accepted for humans, where hESC most confidently represent a state of primed pluripotency, but can be reprogrammed into and maintained in a naïve state (117) .

Other than the isolation of ESC from preimplantation blastocysts, other methods for the generation of PSC have been described (104). A method called somatic cell nuclear transfer (SCNT) transfers the nucleus of a somatic cell into an enucleated oocyte, creating NT-ESC (nuclear transfer embryonic stem cells) (118,119). This method was used to create the first cloned mammal “Dolly”, a sheep, in 1996 (120). Furthermore, PSC can be generated by fusing somatic cells with ESC, creating pluripotent, tetraploid hybrids (121,122).

The next big leap came in 2006 when Yamanaka was able to show the stable reprogramming of somatic cells into PSC, termed “induced pluripotent stem cells” (iPSC) (123). Here, the authors showed that through the retroviral transduction of the transcription factors *Otc3/4*, *Sox2*, *c-Myc* and *Klf4* into adult murine

fibroblasts, pluripotent stem cells could be induced (123). Later, they were able to reprogram adult human fibroblasts into human induced pluripotent stem cells (hiPSC) by retroviral transduction of the same factors (108). HiPSC and miPSC share key features as pluripotency with their respective ESC counterparts but differ to some extent in their gene expression profile, when compared with ESC (108,123).

(H)IPSC hold two main advantages over (h)ESC: Since hESC can only be isolated by the destruction of a pre-implantation blastocyst, ethical concerns have been raised and the use of hESC is tightly controlled (124). The reprogramming of adult somatic cells to hiPSC circumvents this problem and therefore diminishes ethical concerns (108,125).

Secondly, patient-specific hiPSC lines can be generated, which allows the study of defined genetic conditions, drug-screening and possibly the development of targeted genetic therapies without immunogenic risks (104,126,127).

Furthermore, (h)iPSC based drug- and toxicity screening can be utilized to reduce animal testing according to the 3R-principle (reduce, replace, refine) (128).

Since 2007 the variety of techniques used for reprogramming increased dramatically (125). Next to the original method by Yamanaka using a lentivirus for retroviral transduction (108), other methods like Sendai virus as a non-integrating virus (129), modified mRNA (130), episomal reprogramming (131), excisable non-viral vector plasmids (132), expression plasmids (133), small molecule assisted reprogramming (134,135) and dCas9 based CRISPRa (136) have been implemented for the generation of hiPSC.

Many different sources for adult somatic cells used for generating hiPSC have been described (125). Dermal fibroblasts acquired by punch biopsies are a widely used cell type. This is because they have been used in the earliest reprogramming protocol and show an easy handling (108,125). Nevertheless, alternatives have emerged with the most broadly used being: (I) blood cells (137), (II) exfoliated cells of the renal-urinary tract (138), and (III) keratinocytes from plucked hair (139). Especially the latter are very intriguing, since they can be acquired non-

invasive by non-medical personnel and plucked hair can be stored and shipped with ease (125).

As a developmental study, this thesis builds upon the use of hiPSC and their directed differentiation. The cell line used – generated through episomal reprogramming – was commercially acquired.

3.8 2D vs. 3D – the rise of organoids

HPSC are a truly versatile tool for developmental studies as well as disease modeling due to their potential to differentiate into a broad range of cells *in vitro*. Shortly after the isolation of hESC, protocols were established to obtain cells of a certain lineage (126). In these directed differentiations, the differentiation of hPSC towards desired cell types *in vitro* is controlled via extrinsic and temporal patterning, mimicking the situation *in vivo* (140). Pattering is achieved by the application of morphogens – biological agents that spatially organize surrounding cells via gradients – and / or small molecules (140,141). Small molecules are of synthetic origin and modulate signaling pathways predictable as well as more potent and cost effective than recombinant morphogens (140,142).

Early on, (I) neural lineages (143,144), (II) hematopoietic cells (145), (III) cardiomyocytes (146) and many more were derived from hESC using these techniques.

Patient derived hiPSC make it possible not only to create lines of specific fates, but also to study the pathophysiology of certain monogenic or sporadic diseases like PD, among others (147,148).

Traditionally, cell culture studies were reliant on 2D and single / oligo cell type protocols, but have limitations for modeling development and studying disease mechanisms (148,149). *In vivo*, cells reside in complex tissue and organ structures within a pluralistic extracellular environment, reliant on dynamic and reciprocal interaction (148). However, in a classical monolayer cell culture, this complex environment, extracellular matrix (ECM) and cell contacts with a high order of organization are absent (148). These unphysiological conditions impose limits on disease modeling capacity (148), maturation ability (150) and lead to an

aberrant cell morphology (148). These limitations can – at least partly – be overcome using 3D cell cultures.

The first method for 3D culture were the so called EB (107). PSC can aggregate into these 3D structures which recapitulate some developmental aspects of early pre-implantation blastocysts (107). EB show the ability to self-organize and exhibit axis formation, reminiscent of the developing embryo (151,152). EB – just like teratoma – give rise to many organized tissues and can be subject to directed differentiation (107). In many adherent protocols an initial EB step is used to create cells of certain lineages (144,153).

A further methodological evolution of EB are the so called “organoids” (149). Organoids – 3D cell aggregates which resemble the structure and function of an organ or tissue *in vitro* – can be generated using 3D cell culture systems (149).

There are several necessities for the correct definition of an organoid: (I) several organ specific cell types, (II) organ specific functional aspect, (III) cells grouped and organized similar to resembling organ, (IV) development mirrors *in vivo* situation (149). Lancaster and colleagues therefore proposed the following definition:

> “A collection of organ-specific cell types that develops from stem cells or organ progenitors and self-organizes through cell sorting and spatially restricted lineage commitment in a manner similar to *in vivo*” (149).

Organoid models often induce multiple tissues within one aggregate, enabling development and further maturation (96). This co-induction of different lineages facilitates tissue-crosstalk, similar to the situation *in vivo* and hence allows proper tissue formation mirroring the embryological situation (89,96,154).

Organoid technology often makes use of ECM components obtained from the Engelbreth-Holm-Swarm tumor line (155) made commercially available as Matrigel®, which creates a complex environment supportive of organoid formation and maturation (72). Likewise, a high order of organization is obtained (72).

Organoids as model systems have several limitations, most important being a high variability, paired with low controllability, slow production time and limited efficiency (148,149,154).

Nevertheless, their outweighing benefits render them important tools in molecular and cell biology, which led to the creation of numerous human organoid models for: Skin (156), inner ear (96), brain / brain regions (72,157,158), pituitary (89), retina (159), mammary gland (160), bone (161), cardiac muscle (162), skeletal muscle (163), kidney (164), intestine (165), liver (166), lung (167), stomach (168), pancreas (169), blood vessels (170), prostate (171) and endometrium (172).

3.8.1 Brain organoids

Brain organoids are of special interest to gain a better understanding of the development and functional impairments of the CNS (157). The limited excess to fetal brain tissue as well as the lack of good model organisms led to the development of 3D neuronal protocols (149). Mice are limited in their capacity to model human brain development since they and humans diverged ~ 70-80 million years ago and hence show substantial interspecies differences (148). Human cortex development shows a differing cytoarchitecture with unique cell types and more pallial thickness than found in the murine system (72,158). The group of Yoshiki Sasai was able to show the differentiation of murine and human ES into telencephalic precursors using a defined, partly 3D culture system termed SFEB (serum-free, floating culture of embryoid body–like aggregates) which recapitulated key aspects of developmental patterning (83,173). The group later refined their method, now termed SFEBq (SFEB, quick aggregation) and turned to a fully 3D approach, yielding polarized neuroepithelium expressing telencephalic markers and showing characteristics of early brain development (80). This led to the creation of a self-organizing, polarized neuroepithelia from hESC in suspension culture, showing human specific cell types like oRG and distinct inside-out layering, resembling the fetal development (158). Lancaster and colleagues showed in 2013 the generation of 3D, self-organizing “brain-organoids” from hPSC by embedding EB derived neuroectoderm in Matrigel® as an extracellular scaffold (72). This approach – which unlike SFEBq does not rely on extrinsic patterning – yields tissues of multiple brain regions within one organoid, as well as human specific organization and cell-types like oRG (72). Pasca et al. later created reproducible, 3D human cortical spheroids (hCS) from hPSC, using dSMADi as extrinsic patterning, without Matrigel® embedding, which showed improved maturation and

also generation of glial cell types (82,157). These hCS could be patterned externally to generate brain region specific tissues (75,157). The group of Lorenz Studer later showed in an elegant study that an axis could be generated within forebrain organoids using an inducible SHH system, in which some cells of the organoid can be prompted to secrete SHH, leading to a D-V axis formation (76).

Brain organoids, although showing huge potential due to their self-organization as well as resemblance of complex cytoarchitecture, developmental process and disease modeling capabilities, have limitations due to their limited reproducibility and difficult region patterning (80,149).

3.8.2 Organoids in PPR-derived tissues

Insights into the development of the PPR and its placodal derivatives are – due to their transient occurrence in ontogenesis – mostly limited to animal models like mice, chick, and zebrafish (9). Previous efforts to induce PPR and CP-like cells from hPSC in a 2D culture were focused on elucidating molecular mechanisms of cell specification and cellular properties (94,95). Since these protocols yield rather homogeneous cell populations and hence lack tissue-crosstalk important for placodal induction, they are limited in their potential to generate mature placodal derivatives (61,94). Through 3D cell culture systems these limitations can be overcome, and more mature cell lineages can be obtained, similar to the situation in brain organoids (72,96).

Adapting the SFEB(q) culture method, organoids of the anterior pituitary (89,154,174) and inner-ear (96,175) were generated. Both groups first established a mPSC model (174,175), followed by hESC (89,96) and later hiPSC (96,154) models. For both structures significant differences between the mESC and hESC culture had to be made, highlighting inter-species variation (89,96). Likewise, compared to hESC, hiPSC needed adaptation in some aspects of directed differentiation (96,154).

The 3D approach utilized the co-induction of different tissues, enabling tissue cross-talk and improved maturation, recapitulating key steps of murine and human development (89,96,174,175).

For the anterior pituitary, an oral-head-like ectoderm (PITX1^{+}/pan-Cytokeratin^{+}) was induced around a hypothalamic-like core (NKX2.1^{+}/RX^{+}), resulting in the invagination of structures similar to the Rathke-pouch in vertebrate development (61,89,174) These pituitary organoids rescued hypopituitary mice upon transplantation, proving their functionality (174).

In inner-ear organoids, NNE – yielding epidermis and PPR – is co-induced with a NC-derived head-like mesenchyme, enabling the important mesenchymal cross-talk, similar to the *in vivo* situation (61,175).

Although these organoids show great promise for regenerative medicine and developmental biology, they share the limitations of other organoid model systems – especially brain organoids – being low efficiency and high batch-to-batch variability (149,154).

3.9 Aim of the thesis

The study of the development of the human olfactory system has long been neglected due to a lack of broad interest and difficult access to the early development in humans. Since the ORN of the OE are capable of lifelong neurogenesis from stem cells, insight on the olfactory development will enable research on adult neurogenesis and neuroregeneration. A 3D organoid model system of the OP and OE would pose as a powerful tool in neuroscience for the study of neurodegeneration and neuro-pharmacological delivery methods. The aim of this thesis was to establish and analyze a hiPSC based 3D organoid protocol modeling the early human development towards the OP. To verify their olfactory identity and gain first insight on the human olfactory development, the organoids (DOPEoids) were characterized on a morphological and protein level, establishing a timeline from day 4 to day 31. Key features found in the DOPEoids were further examined and four distinct compartments – a surface ectoderm, olfactory placodal patches, a head mesenchyme and neural tubuli – were validated and characterized. The DOPEoids were then analyzed on an RNA level to verify the protein data and analyze the expression and timeline of more key markers in early head development. Finally, the differentiation protocol was modified to promote further maturation and preliminary analyzed on a protein and morphological level. In summary, this thesis establishes a complex, multi-tissue organoid of olfactory fate, recapitulating key features of olfactory development *in vitro* and poses a major milestone in the development of a fully functional 3D olfactory model *in vitro*.

4 Material

4.1 Cell lines

Table 1: Cell line used for differentiation

Cell line	Origin	Company	Order No.
Gibco™ episomal hiPSC line	Cord blood-derived $CD34^+$ progenitors	Thermo Fisher Scientific, Waltham, MA, USA	A18945

4.2 Media

4.2.1 Basal media

Table 2: List of basal media used

Media	Company	Order No.
DMEM/F12 + GlutaMAX™	Thermo Fisher Scientific, Waltham, MA, USA	31331-028
Essential 8™ Basal Medium	Thermo Fisher Scientific, Waltham, MA, USA	A15169-01
F12 Nutrient Mix + GlutaMAX™	Thermo Fisher Scientific, Waltham, MA, USA	31765-035
IMDM + GlutaMAX™	Thermo Fisher Scientific, Waltham, MA, USA	31980-022
KnockOut™ DMEM	Thermo Fisher Scientific, Waltham, MA, USA	10829-018
Neurobasal™ Medium	Thermo Fisher Scientific, Waltham, MA, USA	21103-049

4.2.2 Media supplements

Table 3: List of media supplements used

Supplement	Company	Order No.
(±) Blebbistatin	SantaCruz Biotechnology, Dallas, TX, USA	sc-203532B
1-Thioglycerol	Sigma Aldrich, St. Louis, MO, USA	M6145-25ML
Anti-Anti (100X)	Thermo Fisher Scientific, Waltham, MA, USA	15240-062
B-27® Supplement without Vitamin A	Thermo Fisher Scientific, Waltham, MA, USA	12587-010
Bovine Serum Albumin (BSA) 25%	Thermo Fisher Scientific, Waltham, MA, USA	A10008-01
CD Lipid Concentrate (CDL)	Thermo Fisher Scientific, Waltham, MA, USA	11905-031
Dibutyryl-cAMP	Enzo Life Sciences, Framingdale, NY, USA	NC1539057
Essential 8™ Supplement (50x)	Thermo Fisher Scientific, Waltham, MA, USA	A15171-01
GlutaMAX™ (100X)	Thermo Fisher Scientific, Waltham, MA, USA	35050-038
Human FGF-basic (FGF2)	PeproTech, Hamburg, Germany	100-18B-1MG
Human GDNF (GDNF)	PeproTech, Hamburg, Germany	450-10-250UG
Human/Murine FGF-8b (FGF8)	PeproTech, Hamburg, Germany	100-25-500UG
Human/Murine/Rat BDNF (BDNF)	PeproTech, Hamburg, Germany	450-02-500UG
IWP-2	Selleckchem, München, Germany	S7085
IWR1e	Selleckchem, München, Germany	S7086

KnockOut™ SR (KOSR)	Thermo Fisher Scientific, Waltham, MA, USA	10828-028
L(+)-Ascorbic acid (Vitamin C)	Carl Roth, Karlsruhe, Germany	3525.1
LDN193189 hydrochloride (LDN)	Sigma Aldrich, St. Louis, MO, USA	SML0559-5MG
MEM NEAA (100X)	Thermo Fisher Scientific, Waltham, MA, USA	11140-050
N-2 Supplement	Thermo Fisher Scientific, Waltham, MA, USA	17502-048
Phenanthroline	Sigma Aldrich, St. Louis, MO, USA	131377
Recombinant Human BMP-4 (BMP4)	PeproTech, Hamburg, Germany	120-05ET
RevitaCell™ Supplement	Thermo Fisher Scientific, Waltham, MA, USA	A26445-01
SB431542	Selleckchem, München, Germany	S1067
Y-27632	Selleckchem, München, Germany	S1049

4.2.3 Starting media for differentiations

Table 4: Growth-factor free chemically defined medium (gfCDM) composition

	Basal media	**Supplement**	**Concentration**
gfCDM	50 % IMDM + GlutaMAX™	CDL	1 %
		BSA	0.5 %
	50 % F12 Nutrient Mix + GlutaMAX™	KOSR	5 %
		1-Thioglycerol	450 µM

As described previously in (89).

Table 5: DOPEoid maturation medium (DMM) composition

	Basal media	Supplement	Concentration
DMM	50 % DMEM/F12 + GlutaMAX™	N2	0.5 %
		B-27 w/o Vit.A	0.5 %
		GlutaMAX™	0.5 %
	50 % Neurobasal™ Medium	NEAA	0.5 %
		CDL	1 %
		KOSR	5 %
		1-Thioglycerol	450 µM

4.2.4 Differentiation media

Table 6: List of differentiation media used for the differentiation protocols

Name	Starting medium	Supplement	Concentration
d0	gfCDM	Y-27632	10 µM
		(±) Blebbistatin	10 µM
		SB431542	10 µM
		IWP-2	2 µM

Name	Starting medium	Supplement	Concentration
d3	gfCDM	BMP4	65 ng/ml
		Phenanthroline	10 µM
		SB431542	10 µM
		IWP-2	2 µM

Name	Starting medium	Supplement	Concentration
d5/6	gfCDM	LDN	100 nM
		SB431542	10 µM
		IWP-2	2 µM

Name	Starting medium	Supplement	Concentration
d9+	gfCDM	FGF2	20 ng/ml
		FGF8	100 ng/ml
		SB431542	10 µM

Name	Starting medium	Supplement	Concentration
d27+	gfCDM	GDNF	10 ng/ml
		BDNF	10 ng/ml
		Vitamin C	50 µg/ml
		cAMP	500 nM

Name	Starting medium	Supplement	Concentration
DMM d21+	DMM	FGF2	20 ng/ml
		FGF8	100 ng/ml
		SB431542	10 µM

Name	Starting medium	Supplement	Concentration
DMM d27+	DMM	FGF2	20 ng/ml
		GDNF	20 ng/ml
		BDNF	20 ng/ml
	(From day 30)	(Anti-Anti)	(1 %)

4.3 Chemicals, enzymes, and additives

Table 7: List of chemicals, enzymes & additives used

Product	Company	Order No.
Ampuwa	Fresenius, Bad Homburg, Germany	B102409 Rev.00
Aquaguard-2	Sartorius, Göttingen, Germany	01-916-1E
DAPI	Sigma Aldrich, St. Louis, MO, USA	D9542
DMSO	AppliChem, Darmstadt, Germany	a3672,0250
DPBS, without Ca^{2+}, without Mg^{2+}	Thermo Fisher Scientific, Waltham, MA, USA	14190-094
Ethanol 99 %, denatured	SAV-LP, Flintsbach am Inn, Germany	ETO-10000-99-1
GE 96.96 Dynamic Array™ Sample & Assay Loading Reagent	Fluidigm Corporation, South San Francisco, CA, USA	85000802-R
Matrigel® Matrix, hESC-qualified	Corning, Corning, NY, USA	534277
Moviol® 4-88 Histology grade	AppliChem, Darmstadt, Germany	A9011,0100
Normal donkey serum (NDS)	Sigma Aldrich, St. Louis, MO, USA	D9663
NutriFreez™ D10	Sartorius, Göttingen, Germany	05-713-1C
O.C.T.™ Compound	Sakura, Tokyo, Japan	SA62550
Paraformaldehyde Solution 4 % in PBS (PFA)	SantaCruz Biotechnology, Dallas, TX, USA	sc-281695
ProLong® Gold Antifade Mountant with DAPI	Thermo Fisher Scientific, Waltham, MA, USA	P36935
Skimmed milk powder	TSI, Zeven, Germany	4021155023078

StemPro® Accutase®	Thermo Fisher Scientific, Waltham, MA, USA	A11105-01
Sucrose	Sigma Aldrich, St. Louis, MO, USA	S-0389
Synth-a-Freeze®	Thermo Fisher Scientific, Waltham, MA, USA	A12542-01
TaqMan™ universal-mastermix for PCR, no AmpErase™ UNG	Thermo Fisher Scientific, Waltham, MA, USA	4324018
TE buffer, pH 7.0, RNase-free	Thermo Fisher Scientific, Waltham, MA, USA	AM9861
Triton™ X-100	Sigma Aldrich, St. Louis, MO, USA	T8787-50ML
Versene (1X)	Thermo Fisher Scientific, Waltham, MA, USA	15040-066
Water, demineralized, non-sterile	Carl Roth, Karlsruhe, Germany	3175.1

4.4 Buffer and solutions

Table 8: List of buffers & solutions used

Buffer	Ingredients
Sucrose solution	$PBS^{-/-}$
	Sucrose (30 %)
	Anti-Anti (1 %)
PFA w/ 10% sucrose	4 % PFA solution
	Sucrose (10 %)
Blocking solution	$PBS^{-/-}$
	BSA (1.25 %)
	NDS (10 %)
	Skimmed milk powder (4 %)
	Triton X-100 (0.1 %)

4.5 Kits and assays

Table 9: List of kits & assays used

Kit / Assay	Company	Order No.
Cells Direct One-Step qRT-PCR Kit	Thermo Fisher Scientific, Waltham, MA, USA	11753100
RNeasy Mini Kit	Qiagen, Hilden, Germany	74106

4.6 TaqMan™ probes

Table 10: List of TaqMan™ probes used

Gene name	Order No.
ASCL1	Hs04187546_g1
DACH1	Hs00974297_m1
DLX3	Hs00270938_m1
DLX5	Hs00193291_m1
EBF2	Hs00224081_m1
E-CADHERIN	Hs01023894_m1
EMX2	Hs00244574_m1
EYA1	Hs00166804_m1
EYA2	Hs00193347_m1
EYA4	Hs01012399_m1
FOXG1	Hs01850784_s1
GATA3	Hs00231122_m1
KRT5	Hs00361185_m1
LHX2	Hs00180351_m1
N-CADHERIN	Hs00983056_m1
OTX2	Hs00222238_m1
PAX2	Hs00240858_m1
PAX6	Hs00240871_m1
PAX8	Hs01015257_g1
RAX	Hs00429459_m1

SIX1	Hs01018030_m1
SOX2	Hs01053049_s1
SOX9	Hs01001343_g1
TFAP2A	Hs01029413_m1

4.7 Antibodies

4.7.1 Primary

Table 11: List of primary antibodies used

Antibody	Company	Dilution	Order No.
COLLAGEN IV	Sigma Aldrich, St. Louis, MO, USA	1:50	AB769
DLX3	SantaCruz Biotechnology, Dallas, TX, USA	1:50	sc-514094
EBF2	R&D Systems, Minneapolis, MN, USA	1:50	AF7006
E-CADHERIN	R&D Systems, Minneapolis, MN, USA	1:50	AF648
FOXG1	Abcam, Cambridge, UK	1:100	ab196868
GATA3	SantaCruz Biotechnology, Dallas, TX, USA	1:50	sc-268
KRT5	BioLegend, San Diego, CA, USA	1:100	905501
LAMININ	Sigma Aldrich, St. Louis, MO, USA	1:200	L8271
LHX2	Abcam, Cambridge, UK	1:500	ab184337
N-CADHERIN	BD Biosciences, Franklin Lakes, NJ	1:200	610920
OTX2	Neuromics, Edina, MN, USA	1:200	GT15095
PAX2	Thermo Fisher Scientific, Waltham, MA, USA	1:100	71-6000
PAX3	DSHB, Iowa City, IA, USA	1:19	DSHB AB_528426
PAX6	BioLegend, San Diego, CA, USA	1:100	901301
PAX8	Abcam, Cambridge, UK	1:100	ab97477

SIX1	CellSignaling, Danvers, MA, USA	1:100	12891S
SIX3	Novus, Centennial, CO, USA	1:100	NBP2-57249
SOX2	CellSignaling, Danvers, MA, USA	1:200	9656S
T	R&D Systems, Minneapolis, MN, USA	1:200	AF2085
TFAP2A	SantaCruz Biotechnology, Dallas, TX, USA	1:200	sc-12726
TUBB3	BioLegend, San Diego, CA, USA	1:1000	801202
VIMENTIN	Sigma Aldrich, St. Louis, MO, USA	1:100	MAB3400
ZO1	SantaCruz Biotechnology, Dallas, TX, USA	1:100	61-7300

4.7.2 Secondary

Table 12: List of secondary antibodies used

Antibody	Type	Dilution	Company / No.
Alexa Fluor™ 488	Donkey anti-mouse IgG	1:1000	Thermo Fisher Scientific, Waltham, MA, USA, A32766
Alexa Fluor™ 488	Donkey anti-rabbit IgG	1:1000	Thermo Fisher Scientific, Waltham, MA, USA, A32790
Alexa Fluor™ 546	Donkey anti-mouse IgG	1:1000	Thermo Fisher Scientific, Waltham, MA, USA, A10036
Alexa Fluor™ 546	Donkey anti-rabbit IgG	1:1000	Thermo Fisher Scientific, Waltham, MA, USA, A10040
Alexa Fluor™ 647	Donkey anti-sheep IgG	1:1000	Abcam, Cambridge, UK, ab150179

Alexa Fluor™ 647	Donkey anti-goat IgG	1:1000	Abcam, Cambridge, UK, ab150131

4.8 Consumables

Table 13: List of consumables used

Material	Company	Order No.
1.2 ml Cryogenic vials	Corning, Corning, NY, USA	430487
12-well plate, non-tissue culture treated	Corning, Corning, NY, USA	351143
50 ml syringe	Becton Dickinson, Franklin Lakes, NY, USA	300869
6-well plate, tissue culture treated	Corning, Corning, NY, USA	353046
96 well plate, V-bottom, suspension	Sarstedt, Nümbrecht, Deutschland	83.3926500
Autoclavable, disposure bags	NeoLab, Heidelberg, Germany	1-7105
Carbon steel sterile scalpel #23	Aesculap AG, Tuttlingen, Germany	BA223
Cell scraper	TPP, Trasadingen, Switzerland	99010
Clip Tip™ pipette-tips 1 - 10 µl	Thermo Fisher Scientific, Waltham, MA, USA	94410210
Clip Tip™ pipette-tips 10 - 100 µl	Thermo Fisher Scientific, Waltham, MA, USA	94410310
Clip Tip™ pipette-tips 100 - 1000 µl	Thermo Fisher Scientific, Waltham, MA, USA	94410710
Combitips® advanced 10 ml	Eppendorf SE, Hamburg, Germany	0030089820
Conical tube 15 ml	Sarstedt, Nümbrecht, Deutschland	62.554.502
Conical tube 50 ml	Sarstedt, Nümbrecht, Deutschland	62.547.004

Coverslips 24x50 mm, 0,13 - 0,16 mm	R. Langenbrinck, Emmendingen, Gernamy	01-2450/M
Dako Pen	Agilent Technologies, Santa Clara, CA, USA	S2002
EASYstrainer™, 40 µm	Greiner Bio-One, Frickenhausen, Germany	542040
Kimtech precision wipes	Kimberly-Clark, Surrey, UK	05511
Millex® -GP 0.22 µm sterile filter	Merck Millipore, Cork, Ireland	SLGP033RS
Peha-soft nitrile guard gloves	Paul Hartmann AG, Heidenheim, Germany	9422011
Petri dish 94x16, sterile	Greiner Bio-One, Frickenhausen, Germany	F211134Q
Pipette-tips 10 µl	Biozym, Hessich Oldendorf, Germany	720011
Pipette-tips 1000 µl	Greiner Bio-One, Frickenhausen, Germany	740290
Pipette-tips 200 µl	Sarstedt, Nümbrecht, Deutschland	70.760.002
SafeSeal reaction tube 0.5 ml	Sarstedt, Nümbrecht, Deutschland	72.704.700
SafeSeal reaction tube 1.5 ml	Sarstedt, Nümbrecht, Deutschland	72.706.700
Serological pipette 5 ml	Sarstedt, Nümbrecht, Deutschland	86.1253.001
Serological pipette 10 ml	Sarstedt, Nümbrecht, Deutschland	86.1254.001
Serological pipette 25 ml	Corning, Corning, NY, USA	357525
Serological pipette 50 ml	Corning, Corning, NY, USA	357550

SuperFrost® Plus Slides	R. Langenbrinck, Emmendingen, Gernamy	03-0060
Tissue-Tek® Cryom-old® 10x10x5mm	Sakura, Tokyo, Japan	4565
Tissue-Tek® Cryom-old® 15x15x5mm	Sakura, Tokyo, Japan	4566
Culture-Insert 4 well in µ-Dish 35 mm, high	Ibidi GmbH, Gräfelfing, Germany	80466

4.9 Laboratory equipment

Table 14: List of laboratory equipment used

Equipment	Company
96.96 Dynamic Array™ IFC	Fluidigm, South San Francisco, CA, USA
ApoTome	Zeiss, Oberkochen, Germany
Assistant ® Neubauer counting chamber	Glaswarenfabrik Karl Hecht, Sond-heim vor der Röhn, Germany
BioMark™ HD, Fluidigm	Fluidigm, South San Francisco, CA, USA
BioMark™ IFC controller HX/MX	Fluidigm, South San Francisco, CA, USA
Centrifuges (Heraeus™ Mega-fuge™ 16 Centrifuge, Heraeus™ Fresco 17 Centrifuge)	Thermo Fischer Scientific, Waltham, MA, USA
Cryostat Microm HM 560	Thermo Fischer Scientific, Waltham, MA, USA
Eppendorf Multipette Stream	
Evos FL	Thermo Fischer Scientific, Waltham, MA, USA
F1-ClipTipTM one channel pipette 1 – 10 µl	Thermo Fischer Scientific, Waltham, MA, USA

F1-ClipTipTM one channel pipette 10 – 100 µl	Thermo Fischer Scientific, Waltham, MA, USA
F1-ClipTipTM one channel pipette 100 – 1000 µl	Thermo Fischer Scientific, Waltham, MA, USA
Finnpipette® F2	Thermo Fischer Scientific, Waltham, MA, USA
Fluorescence microscope (Axio Imager M2)	Zeiss, Oberkochen, Germany
Freezer (-20°C)	Liebherr, Biberach, German
Freezer (-80°C)	Thermo Fischer Scientific, Waltham, MA, USA
Fridge (4°C)	Liebherr, Biberach, German
Ice machine, AF103	Scotsman, Great Blakenham, UK
Incubator 37 °C, Heracell™ 240i	Thermo Fischer Scientific, Waltham, MA, USA
InoLab® pH-meter	Xylem Analytics, Weilheim, Germany
Inversion microscope (Axioskop 2 mot plus, Primo Vert)	Zeiss, Oberkochen, Germany
Magnetic stirrer MR3001K	Heidolph, Schwabach, Germany
Mikrowave MW13145W	Amica, Wronic, Poland
Minicentrifuge Sprout	Biozym, Hessisch Oldendorf, Germany
Mr Frosty™ 1° freezing container	Thermo Fischer Scientific, Waltham, MA, USA
NanoPhotometer P330	Implen, München, Germany
NeoVortex D-6012	NeoLab, Heidelberg, Germany
Nitrogen Tank, CryoPlus™ 2	Thermo Fischer Scientific, Waltham, MA, USA
Pipettes, Eppendorf Research® Plus (10µl, 100 µl, 200µl, 1000 µl)	Eppendorf, Hamburg, Germany
Pipetus®	Hischmann, Eberstadt, Germany

Schott Duran® flasks (50 ml, 100 ml, 250 ml, 500 ml, 1000 ml)	Schott, Mainz, Germany
StepOnePlus real-time PCR systems	Thermo Fischer Scientific, Waltham, MA, USA
Stereomicroscope M3	Wild, Heerbrugg, Swizerland
Sterile bench, MSC-Advantage	Thermo Fischer Scientific, Waltham, MA, USA
Systemchannel 165/93 mm safety-hood	Wesemann, Syke, Germany
Thermomixer Pro	CellMedia, Zeitz, Germany
Vacuum pump, Integra Vacusafe	Integra Biosciences, Biebertal, Germany
Vortexer	Bender+ Hobein, Zürich, Switzerland
Water bath, Lab Line waterbath	Thermo Fischer Scientific, Waltham, MA, USA

4.10 Software

Table 15: List of software used

Software	Company	Use
Adobe Illustrator	Adobe Systems Software Ireland Limited, Dublin, Republic of Ireland	Figures
AxioVision	Carl Zeiss AG, Oberkochen, Germany	Microscopy
BioRender	BioRender, Toronto, Canada	Figures
Fluidigm	Fluidigm Corporation, South San Francisco, CA, USA	RT-qPCR
Microsoft Office	Microsoft Corporation, Redmond, WA, SA	Writing, Calculations
Zen	Carl Zeiss AG, Oberkochen, Germany	Microscopy

5 Methods

5.1 Ethics

All work conducted for this thesis was approved by the ethics committee of the medical faculty of the Eberhard Karls Universität Tübingen. The project numbers are 638/2013BO1 for work with hiPSC and 177/2019BO2 for work on the development of the human OE.

5.2 Cell culture

Cells are maintained in an aseptic environment in a 5 % CO_2, fully humidity-saturated incubator with 5 % O_2 (hiPSC, DOPEoids) or 20 % O_2 (DOPEoids) at 37 °C. The cell culture media is pre-warmed to 37 °C before any media changes. Cell culture is performed in a S2 safety-cabinet under aseptic conditions according to German BSL-2 regulations.

5.3 hiPSC culture

5.3.1 Culture & passage

The hiPSC are cultured as colony-based 2D monolayer on Matrigel® coated, tissue treated 6-well plates with 1.5-2 ml hPSC-medium per well with daily media changes. For the coating, 800 µl per well of cold hESC-qualified Matrigel® coating solution is pipetted into a pre-cooled 6-well plate and incubated for 2 hours at 37 °C. The Matrigel® is prepared according to the manufacturer's instructions: 200-300 µl (dependent on batch number) are diluted in 12,5 ml of ice-cold KO-DMEM to obtain Matrigel® coating solution and stored at 4 °C. Coated plates can be stored for up to one week at 4 °C. The hiPSC are maintained in E8 media according to the manufacturer's specifications under hypoxic conditions (5 % CO_2; 5 % O_2). Cells are passaged with a confluency of 70-80 %. Generally, a 6-well-well is splitted in a ratio of 1:6 but other ratios like 1:10, 1:5, 1:4 or 1:3 are sometimes necessary adapting to different cell numbers, attachment ratios, and growth rates.

Prior to passaging, differentiated cells are identified by morphology and are mechanically removed under aseptic conditions using an inversion microscope and a 1-10 or 10-100 µl pipette-tip. For passage, the media is removed, the well is

washed once with 1 ml $PBS^{-/-}$ and 1 ml of Versene is added. The cells are incubated for 6 min at RT until the Versene can be carefully removed and the well is washed once with $PBS^{-/-}$. Afterwards, cells are flushed off with 1 ml of E8 and a cell scraper can be used to lift any remaining cells. The cell suspension in E8 is collected in a 15 ml conical tube and the well washed once with E8. To create the volume of cell suspension to plate 1,5 ml per 6-well well, the necessary amount of E8 is added without breaking up the cell clusters. The cell suspension is plated on a Matrigel®-coated plate after the coating media has been thoroughly removed. The plate is then incubated for 24 h at 37 °C; 5 % CO_2; 5 % O_2 before the first media change.

5.3.2 Freezing iPSC

For cryo-conservation the same procedure is used but the cell suspension is centrifuged for 2 minutes at 423 g (1500 rpm) to pellet the cells. The supernatant is discarded, and the pellet resuspended in 800 µl Synth-a-Freez® or NutriFreez™ D10 without breaking up the clusters and immediately pipetted into a labeled cryotube. The cryotube is transferred into a MrFrosty® and stored at -80 °C for at least 80 min, before the tube can be stored in liquid nitrogen.

5.3.3 Thawing iPSC

To thaw iPSC the cryotube is incubated for 2 min at 37 °C in a water bath before the volume is carefully resuspended in 5 ml E8 and centrifuged for 2 min at 423 g (1500 rpm). The supernatant is discarded, and the pellet carefully resuspended in 1.5 or 3 ml E8 supplemented with RevitaCell™ (1:100), depending on confluency at freezing. The cells are then plated on 1 or 2 Matrigel®-coated 6-well wells.

5.4 DOPEoid differentiation

5.4.1 SFEBq – EB formation

For the DOPEoid differentiation hiPSC at 70-80 % confluency are used. The E8 media is changed and differentiated cells are identified by morphology and mechanically removed under aseptic conditions using an inversion microscope and a 1-10 or 10-100 µl pipette-tip. The cells are then washed with $PBS^{-/-}$ and 600 µl Accutase is added and incubated for 5 min at 37 °C. The reaction is stopped with 1 ml E8, the single cell suspension collected in a 50 ml conical tube and strained. The cells are then counted using a Neubauer counting chamber. Here, the average of four square counts and subsequently the number of cells per ml is calculated. Here, the following formulas are used:

$$\frac{cells\ in\ 4\ large\ squares\ (4 \times 4\ square)}{4} = \frac{cells}{large\ square}$$

$$\frac{cells}{large\ square} \times 10\ 000 = \frac{cells}{ml}$$

To produce standardized EB with 10 000 hiPSC each, the appropriate volume for 1 000 000 cells is transferred to a 15 ml conical tube and centrifuged for 2 min at 428 g (1500 rpm). The supernatant is discarded, and the pellet resuspended in 10 ml d0 media. 100 µl per well of d0 media with $100\ 000\ \frac{cells}{ml}$ are dispensed in a V-bottom shaped 96-well plate using a multi-pipette. The plate is then centrifuged for 5 min at 188 g (1000 rpm).

5.4.2 Differentiation

5.4.2.1 Classical protocol

Differentiation media is changed according to **Table 16**. Here, ~ 100 µl of media is removed without drying out the EB / organoids using an 8-channel pipette. Afterwards, 100 µl of the appropriate media is added and the cells are incubated at 37 °C; 5% CO_2; 5% O_2.

Day of differentiation	Media
0	d0
3	d3
5	d5/6
6	d5/6
9	d9+
12	d9+
15	d9+
18	d9+
21	d9+
24	d9+
27	d27+
30	d27+

Table 16: DOPEoids differentiation – classical protocol

5.4.2.2 Modified protocol

The modified protocol is an adaption of the classical protocol based on brain organoid and other PPR derived organoid technology to enhance maturation (72,96,154,157). The first 21 days of culture are identical to the classical protocol. On day 21, instead of a normal media change, the classical media is removed and 100 µl of DMM d21+ media is added to wells selected for DOPEoids. With a cut 1000 µl pipette-tip, 4-5 DOPEoids are then transferred to a 12-well well with 500 µl DMM d21+ media, resulting in a final volume of 900 – 1000 µl media per 12-well well. The DOPEoids are then cultured from day 21 onwards under normoxic conditions at 37 °C; 5% CO_2; 20% O_2. The media is changed according to **Table 17**. For the media change, the plate is tilted carefully, so that the DOPEoids sink to one side of the well. Then, ~ 500 µl of media (50 %) is removed and replaced with fresh media. On day 27, all of the media (100 %) is changed. From day 30 onwards, 1 % of Anti-Anti is added to prevent contamination. A comparison between the classical and the modified protocol is shown in **Figure 13**.

Day of differentiation	Media
0	d0
3	d3
5	d5/6
6	d5/6
9	d9+
12	d9+
15	d9+
18	d9+
21	DMM d21+ (50 %)
24	DMM d21+ (50 %)
27	DMM d27+ (100 %)
30	DMM d27+ (50 %)
33	DMM d27+ (50 %)
36	DMM d27+ (50 %)
39	DMM d27+ (50 %)

Table 17: DOPEoids differentiation – modified protocol

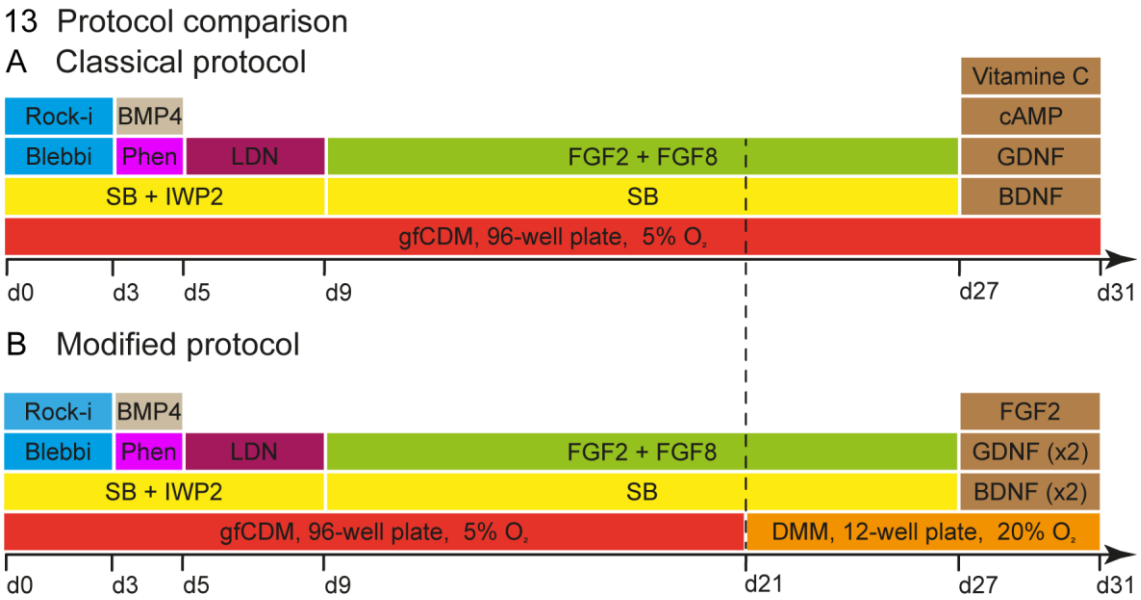

Figure 13: Comparison of classical vs. modified differentiation protocol

Annotated days mark start / end day (day 0 / day 31) of the differentiation and timepoints of changes in media composition. Horizontal bars represent different supplements, basal media and culture conditions, dashed line marks day 21 on which the modified protocol and the classical protocol start to be different. Extension of modified protocol beyond day 31 not shown. **(A)** Classical protocol **(B)** Modified protocol.

5.5 DOPEoid analysis – protein level

5.5.1 DOPEoid fixation

Usually, eight organoids are transferred to a 1.5 ml Epi using a 1000 µl pipette. The media is removed, and the organoids washed once with 500 µl of PBS $^{-/-}$. 500 µl of RT 4 % PFA with 10 % sucrose solution is added and incubated for 20 min at RT. The fixation solution is then removed, and the organoids washed once with 500 µl PBS$^{-/-}$ before 500 µl of 30 % sucrose in PBS$^{-/-}$, supplemented with 1 % Anti-Anti, is added. The tube is then carefully transferred to the fridge and stored for at least 24 h or until the organoids sink to the bottom.

5.5.2 DOPEoid embedding

Fixed organoids can be embedded in OCT embedding medium once they sink to the bottom of the Epi filled with 30 % Sucrose in PBS$^{-/-}$ with 1% Anti-Anti.

5.5.2.1 One-sample block

A 200 µl pipette with a cut tip is used to transfer organoids to a labeled 10x10x5 mm cryomold. Using a stereo microscope, excess medium is removed with an

uncut 200 µl pipette tip without damaging the organoids. Organoids are shifted into the middle of the cryomold with a straight dissecting needle without damaging the organoids. With a 10 µl pipette any excess medium is removed, so that the organoids are dry. OCT embedding medium is applied without air bubbles starting from the edges. If needed, organoids can be shifted into the middle / bottom most level of the cryomold using a straight dissecting needle. The cryomold is then carefully placed into a -80 °C freezing box until the OCT is frozen solid. The cryomold containing the organoids is then transferred to the -80 °C freezer and stored until cryosectioning.

5.5.2.2 Four-sample block

An Ibidi® culture-insert 4 well (Ibidi) is cut horizontally to a height of 4-5 mm. The Ibidi is pressed with its uncut side onto a superfrost slide to ensure a leakproof contact. Starting from the left, chamber # 1 at 9 o'clock is labeled with red and chamber # 4 at 6 o´clock is labeled with blue. A 200 µl pipette with a cut tip is used to transfer the first sample of organoids to chamber # 1. Using a stereo microscope, excess medium is removed with an uncut 200 µl pipette tip without damaging the organoids. Organoids are shifted into the middle of the Ibidi chamber with a straight dissecting needle without damaging die organoids. With a 10 µl pipette any excess medium is removed, so that the organoids are dry. One drop of OCT embedding medium is applied without air bubbles directly on top of the organoids. Likewise, chambers # 2 – 4 are filled. Once all chambers are filled, more OCT embedding medium is applied on top of the whole Ibidi to create a dome-like shape. The slide with the Ibidi is then carefully placed into a -80 °C freezing box until the OCT is frozen solid. A 15x15x5 mm cryomold is labeled, the upper left corner is marked with red, and the lower left corner is marked with blue. OCT embedding medium is applied to cover the base of the cryomold. As soon as the OCT embedding medium has solidified, the slide with the Ibidi is taken out of the freezing box and the Ibidi is carefully separated from the slide using the thin plastic of a cryomold. Afterwards, the Ibidi is removed with tweezers and the block is pressed into the prepared 15x15x5 mm cryomold with the organoids facing downwards, respecting the correct color-coded orientation. More OCT embedding medium is added to the cryomold which is then placed into a -80°C

freezing box until the OCT is frozen solid. The cryomold is then transferred to the -80 °C freezer and stored until cryosectioning.

5.5.3 DOPEoid cryosectioning

The cryomold with the sample(s) for cryosectioning is retrieved from -80 °C and placed in the cryostat. Before removing a four-sample block from the cryomold the position of the red sample is marked to ensure proper orientation. The block is then pressed out and molded with OCT embedding medium to the sectioning platform, with the red sample facing 12 o´clock when using a four-sample block. The sectioning platform with the block is then clamped into the object console with any edge parallel to the blade using a one-sample block or sample # 3 at 6 o´clock with all edges at 45° to the blade using a four-sample block. The console is then adjusted so that the whole block and the blade are in plain. Slides are cut with a thickness of 12 µm or 14 µm for one-sample blocks and four-sample blocks, respectively. Three sections are adsorbed to a superfrost slide for one-sample blocks. For four-sample blocks, two sections are adsorbed to a superfrost slide with sample # 1 (red) faced towards the label. Slides are stored in a slide-box short term a 4 °C or long term at -80 °C prior to staining.

5.5.4 DOPEoid immunofluorescence staining

Slides are retrieved from 4 °C / -80 °C and left to thaw to RT. The cryosections are circled with a DAKO®-Pen and the line is left to dry before placing the slides in a cuvette filled with $PBS^{-/-}$ to rehydrate for ~ 5 min. Then, an ethanol series is performed with 30 s incubation in cuvettes with 70 %, 95 %, 100 %, 95 % and 70 % ethanol in that order. The slides are washed again in a cuvette filled with $PBS^{-/-}$ for ~ 5 min. The slides are removed from the cuvette and excess $PBS^{-/-}$ is removed through tapping the side of the slides on a flat surface. For blocking, slides are incubated for 1 h at RT with 40 µl per section of blocking solution containing 1.25 % BSA, 10 % NDS, 4 % skimmed-milk-powder-solution and 0.1 % Triton-X. Primary antibodies are diluted in this blocking solution at the dilutions given in **Table 11**. After blocking, the blocking solution is removed by tapping and the DAKO®-Pen line can be dried using a Q-tip if necessary. 40 µl of primary antibody solution are pipetted onto the sections and are incubated over night at 4 °C in a

humidity chamber to prevent drying out of the samples. The next day the slides are tapped on the side to remove the antibody solution and are then washed in a cuvette containing $PBS^{-/-}$ for ~ 5 min. Secondary antibodies for the given species of primary antibodies and DAPI are diluted 1:1000 in $PBS^{-/-}$. The slides are removed from the cuvette, excess $PBS^{-/-}$ is removed and the DAKO®-Pen line is dried. Now, 40 µl of secondary antibody solution is applied to each appropriate section and incubated for 1 h at RT in a humidity chamber under the exclusion of light. After incubation, the slides are washed two times in a cuvette filled with $PBS^{-/-}$ and any remaining $PBS^{-/-}$ is removed. One drop of Moviol or ProLong® Gold Antifade is applied per section and a coverslip is placed carefully on the slide, avoiding air bubble trapping. The stained slides are let out to dry for 1-2 h at RT and are then either analyzed with a microscope or stored at 4°C.

5.5.5 Picture acquisition

The AxioImager M2 fluorescent microscope with ApoTome is used. For picture acquisition and analysis, the software AxioVision and Zen by Zeiss® are used.

5.6 DOPEoid analysis – RNA level

5.6.1 DOPEoid selection & RNA isolation

To select DOPEoids for RNA extraction, a double contrast inversion microscope is used to assess the organoids gross morphology. Here, the 96-well plate containing the living organoids is placed under the microscope and organoids were classified as DOPEoid or non-DOPEoid based on their morphology. A DOPEoid exhibits (I) a thin, clearly demarked surface epithelium, (II) a denser core, and sometimes, depending on DOPEoid maturation and batch (III) one or more translucent vesicles in the core (**Fig. 14**). A non-DOPEoid does not show this clear structure and is more homogenous. Also, non-DOPEoids are on average larger than DOPEoids (**Fig. 14**). Per timepoint, four DOPEoids are transferred to a 1.5 µl Epi using a cut 1 000 µl pipette-tip. The supernatant is discarded and the DOPEoids washed once with $PBS^{-/-}$. Then, 200 µl of RLT buffer of the RNeasy Mini Kit containing 0.2 µl β-Mercaptoethanol (14.3 M) is added, and the tube is immediately transferred to -80 °C or used directly. The RNeasy Mini Kit is then used to isolate the RNA according to the manufacturer's instructions.

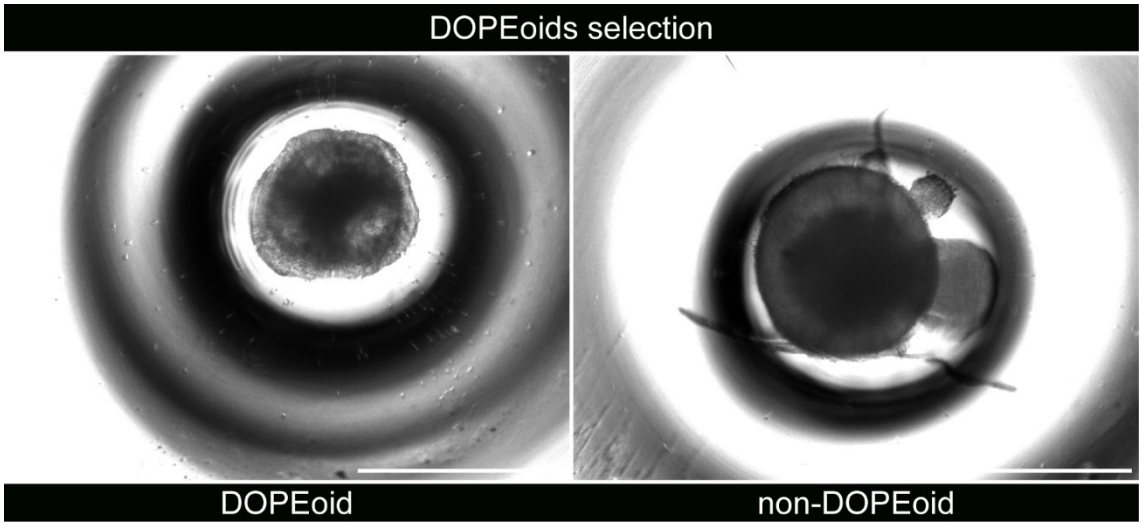

Figure 14: Live cell comparison of DOPEoid & non-DOPEoid

DOPEoid **(Left)** exhibits a translucent epithelium and a denser core with 3 translucent vesicles. Non-DOPEoid **(Right)** is larger and shows a thick translucent epithelium with a dense core and 2 homogenous outgrows (right). Scalebar 1 000 µm.

5.6.2 RT-qPCR – Biomark™ Fludigm

For the reverse transcriptase quantitative real time PCR (RT-qPCR) the Biomark™ Fluidigm system is used. First in a 48 or 96-well plate, in each well 3 µl assay loading reagent and 3 µl respective assay (**Tab. 10**) are pipetted, and the plate then centrifuged and stored at -20 °C or used directly. An assay-mix is made using all assays diluted 1:100 in TE buffer to reach a final volume of 2.5 µl per sample. The assay mix is either used directly or stored at -20 °C. Now, for the cDNA synthesis and pre-amplification, the RNA concentration of the isolated RNA is measured, and 20 ng diluted in 1 – 3 µl volume are used together with 5 µl 2x RXN buffer, 1.3 µl TE buffer, 0.2 µl SuperScript™ III RT/Platinum™ Taq-Mix and 2.5 µl assay mix. The final volume of 10 – 12 µl is then pipetted to a 96-well plate, vortexed, centrifuged and loaded into the StepOnePlus™ cycler. The following settings are used for a total of 18 cycles:

Temperature	Duration
50 °C	15 min
95 °C	2 min
95 °C – cycle	15 s
60 °C – cycle	4 min
8 °C – storage	Infinite

Table 18: cDNA synthesis & pre-amplification cycler settings

To dilute the pre-amplified cDNA 1:5, 40 µl of TE buffer are added. In a new 96-well plate, per sample 3 µl Universal TaqMan™ PCR Master Mix, No AmpErase™, 0.3 µl GE Sample Loading Reagent and 2.7 µl sample cDNA are added. A 96.96 Dynamic Array™ For Gene Expression plate is loaded with oil according to the manufacturers protocol in the MX / HX controller using “prime”. Now, 5.2 µl of array and sample are added on the respective side of the chip and the plate is loaded according to the manufacturers protocol in the MX / HX controller using “load”. Now the RT-qPCR is run in the BioMark™ machine using the “GE standard v1.pcl” protocol and analyzed. The CT-values of the respective samples are analyzed relative to *GAPDH* and standardized to the hiPSC samples using Excel.

6 Results

This study shows the generation of 3D OP-organoids (DOPEoids) from hiPSC. To verify their DOPEoid identity, a timeline of their development and a characterization of their distinctive architectural features and cell types are shown using extensive immunofluorescence staining. Furthermore, RT-qPCR data shows the expression patterns of key markers of craniofacial development during different timepoints of the differentiation. Finally, an outlook for possible differentiation protocol adaption is shown. This is based on an adapted differentiation protocol with improved organoid maturation and key features of olfactory development, shown with immunofluorescence staining.

6.1 DOPEoids generation & definition

For this study organoids were generated using the methods described in section **5.4.** These organoids were then fixed, cryo-sectioned and stained, according to section **5.5**. For RNA analysis, organoids were selected for DOPEoids, RNA collected and a qRT-RCR performed as described in section **5.6**. A total of three independent batches using the same differentiation protocol (n=3) were used for the morphological and developmental analysis on a protein level shown here. RNA of three independent differentiations was collected, although data of all three differentiations only contributed to one timepoint (n=3), with the other timepoints being n=1 or n=2.

Not all organoids of each differentiation batch were DOPEoids. Organoids, which did not exhibit OP character (non-DOPEoids) can be discriminated using a double contrast inversion microscope, as described in section **5.6.1**. However, the final definition of DOPEoids is based on immunofluorescence findings. To be defined as a DOPEoid, an organoid must have: (I) a TFAP2A^{+}/E-CADHERIN^{+} surface epithelium on the outside with an outside-out orientation, (II) thickened SIX1^{+}/TFAP2A^{-}/E-CADHERIN^{+} placodal patches within this epithelium, (III) neural tubuli expressing telencephalic markers in the core, and (IV) a developing head-like mesenchyme between the surface epithelium and the neural tubuli with (V) a basement membrane for each (**Fig. 15**).

The efficiency of DOPEoid formation was ~ 40-70 % of all organoids, with great variation between differentiations, a problem described previously by others working with PPR-like organoids (154). A comparison of morphology and RNA expression of a DOPEoid and a non-DOPEoid on day 31 can be found in **Supplemental Figure S1** and **Supplemental Figure S2**, respectively. All pictures and RNA results shown in the results part of this thesis were obtained from pre-selected DOPEoids.

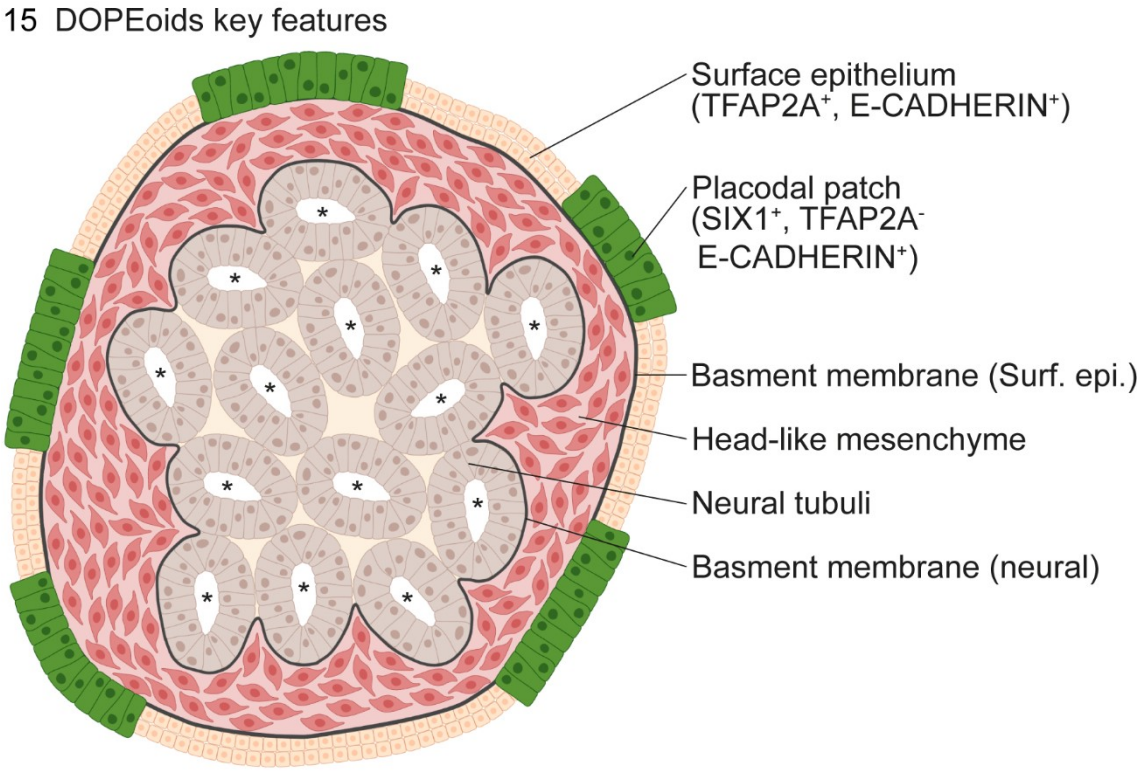

Figure 15: Defining features of DOPEoids

Schematic, idealized drawing of a cross section view of a DOPEoid. Defining features annotated: Placodal patch (green), (stratified) surface epithelium (yellow), neural tubuli (brown), head-like mesenchyme (red), basement membranes (grey). Lumen of neural tubuli marked by asterisks. Figure created with BioRender.com.

6.2 DOPEoids timeline

To establish a developmental timeline of the DOPEoids generated in this differentiation, the DOPEoids were stained for TFAP2A, SIX1 and E-CADHERIN at different timepoints from day 4 to day 31 of the differentiation. TFAP2A is an important marker for the NNE, as well as the PPR. SIX1 is also expressed in the PPR but its expression is later restricted to the neurogenic placodes, especially the OP. E-CADHERIN is a cell-adhesion molecule expressed in the surface epithelium, but not elsewhere. The pictures shown in the timeline highlight the hallmarks of DOPEoid development.

6.2.1 DOPEoids timeline – day 4 & day 8

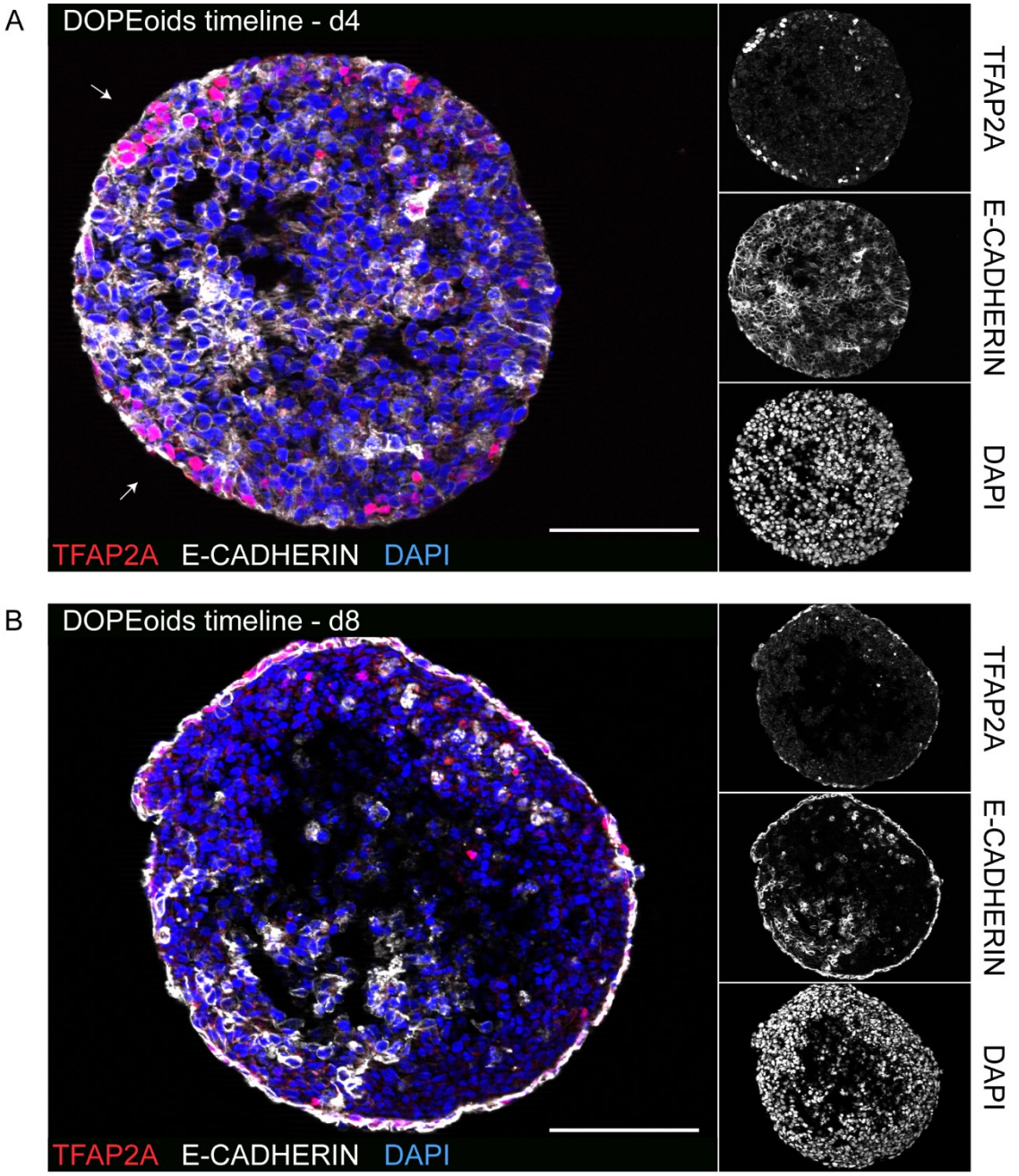

Figure 16: DOPEoids timeline – day 4 & day 8

Organoids stained for TFAP2A (red) and E-CADHERIN (white). Nuclei counterstaining with DAPI (blue). Arrows marking superficial TFAP2A expression. Scalebars: 100 µm. **(A+B)** TFAP2A, E-CADHERIN & DAPI.

6.2.2 DOPEoids timeline – day 10

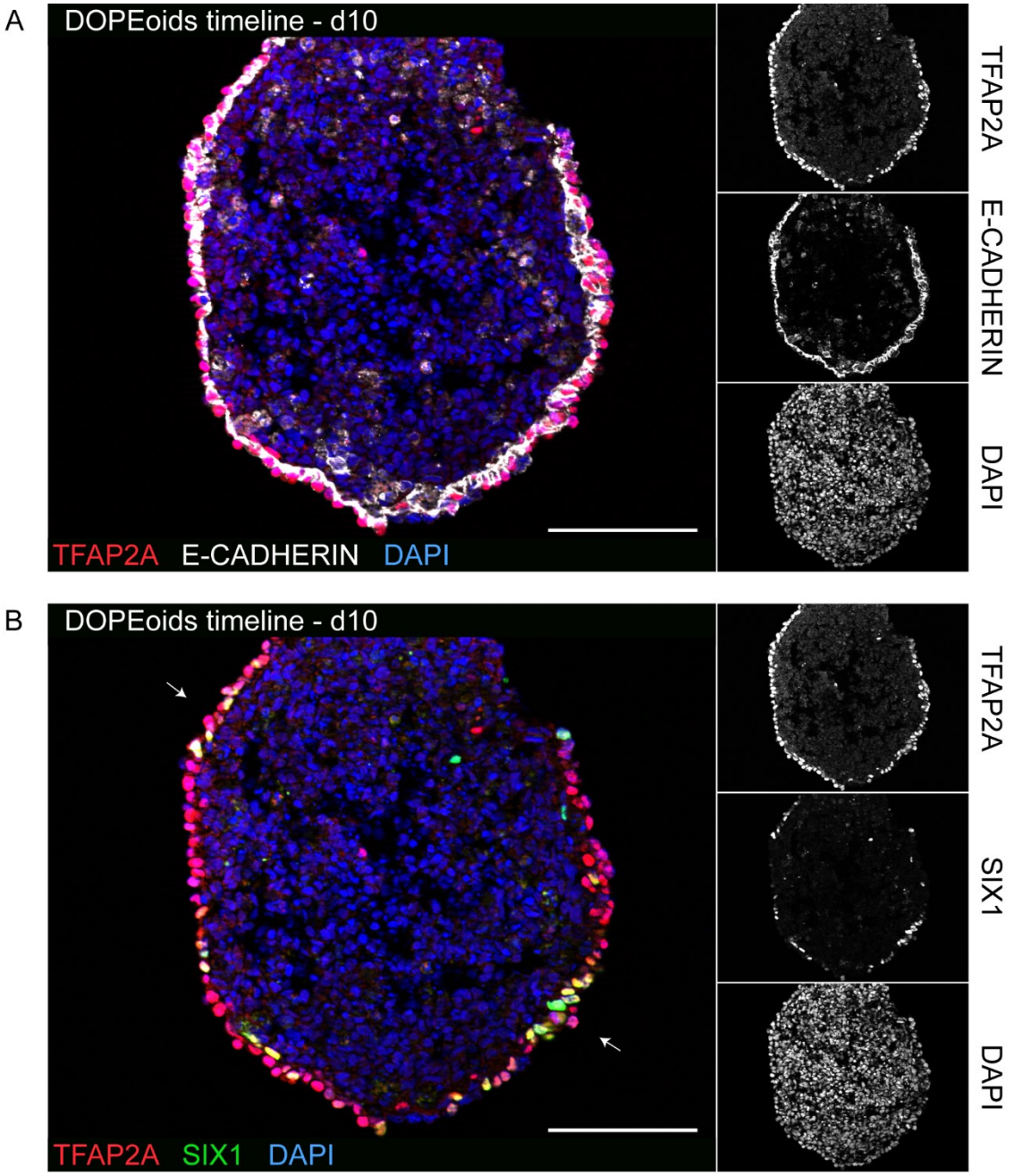

Figure 17: DOPEoids timeline – day 10

Organoid stained for TFAP2A (red), SIX1 (green) and E-CADHERIN (white). Nuclei counterstaining with DAPI (blue). Arrows marking co-expression of SIX1 and TFAP2A. Scalebars: 100 µm. **(A)** TFAP2A, E-CADHERIN & DAPI **(B)** TFAP2A, SIX1 & DAPI.

6.2.3 DOPEoids timeline – day 13

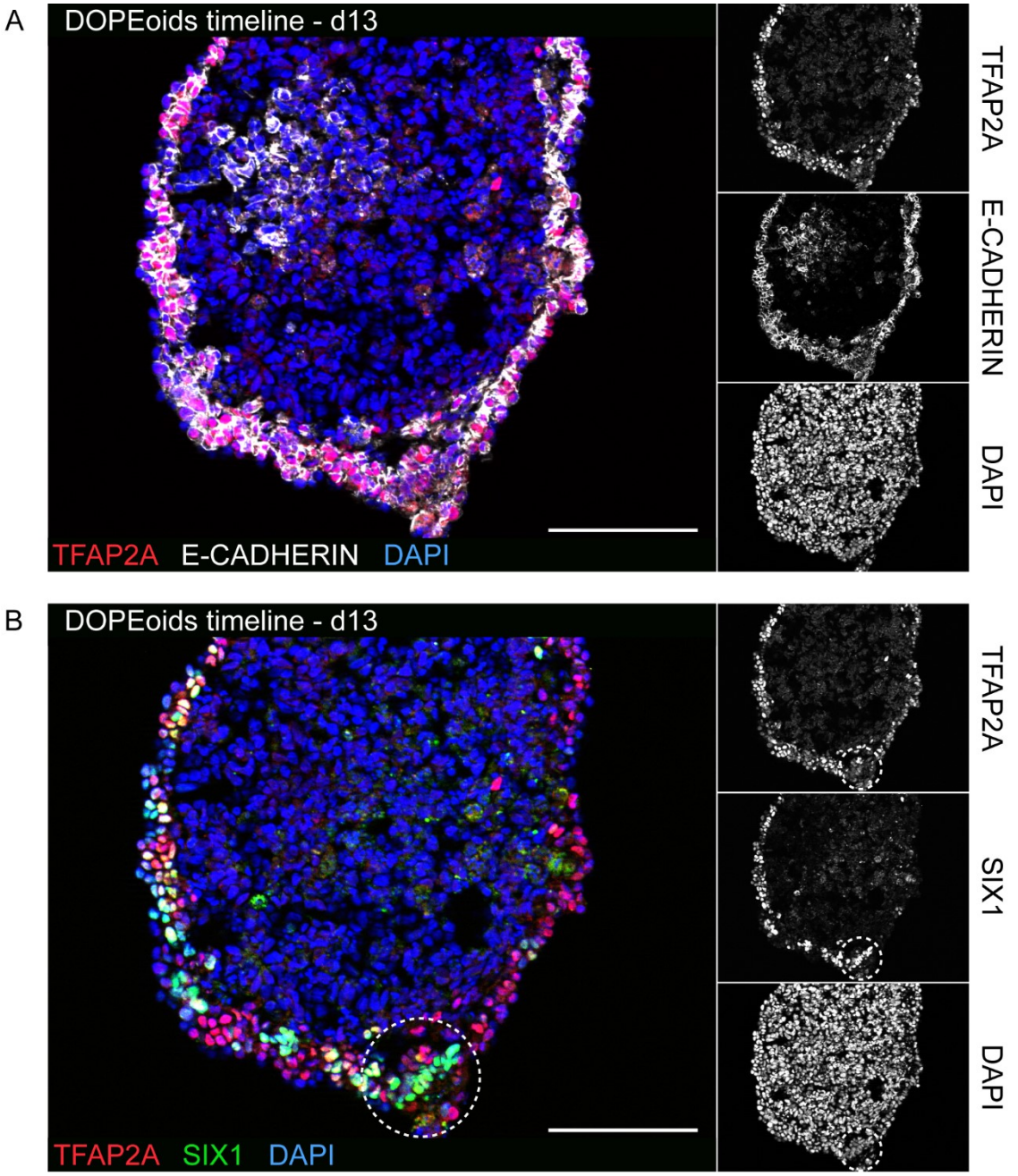

Figure 18: DOPEoids timeline – day 13

Organoid stained for TFAP2A (red), SIX1 (green) and E-CADHERIN (white). Nuclei counterstaining with DAPI (blue). Dotted circle marking patch of SIX1^{+}/TFAP2A$^{-/low\ cells}$. Scalebars: 100 µm. **(A)** TFAP2A, E-CADHERIN & DAPI **(B)** TFAP2A, SIX1 & DAPI.

6.2.4 Summary: DOPEoids timeline day 4 – day 13

On day 4 of the differentiation, the first superficial TFAP2A expression (arrows) indicates the start of NNE commitment in the surface layers of the organoid, whilst the diffuse and strong E-CADHERIN signal is a remnant of the stem cell state.

Day 8 marks the first appearance of a simple squamous epithelium expressing TFAP2A and E-CADHERIN, which represents the early NNE. The decrease in diffuse E-CADHERIN expression on day 8 marks the final loss of pluripotency.

On day 10, the TFAP2A^{+}/E-CADHERIN^{+} surface epithelium becomes a simple cuboid epithelium, marking the NNE. Also on day 10, parts of the epithelium show a significant co-expression of SIX1 and TFAP2A, which represents PPR-like cells (arrows), whilst SIX1$^{-/low}$/TFAP2A^{+} cells represent the remaining NNE.

On day 13 of the differentiation, the surface epithelium of the organoids becomes stratified for the first time and comprises multiple cell populations. Many cells are TFAP2A^{+}/SIX1^{+} and resemble PPR-like cells, whilst TFAP2A^{+}/SIX1$^{-/low}$ cells indicate surface ectoderm. A patch of SIX1^{+}/TFAP2A$^{-/low}$ cells can be first observed on day 13 on 6 o´clock of the organoid (dotted circle). This patch resembles the late PPR or CP-like cells and is termed “placodal patch”.

6.2.5 DOPEoids timeline – day 16

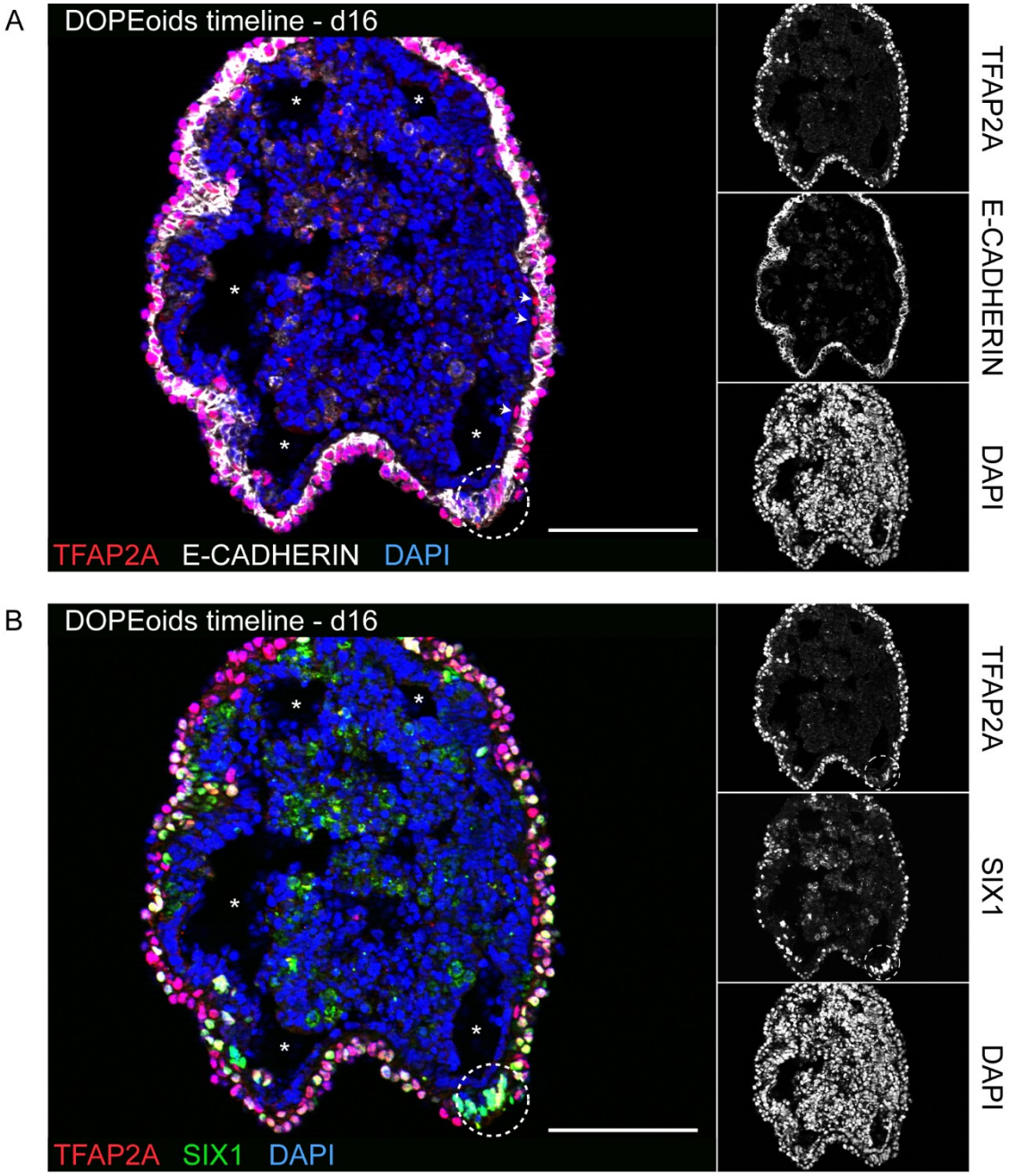

Figure 19: DOPEoids timeline – day 16

Organoid stained for TFAP2A (red), SIX1 (green) and E-CADHERIN (white). Nuclei counterstaining with DAPI (blue). Dotted circle marking SIX1^{+}/TFAP2A$^{-/low}$ late PPR / CP patch, asterisk marking neural tubuli with flat or cuboidal cell morphology, arrowheads marking TFAP2A^{+}/E-CADHERIN^{-} head-like mesenchyme. Scalebars: 100 µm. **(A)** TFAP2A, E-CADHERIN & DAPI **(B)** TFAP2A, SIX1 & DAPI.

6.2.6 DOPEoids timeline – day 25

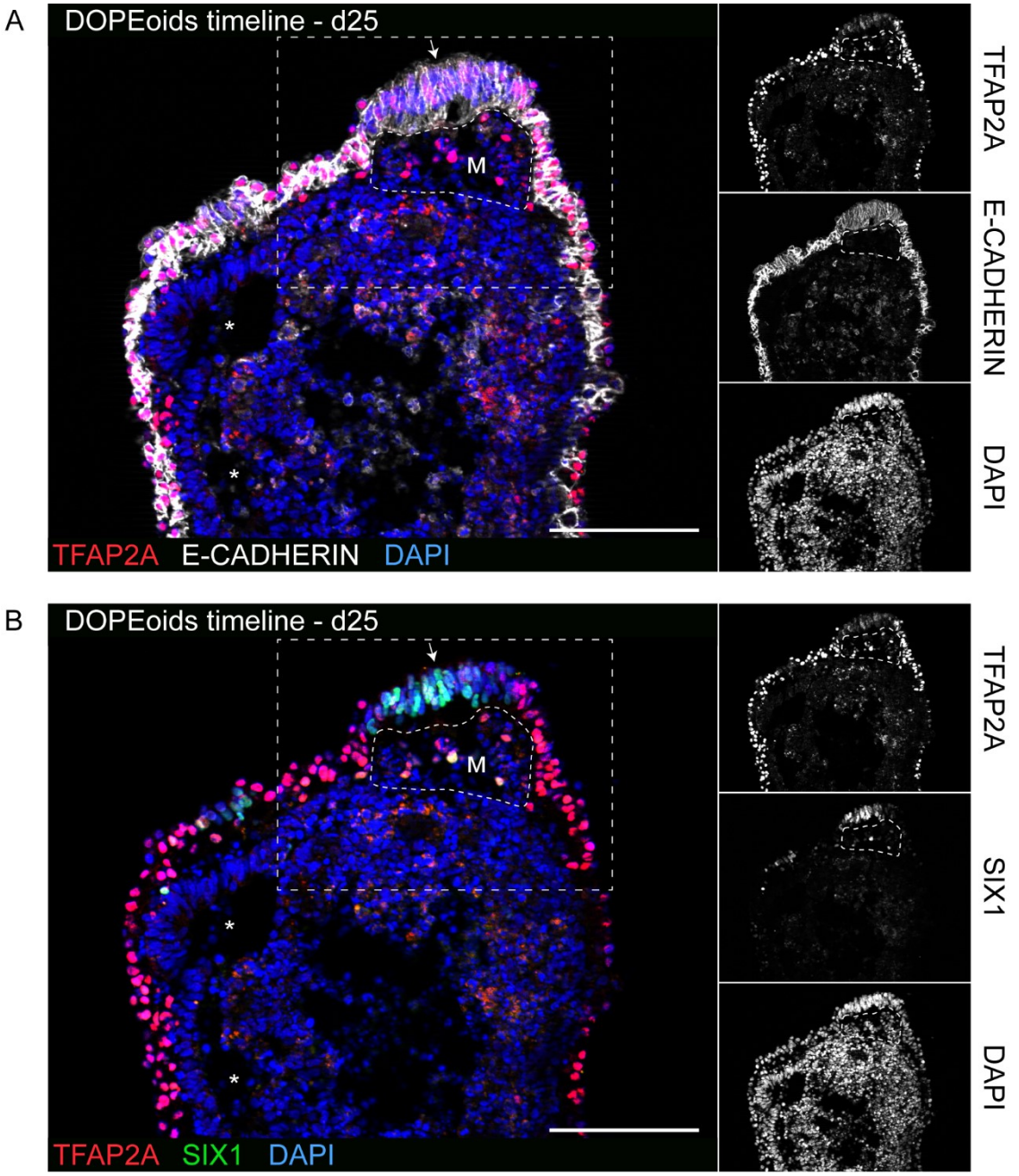

Figure 20: DOPEoids timeline – day 25

Organoid stained for TFAP2A (red), SIX1 (green) and E-CADHERIN (white). Nuclei counterstaining with DAPI (blue). Arrow marking SIX1^{+}/TFAP2A$^{-/low}$ placodal patch, asterisks marking neural tubuli, dashed outline / M marking head-like mesenchyme. Dotted rectangle indicates area of higher magnification in **(Fig. 21)**. Scalebars: 100 µm. **(A)** TFAP2A, E-CADHERIN & DAPI **(B)** TFAP2A, SIX1 & DAPI.

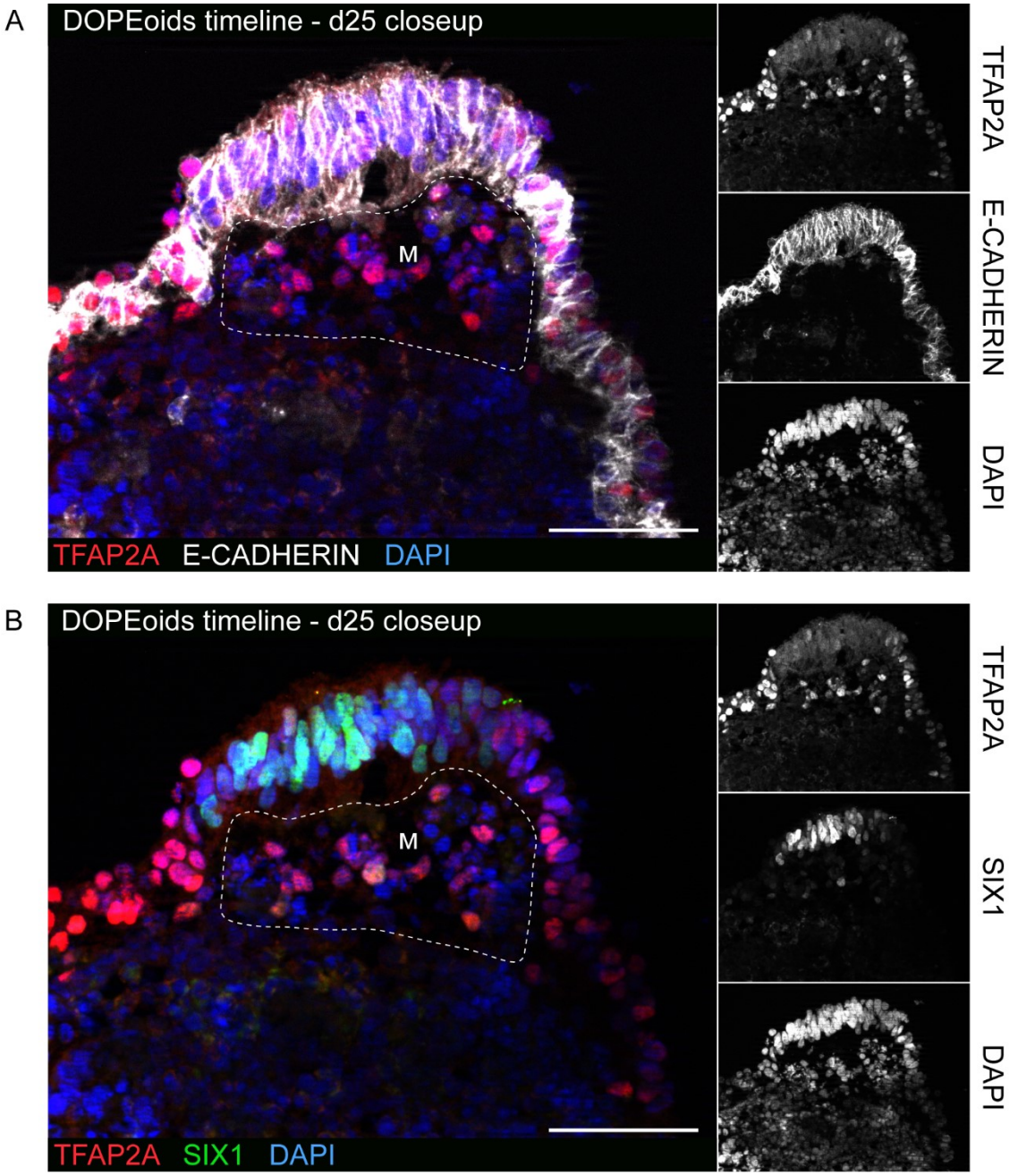

Figure 21: DOPEoids timeline – day 25 closeup

Organoid stained for TFAP2A (red), SIX1 (green) and E-CADHERIN (white). Nuclei counterstaining with DAPI (blue). Dashed outline / M marking head-like mesenchyme. Higher magnification of dotted rectangle from **(Fig. 20)**. Scalebars: 50 µm. **(A)** TFAP2A, E-CADHERIN & DAPI **(B)** TFAP2A, SIX1 & DAPI.

6.2.7 DOPEoids timeline – day 31

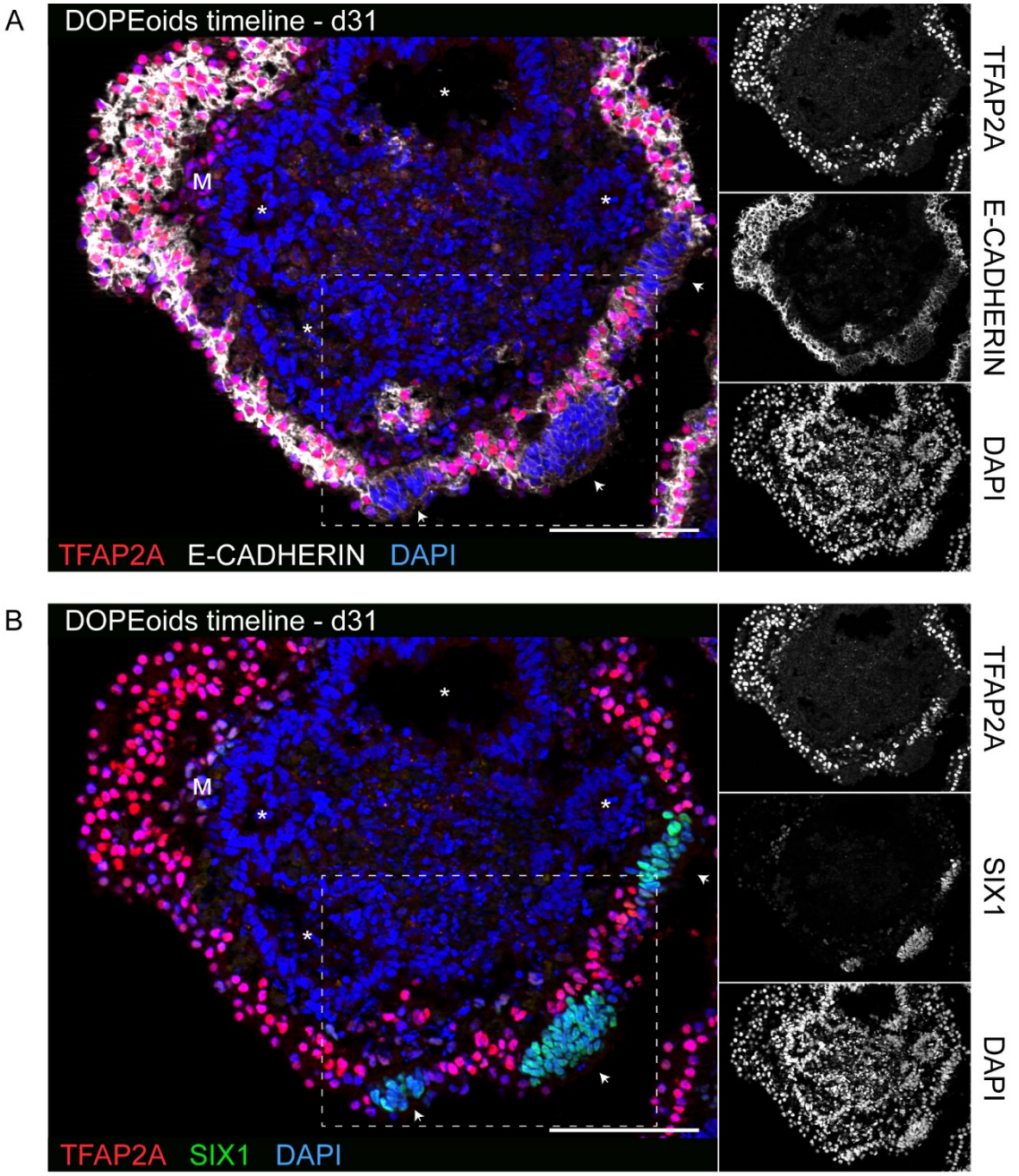

Figure 22: DOPEoids timeline – day 31

Organoid stained for TFAP2A (red), SIX1 (green) and E-CADHERIN (white). Nuclei counterstaining with DAPI (blue). Arrowheads marking SIX1^{+}/TFAP2A$^{-/low}$ placodal patches, asterisks marking neural tubuli, M marking head-like mesenchyme. Dotted rectangle indicates area of higher magnification in **(Fig. 23)**. Scalebars: 100 µm. **(A)** TFAP2A, E-CADHERIN & DAPI **(B)** TFAP2A, SIX1 & DAPI.

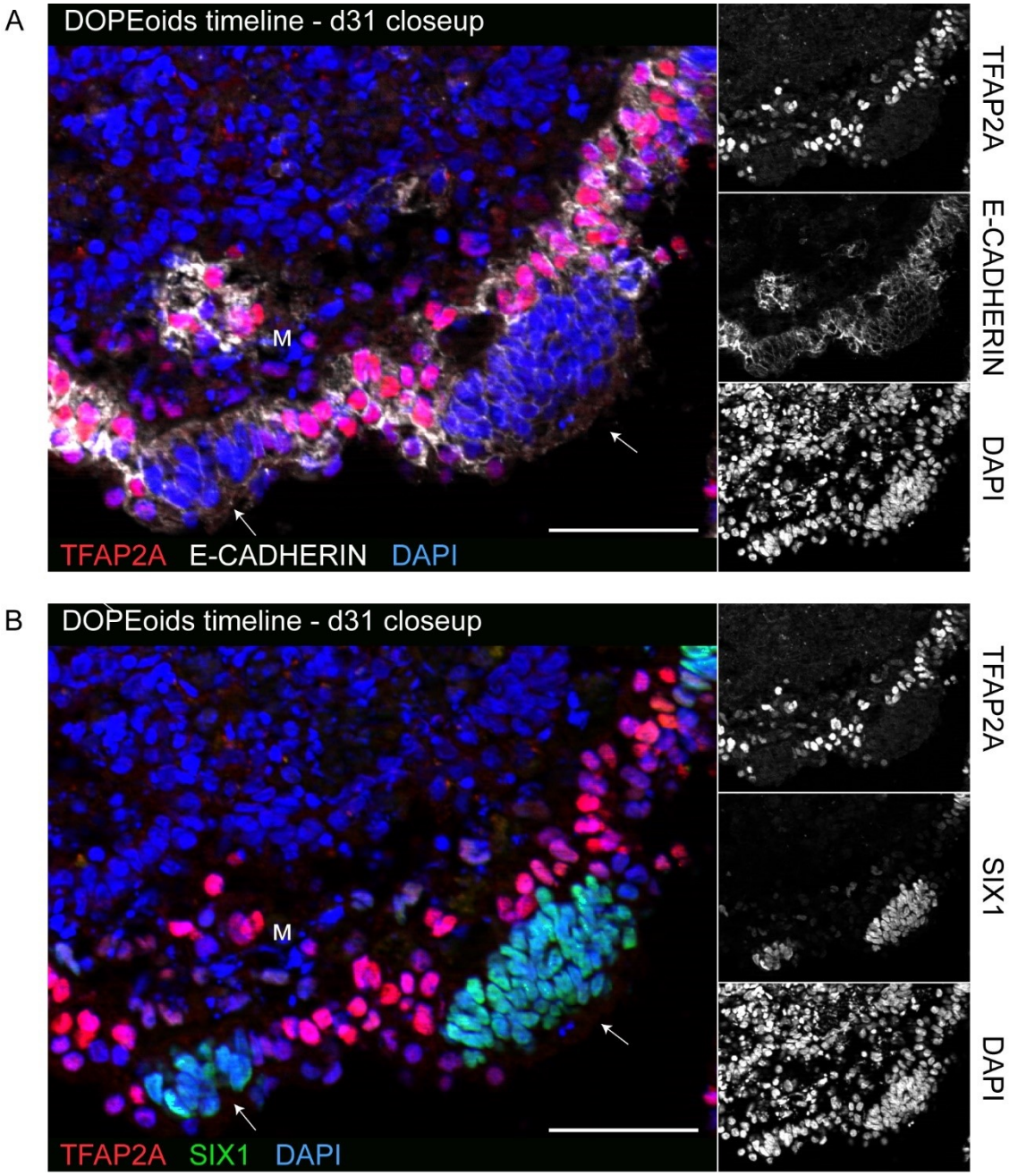

Figure 23: DOPEoids timeline – day 31 closeup

Organoid stained for TFAP2A (red), SIX1 (green) and E-CADHERIN (white). Nuclei counterstaining with DAPI (blue). Arrows marking SIX1^{+}/TFAP2A$^{-/low}$ placodal patches, M marking head-like mesenchyme. Higher magnification of dotted rectangle from **(Fig. 22)**. Scalebars: 50 µm. **(A)** TFAP2A, E-CADHERIN & DAPI **(B)** TFAP2A, SIX1 & DAPI.

6.2.8 Summary: DOPEoids timeline day 16 – day 31

On day 16 of the differentiation most cells within the TFAP2A^{+}/E-CADHERIN^{+} stratified cuboidal surface epithelium are also TFAP2A^{+}/SIX1^{+}, representing PPR-like cells. The few TFAP2A^{+}/SIX1$^{-/low}$ cells resemble the NNE / surface epithelium. At 5 o´clock of the organoid, a thickened columnar placodal patch made up of SIX1^{+}/TFAP2A$^{-/low}$ cells with elongated nuclei represents the late PPR or CP (dotted circle). Day 16 marks the first appearance of neural tubuli with flat or cuboidal cell morphology within the organoids (lumen marked by asterisks). Also, the first scattered TFAP2A^{+}/E-CADHERIN^{-} cells can be observed by day 16 between the surface epithelium and the tubuli / inner parts of the organoids (arrowheads). These cells resemble cells of the head-like mesenchyme.

By day 25, the TFAP2A^{+}/E-CADHERIN^{+} stratified cuboidal surface epithelium has increased in thickness. Now, the proportion of TFAP2A^{+}/SIX1^{+} PPR-like cells has decreased, and more cells resemble the TFAP2A^{+}/SIX1$^{-/low}$ surface epithelium. The SIX1^{+}/TFAP2A$^{-/low}$ placodal patch at 12 o´clock of the organoid is now pseudostratified and more thickened, with its elongated nuclei residing in different levels of the patch (arrow). This placodal patch exhibits the expression of E-CADHERIN, although at lower levels and with different morphology than the remaining surface epithelium. The morphology of the neural tubuli also changes by day 25, when the tubuli become columnar and pseudostratified (lumen marked by asterisks). On day 25, accumulations of polygonal cells with TFAP2A and / or SIX1 but no E-CADHERIN expression can be observed in clusters between the surface epithelium and the neural tubuli / inner parts of the organoids as a distinct compartment (M, dashed outline). These cell accumulations resemble the developing head-like mesenchyme.

On day 31 the TFAP2A^{+}/E-CADHERIN^{+} stratified cuboidal surface epithelium has reached its maximum thickness. Now, all cells are of TFAP2A^{+}/SIX1$^{-/low}$ surface epithelium lineage and TFAP2A^{+}/SIX1^{+} PPR-like cells cannot be observed anymore. Three thick, pseudostratified placodal patches made up of SIX1^{+}/TFAP2A$^{-/low}$ cells with a distinct E-CADHERIN morphology can be seen (arrowheads). These patches have further increased in thickness and cell density compared to day 25. Also, the neural tubuli show increased wall thickness and

prominent pseudostratification (lumen marked by asterisks). On day 31, E-CADHERIN^{-} and TFAP2A^{+} and / or SIX1^{+} head mesenchyme-like cells can be observed as a continuous compartment between the surface epithelium / placodal patches and the neural tubuli (M).

An overview of the hallmarks in the DOPEoid differentiation can be found in **Figure 24**.

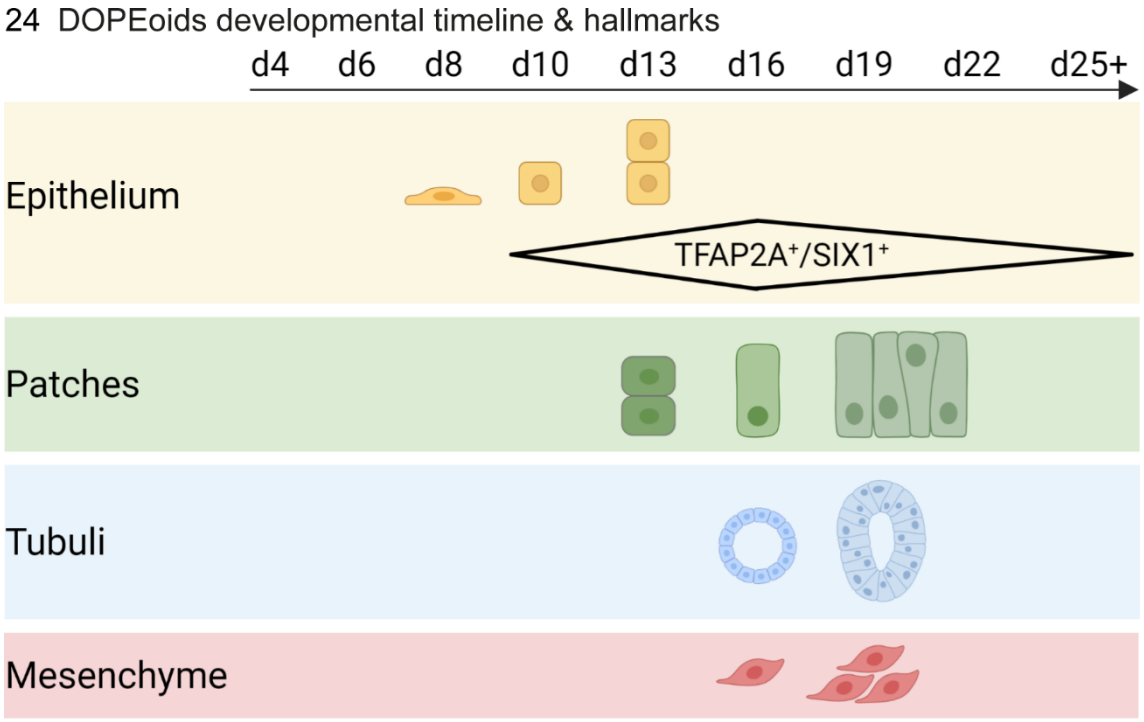

Figure 24: Timeline & hallmarks of DOPEoid development

Visualization of the developmental hallmarks of the four compartments in the DOPEoid differentiation. Timeline (top) from day 4 (left) to days 25+ (right). The appearance of the symbols marks the first appearance in DOPEoids. Epithelium (yellow) with first squamous cells on day 8, cuboid cells on day 10 and stratified appearance from day 13 onwards. TFAP2A^{+}/SIX1^{+} cells marking the PPR with their maximum abundancy on day 16. Placodal patches (green) first appearing cuboid-like on day 13, columnar on day 16 and pseudostratified from day 19 onwards. Neural tubuli (blue) first appearing as simple cuboid on day 16 and pseudostratified from day 19 onwards. Head-like mesenchyme (red) first appearing as single cells on day 16, becoming more abundant as distinct compartment from day 19 onwards. Figure created with BioRender.com.

6.3 DOPEoids characterization

To further characterize the structures found in the DOPEoids, which are highlighted in **Figure 15 & 24** and to prove their tissue identity, immunofluorescence staining for different markers are shown here. A variety of neural markers can be found in the neural tubuli as well as the placodal patches. Multiple mesenchymal markers can be found in the suggested head-like mesenchyme. Furthermore, morphological changes found in the DOPEoids closely resemble the development *in vivo*, further highlighting the OP character of the DOPEoids.

6.3.1 DOPEoids characterization A

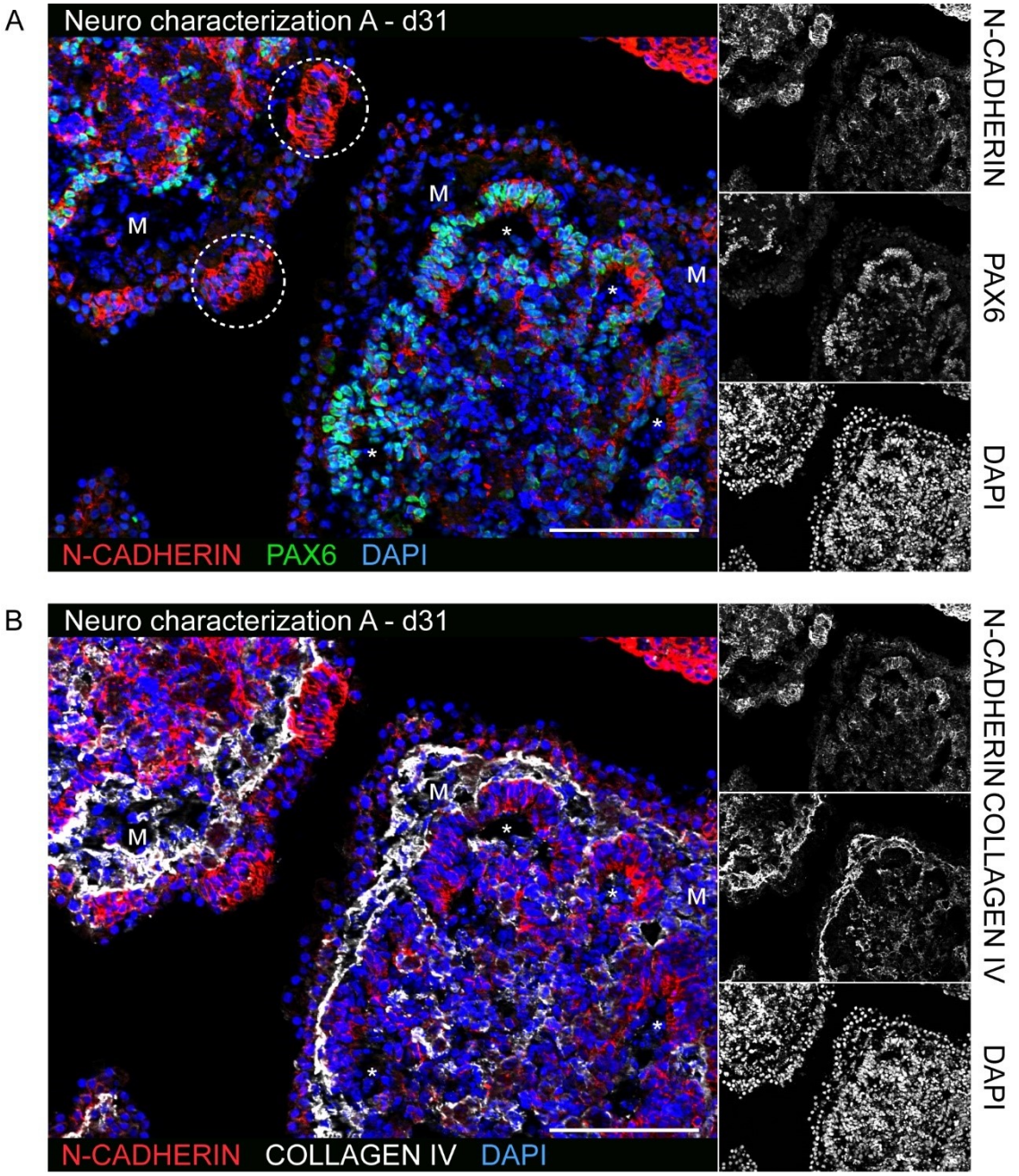

Figure 25: DOPEoids characterization A – day 31

Organoid stained for N-CADHERIN (red), PAX6 (green) and COLLAGEN IV (white). Nuclei counterstaining with DAPI (blue). Dotted circles marking placodal patches, asterisks marking neural tubuli, M marking head-like mesenchyme. Scalebars: 100 µm. **(A)** N-CADHERIN, PAX6 & DAPI (**B)** N-CADHERIN, COLLAGEN IV & DAPI.

The tubuli inside the organoids (lumen marked with asterisks) show a high expression of the early neural / forebrain marker PAX6 and the neural cell-adhesion marker N-CADHERIN. Low-level expression of PAX6 and N-CADHERIN can be observed in the surface epithelium. The two pseudostratified patches within the surface epithelium in the upper organoid also show a high expression of N-CADHERIN (dotted circle). In between the surface epithelium and the tubuli inside the organoids, a mesenchymal compartment with loose, polygonal cells with a high signal for ECM component COLLAGEN IV and no expression of neural marker N-CADHERIN can be observed (M). This COLLAGEN IV signal, although present in the whole mesenchyme, is most prominent as two concentrated *laminae* directly adjacent to the surface epithelium and the tubuli, indicating the presence of two separate basement membranes for the surface epithelium and the neural tubuli.

6.3.2 DOPEoids characterization B

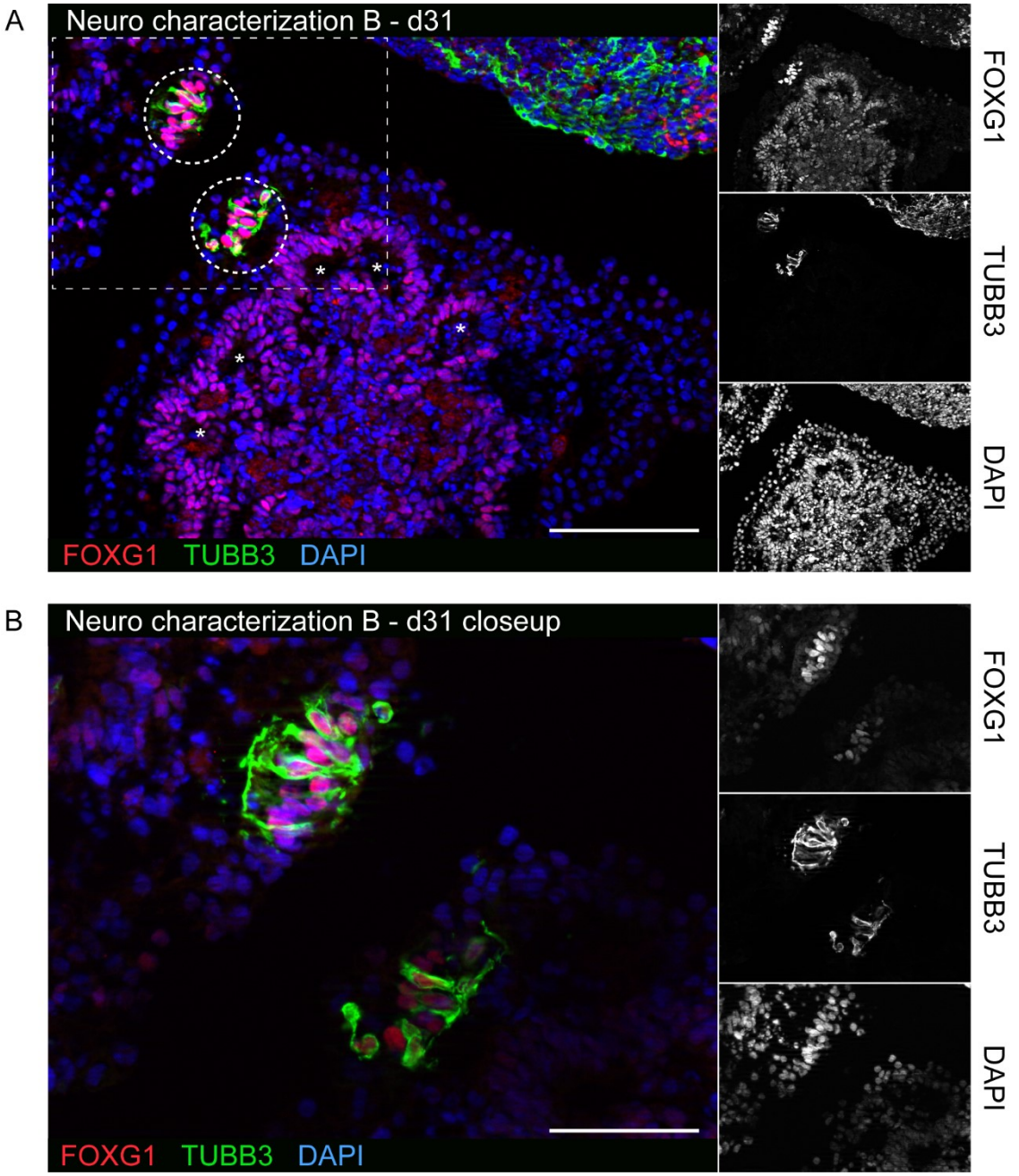

Figure 26: DOPEoids characterization B – day 31

Serial section of organoid from (**Fig. 25)** stained for FOXG1 (red) and TUBB3 (green). Nuclei counterstaining with DAPI (blue). Dotted rectangle in (A) indicates area of higher magnification shown in (B). Dotted circles marking placodal patches, asterisks marking neural tubuli. Scalebars: (A) 100 µm, (B) 50 µm. **(A+B)** FOXG1, TUBB3 & DAPI.

The tubuli inside the organoids (lumen marked with asterisks) show expression of the early neural / forebrain marker FOXG1. Low-level expression of FOXG1 can also be observed in the surface epithelium. The two pseudostratified patches within the surface epithelium show a high expression of FOXG1 and postmitotic neural marker TUBB3 (dotted circles), which cannot be found in the neural tubuli. The $FOXG1^{+}$/$TUBB3^{+}$ cells in the patches exhibit a bipolar neuron-like morphology with structures resembling axons projecting towards the inside of the organoid.

6.3.3 DOPEoids characterization C

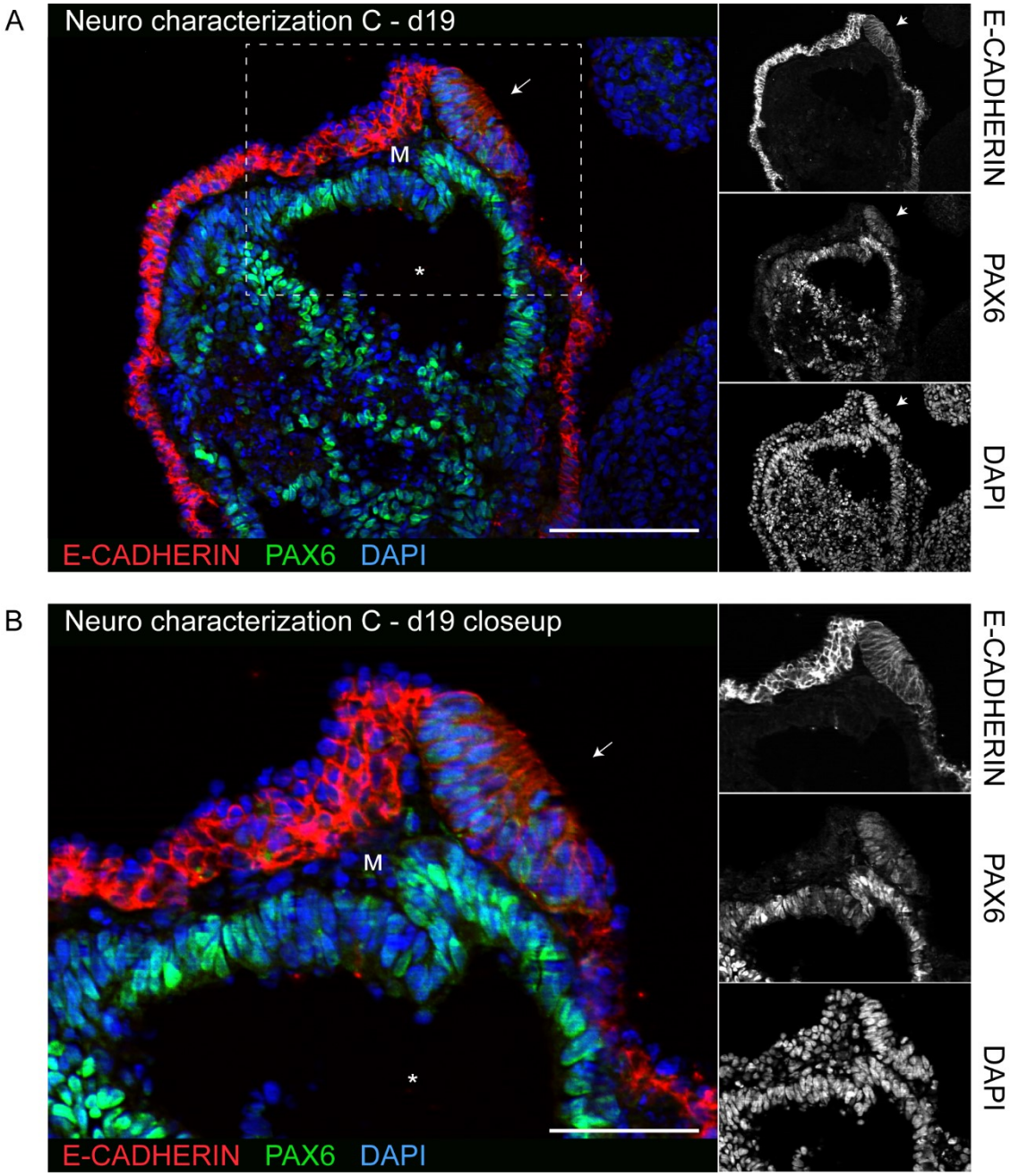

Figure 27: DOPEoids characterization C – day 19

Organoid stained for E-CADHERIN (red) and PAX6 (green). Nuclei counterstaining with DAPI (blue). Dotted rectangle in (A) indicates area of higher magnification shown in (B). Arrow / Arrowhead marking placodal patch, asterisk marking neural tubulus, M marking head-like mesenchyme. Scalebars: (A) 100 µm, (B) 50 µm. **(A+B)** E-CADHERIN, PAX6 & DAPI.

Similar to **Figure 25A**, the columnar / pseudostratified tubuli inside the organoids (lumen marked with asterisks) show expression of the early neural / forebrain marker PAX6. In contrast to **Figure 25A**, the pseudostratified, slightly concave epithelial patch at 1 o´clock (arrow) also shows a high expression of PAX6, which is also a marker of the anterior placodal region. E-CADHERIN is also expressed in this patch, although at a lower level and with a different morphology compared to the rest of the surface epithelium (see also **Fig. 20-23**). The thin mesenchyme between the surface epithelium and the neural tubuli does not show expression of either PAX6 or E-CADHERIN.

6.3.4 DOPEoids characterization D

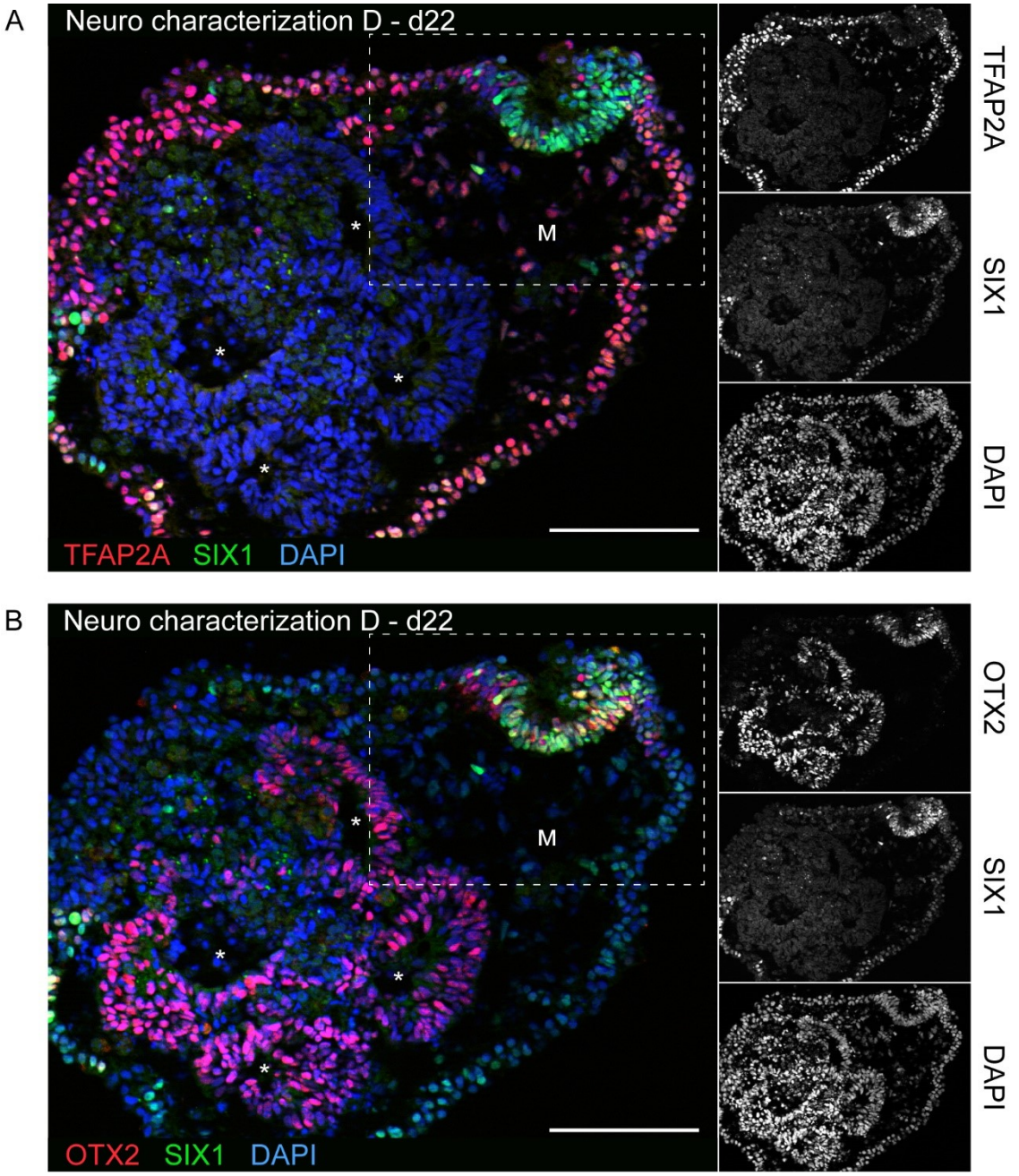

Figure 28: DOPEoids characterization D – day 22

(A) organoid stained for TFAP2A (red) and SIX1 (green). (B) same section as (A) stained for OTX2 (red) and SIX1 (green). Nuclei counterstaining with DAPI (blue). Dotted rectangle indicates area of higher magnification shown in **(Fig. 29)**. Asterisks marking neural tubuli, M marking head-like mesenchyme. Scalebars: 100 µm. **(A)** TFAP2A, SIX1 & DAPI. **(B)** OTX2, SIX1 & DAPI.

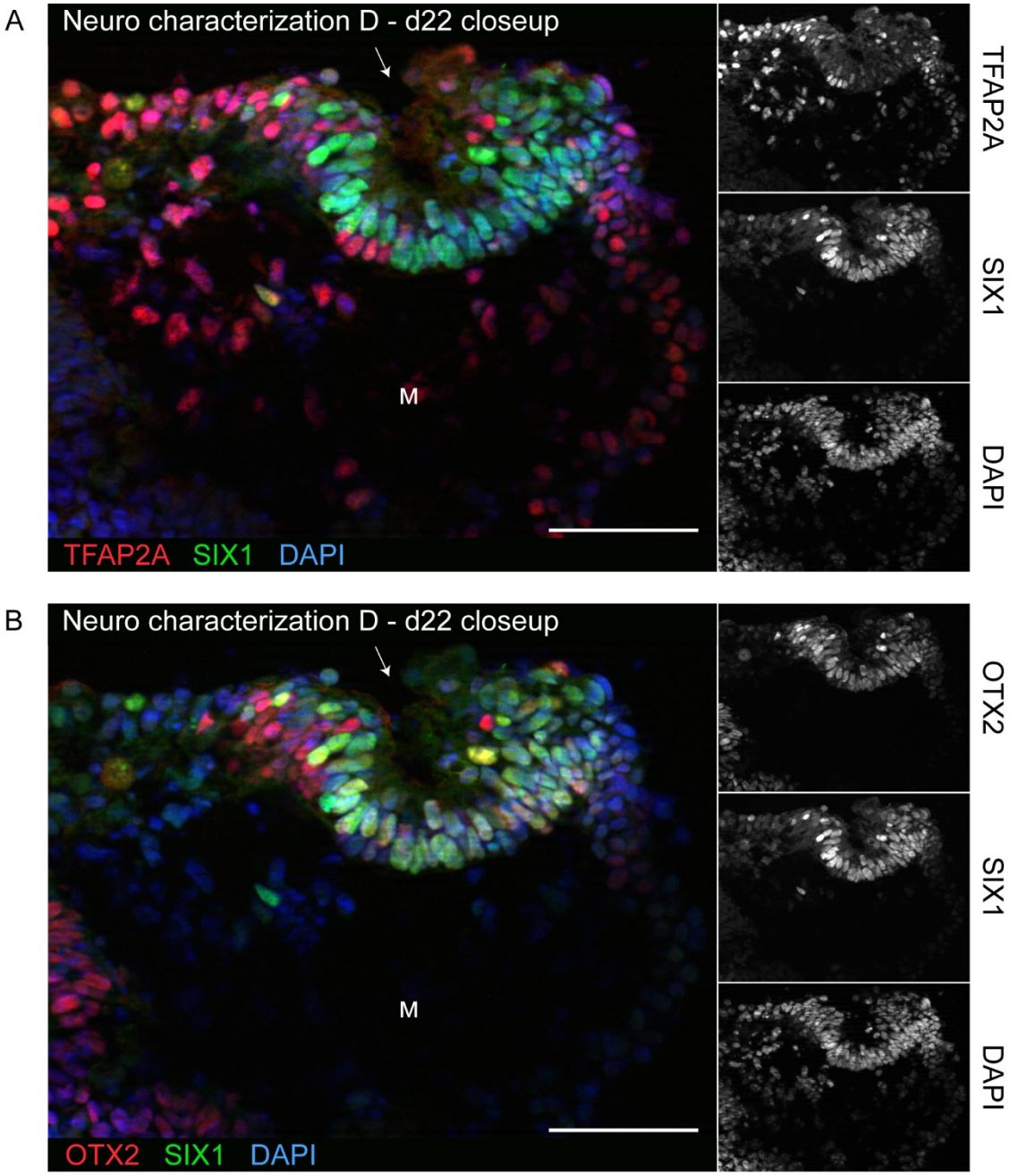

Figure 29: DOPEoids characterization D – day 22 closeup

(A) organoid stained for TFAP2A (red) and SIX1 (green). (B) same section as (A) stained for OTX2 (red) and SIX1 (green). Nuclei counterstaining with DAPI (blue). Higher magnification of dotted rectangle from **(Fig. 28)**. Arrow marking invaginating placodal patch, M marking head-like mesenchyme. Scalebars: 50 µm. **(A)** TFAP2A, SIX1 & DAPI. **(B)** OTX2, SIX1 & DAPI.

The pseudostratified tubuli inside the organoids (lumen marked with asterisks) show expression posterior / ventral forebrain marker OTX2. The surface epithelium is made up of TFAP2A^{+}/SIX1$^{low/-}$ cells, resembling definite NNE (see also **Fig. 5-8**). The placodal patch at 1 o´clock of the organoid (arrow in B) shows strong expression of PPR / CP marker SIX1 and anterior placodal region / olfactory marker OTX2. The pseudostratified placodal patch invaginates into the underlying mesenchyme, similar to the formation of the nasal pit *in vivo*. The head mesenchyme-like compartment is prominent between the surface epithelium / placodal patch and the neural tubuli and is made up of polygonal cells expressing TFAP2A and sometimes also SIX1 but not OTX2.

6.3.5 DOPEoids characterization E & F

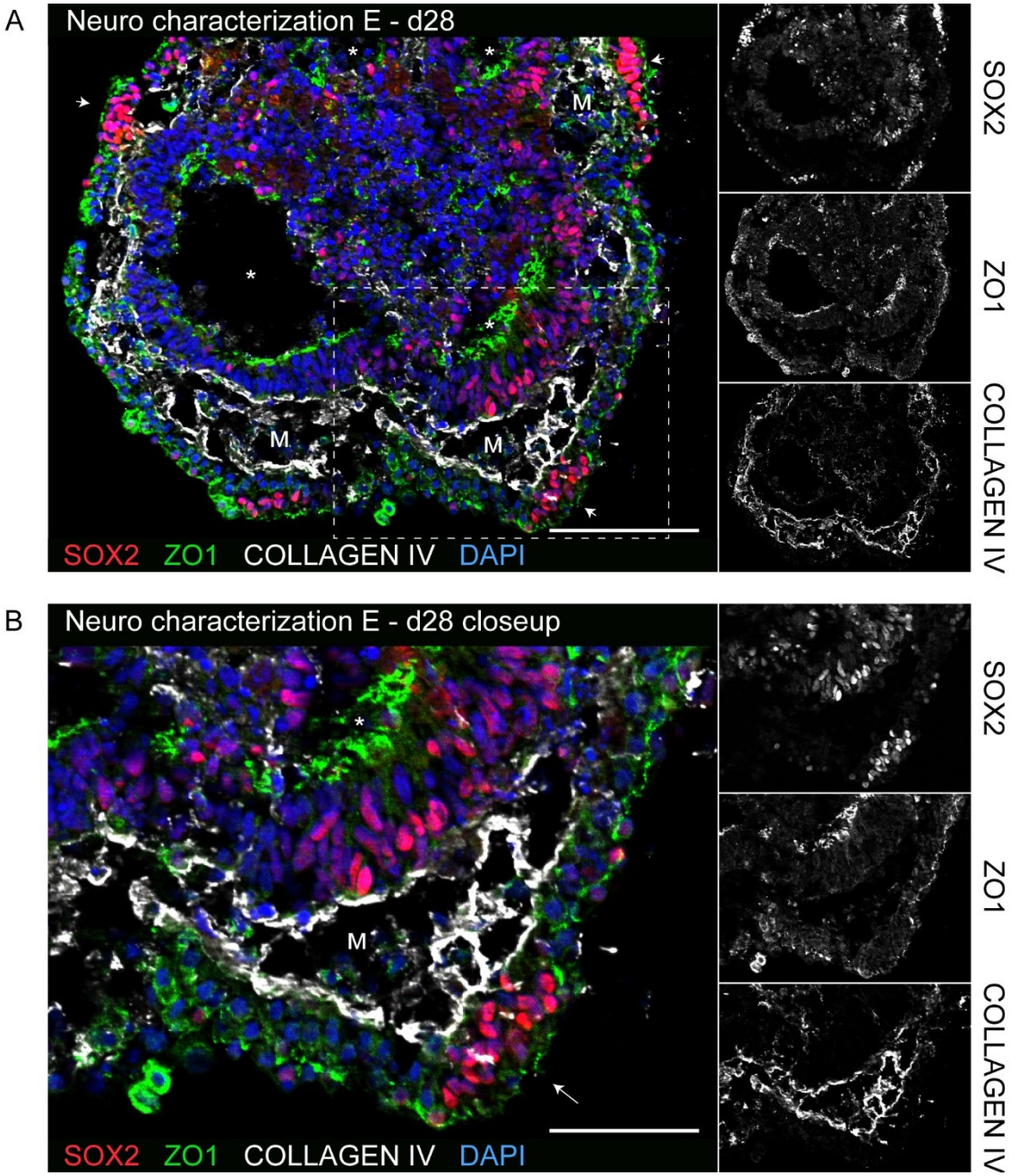

Figure 30: DOPEoids characterization E – day 28

Organoid stained for SOX2 (red), ZO1 (green) and COLLAGEN IV (white). Nuclei counterstaining with DAPI (blue). Dotted rectangle in (A) indicates area of higher magnification shown in (B). Arrows / Arrowheads marking placodal patches, asterisks marking neural tubuli, M marking head-like mesenchyme. Scalebars: (A) 100 µm, (B) 50 µm. **(A+B)** SOX2, ZO1, COLLAGEN IV & DAPI.

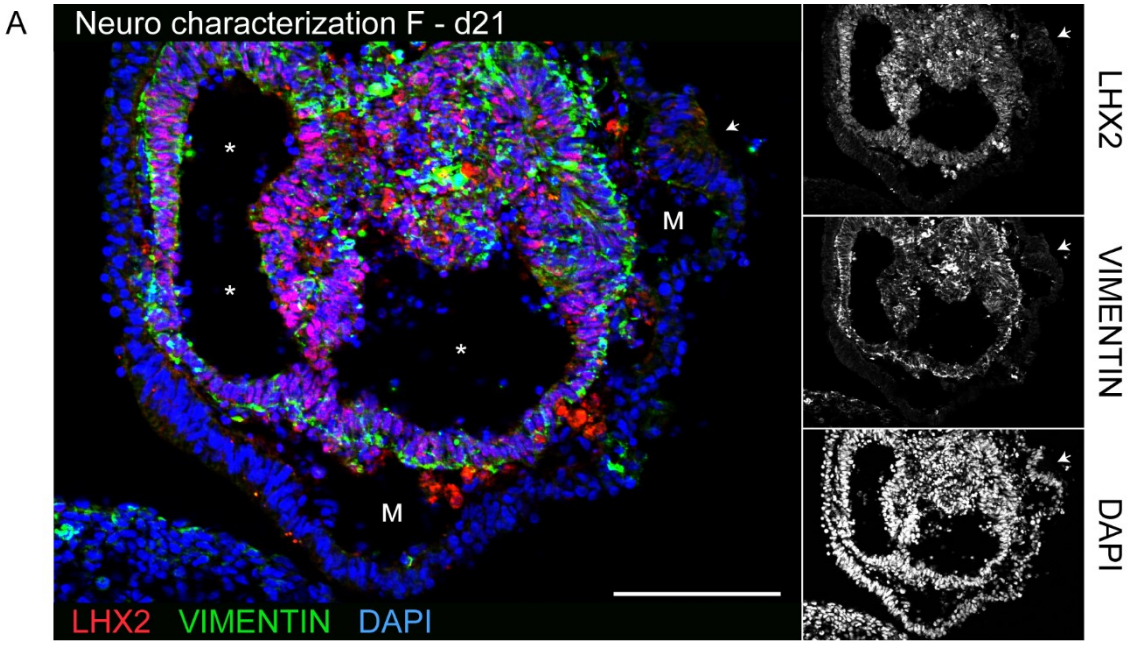

Figure 31: DOPEoids characterization F – day 21

Organoid stained for LHX2 (red) and VIMENTIN (green). Nuclei counterstaining with DAPI (blue). Arrowhead marking placodal patch, asterisks marking neural tubuli, M marking head-like mesenchyme. Scalebar: 100 µm.

The tubuli inside the organoids (lumen marked with asterisks) show expression of neural progenitor / stem cell marker SOX2 and dorsal forebrain marker LHX2. The pseudostratified neural tubuli are also expressing high levels of VIMENTIN, a known marker for RG. SOX2 expression can also be found in the epithelial patches (arrows), indicating neurogenic placodal fate. The mesenchyme between the surface epithelium and the neural tubuli (M) is rich in COLLAGEN IV (see also **Fig. 25**) and shows some low-level expression of VIMENTIN, which is also a mesenchymal marker. Again, two separate basement membranes for the neural tubuli and the surface epithelium can be identified (see also **Fig. 25**). A high signal for ZO1 (marking the apical side of epithelia) can be observed on the outside of the surface epithelium and the patches, as well as on the inside of the neural tubuli inside the organoid. This orientation (neural: apical inside; surface epithelium: apical outside) is in accordance with the two separate basement membranes, marking the basal sides of the epithelium and the neural tubuli, facing each other back-to-back.

6.3.6 DOPEoids characterization G

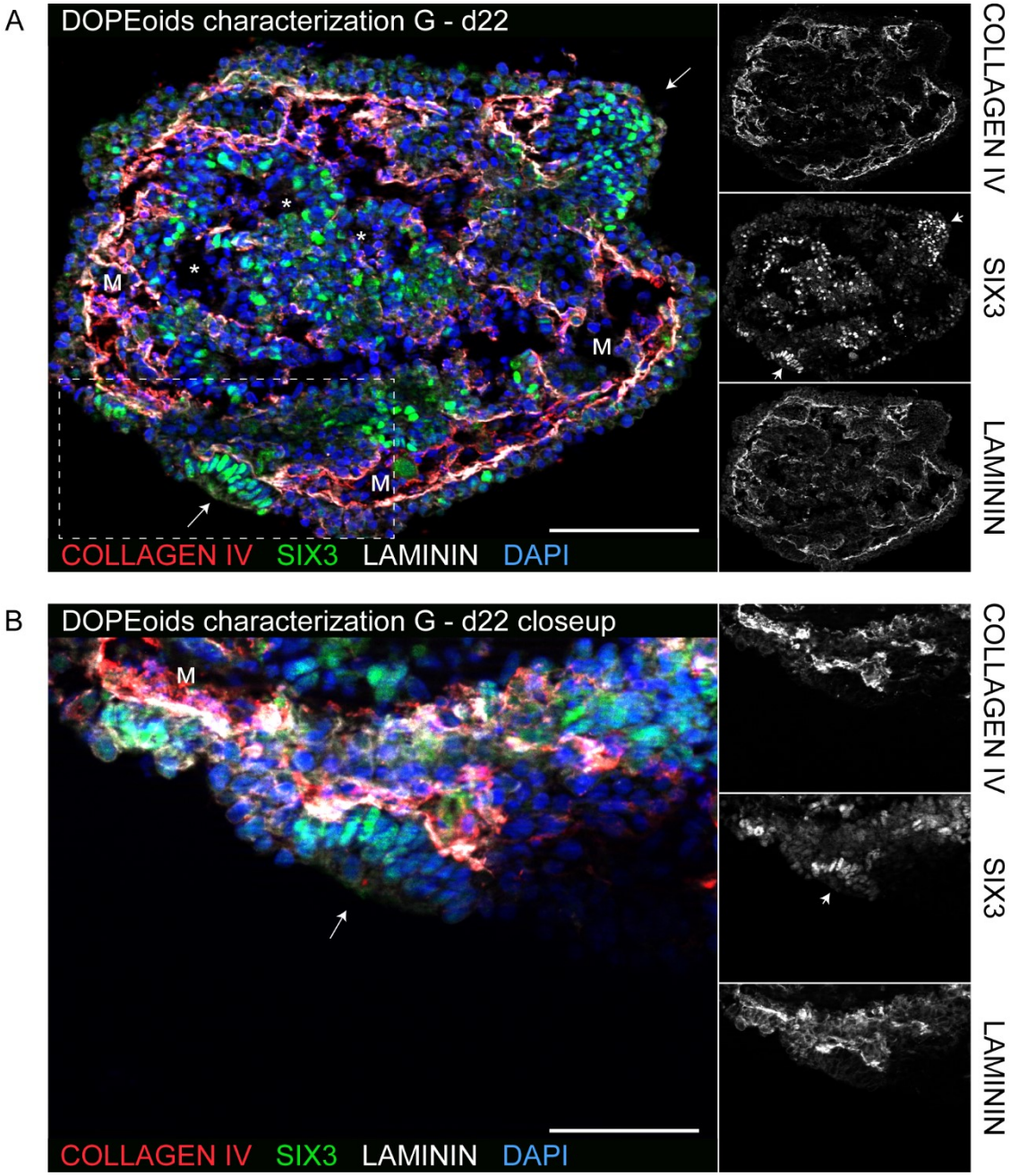

Figure 32: DOPEoids characterization G – day 22

Organoid stained for COLLAGEN IV (red), SIX3 (green) and LAMININ (white). Nuclei counter-staining with DAPI (blue). Dotted rectangle in (A) indicates area of higher magnification shown in (B). Arrows marking placodal patches, asterisks marking neural tubuli, M marking head-like mesenchyme. Scalebars: (A) 100 µm, (B) 50 µm. **(A+B)** COLLAGEN IV, SIX3, LAMININ & DAPI.

The tubuli inside the organoids (lumen marked with asterisks) show expression of early neuroectodermal marker SIX3. Also, as a marker of the anterior placodal region, prominent SIX3 expression can also be observed in pseudostratified patches within the surface epithelium (arrows). The mesenchyme (M) shows faithful overlapping signals of ECM / basement membrane components COLLAGEN IV (see also **Fig. 25 & 30**) and LAMININ, demarking two separate basement membranes. The polygonal mesenchymal cells also show cytoplasmatic expression of these two markers.

6.3.7 DOPEoids characterization summary

Figure 33 shows a summary of the identified marker expression found in the distinct compartments of the DOPEoids.

33 DOPEoids compartmental protein expression

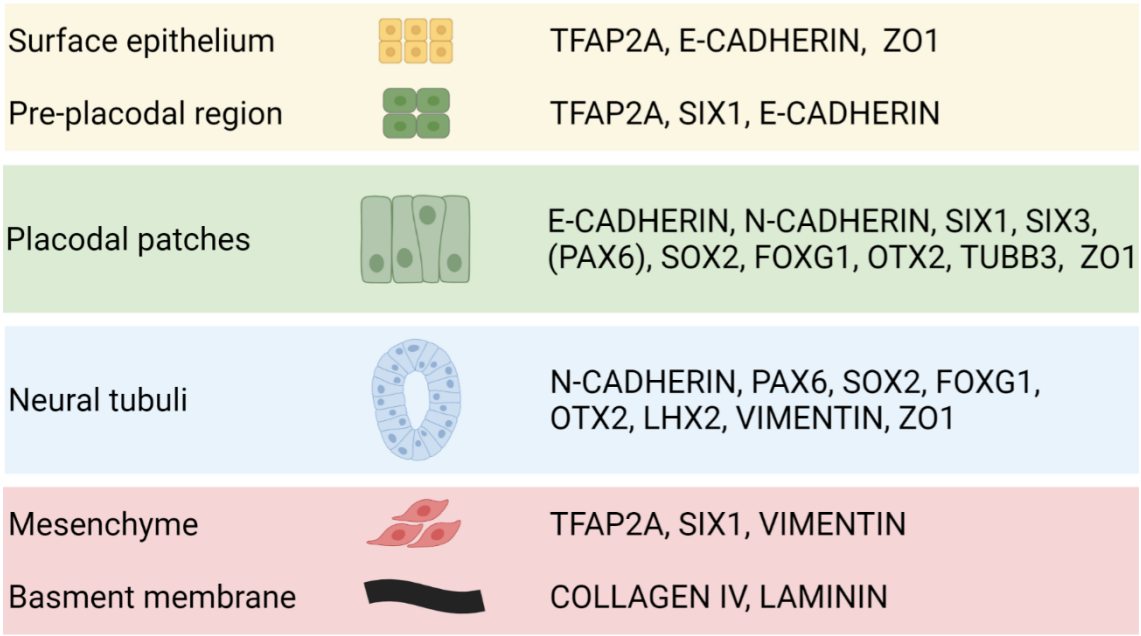

Figure 33: Compartmental protein expression in DOPEoids

Visualization of the marker expression found in the four compartments of the DOPEoids. Figure created with BioRender.com.

6.4 RNA data

To demonstrate the developmental timeline of the DOPEoids also on RNA level, as well as to introduce some new markers to prove OP identity, a RT-qPCR of bulk RNA from pre-selected DOPEoids was performed on different timepoints (day 4 – day 40). The expression shown here is relative to *GAPDAH* and normalized for hiPSC (n=3). Timepoints “day 4” – “day 28” originate from one differentiation (n=1), whilst “day 31” and “day 40” come from three and two differentiations, respectively (n=3; n=2).

The mRNA expression timeline is analyzed in four different clusters: The first cluster shows epithelial markers (***6.4.1***), the second PPR markers (***6.4.2***), the third neural / forebrain markers (***6.4.3***), and the last cluster shows placodal and mesenchymal markers (***6.4.4***).

6.4.1 DOPEoids RNA expression timeline – epithelial markers

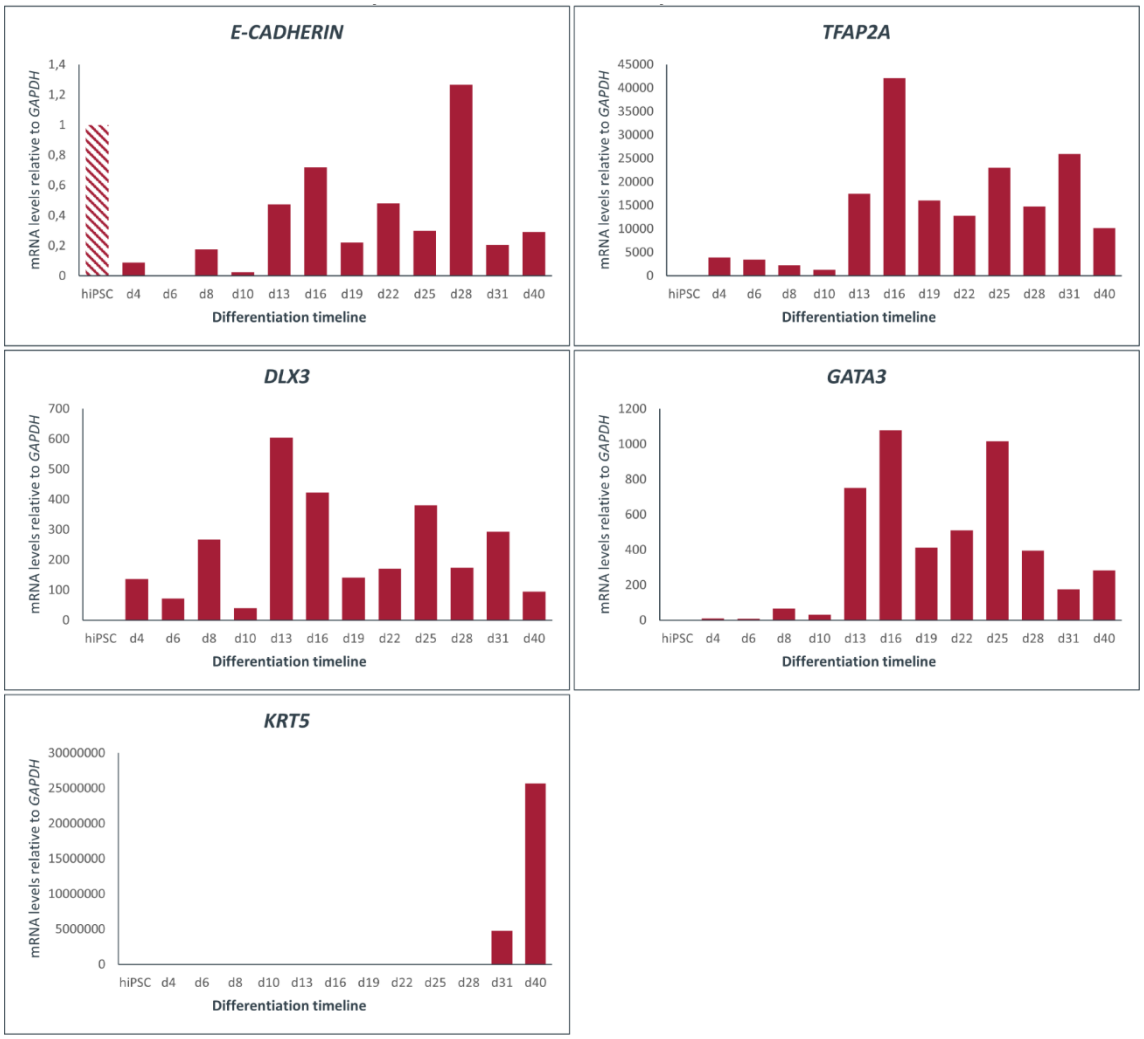

Figure 34: DOPEoids RNA expression timeline – epithelial markers

Relative mRNA expression to *GAPDH*, normalized to hiPSC expression on days 4 to 40 of the DOPEoid differentiation. Exception: *KRT5* expression normalized to day 19 since no expression was detected before.

The *E-CADHERIN* expression during the differentiation is relatively low, compared to hiPSC, since it is only expressed in the DOPEoids surface epithelium, whilst *E-CADHERIN* is highly expressed in hiPSC. Remnant *E-CADHERIN* expression can be detected on day 4 and prominent expression from day 13 onward. From day 16 to day 40 the expression is generally down trending with exceptional high expression on day 28.

The expression of NNE, PPR and mesenchymal marker *TFAP2A* increases by day 4 and peaks on day 16, from whereon it is trajectory is down trending.

DLX3 and *GATA3* are both important early NNE genes and show a peak in their expression on day 13 and day 16, respectively. From this peak, their expression is down trending towards day 40.

The expression of *KRT5*, a marker for basal layers of the developing skin can first be detected on day 19. From here, the expression increases to peak on day 40.

6.4.2 DOPEoids RNA expression timeline – PPR markers

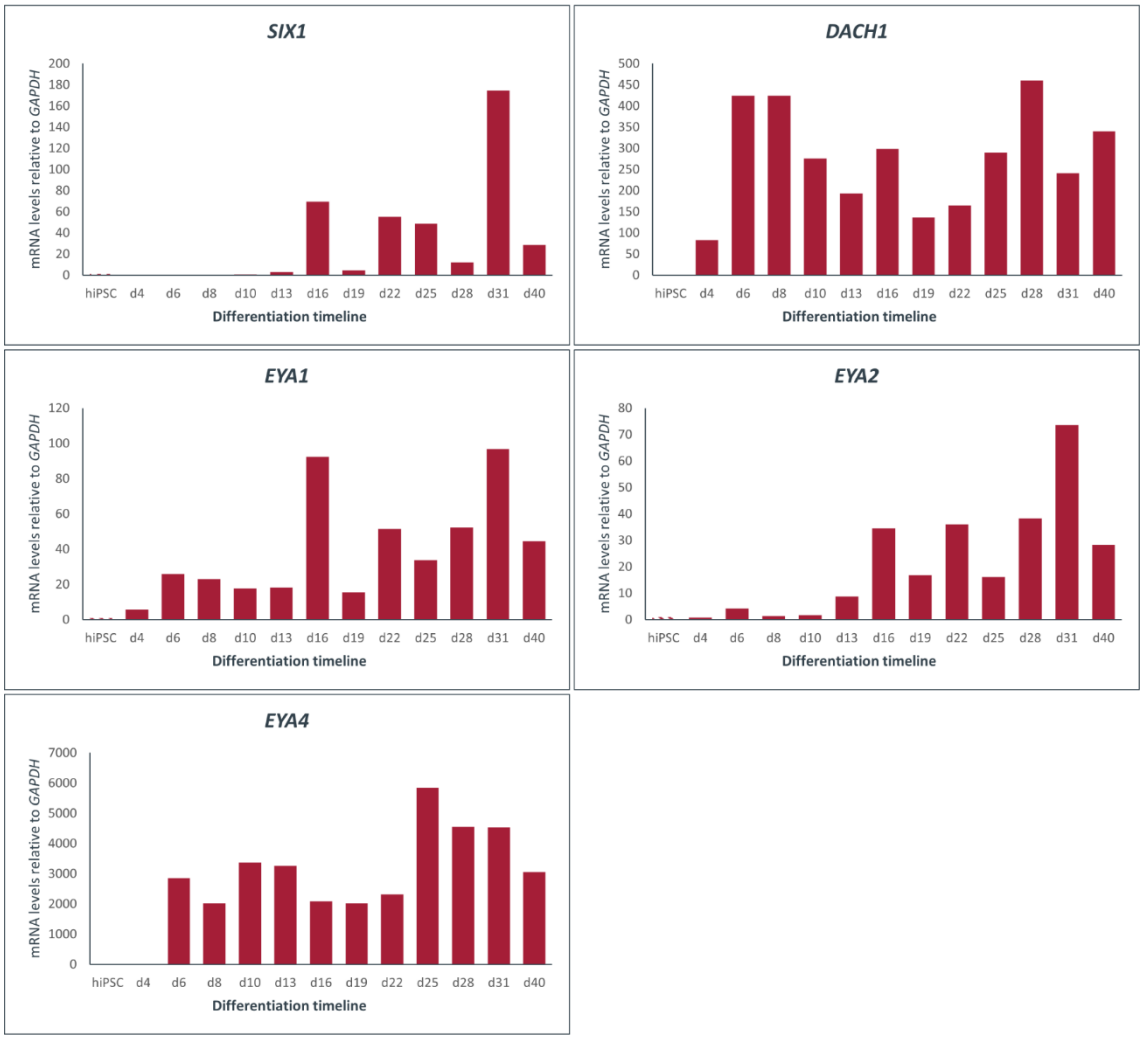

Figure 35: DOPEoids RNA expression timeline – PPR markers

Relative mRNA expression to *GAPDH*, normalized to hiPSC expression on days 4 to 40 of the DOPEoid differentiation.

The expression of *SIX1*, a key marker for the PPR, the anterior placodal region and later the OP, starts to exceed expression in hiPSC in the DOPEoids by day 13. From day 16 onwards, *SIX1* is generally highly expressed in the DOPEoids, with some fluctuations.

Elevated expression of *DACH1*, also a key regulator of the primitive NNE and PPR / CP, can be observed by day 4. Hereafter, high expression of *DACH1* can be measured in the DOPEoids with some fluctuations.

Compared to hiPSC, elevated expression of *EYA1* and *EYA2* can first be observed on day 4 and day 6, respectively. The expression of these PPR and CP marker genes can be observed as high / rising hereon after in the differentiation with some fluctuations.

Elevated expression of *EYA4*, also an important PPR / pan-placodal marker can be first observed on day 4, but higher can be seen from day 6. From day 8 to day 40, the expression stays generally high, with some fluctuations.

6.4.3 DOPEoids RNA expression timeline – forebrain markers

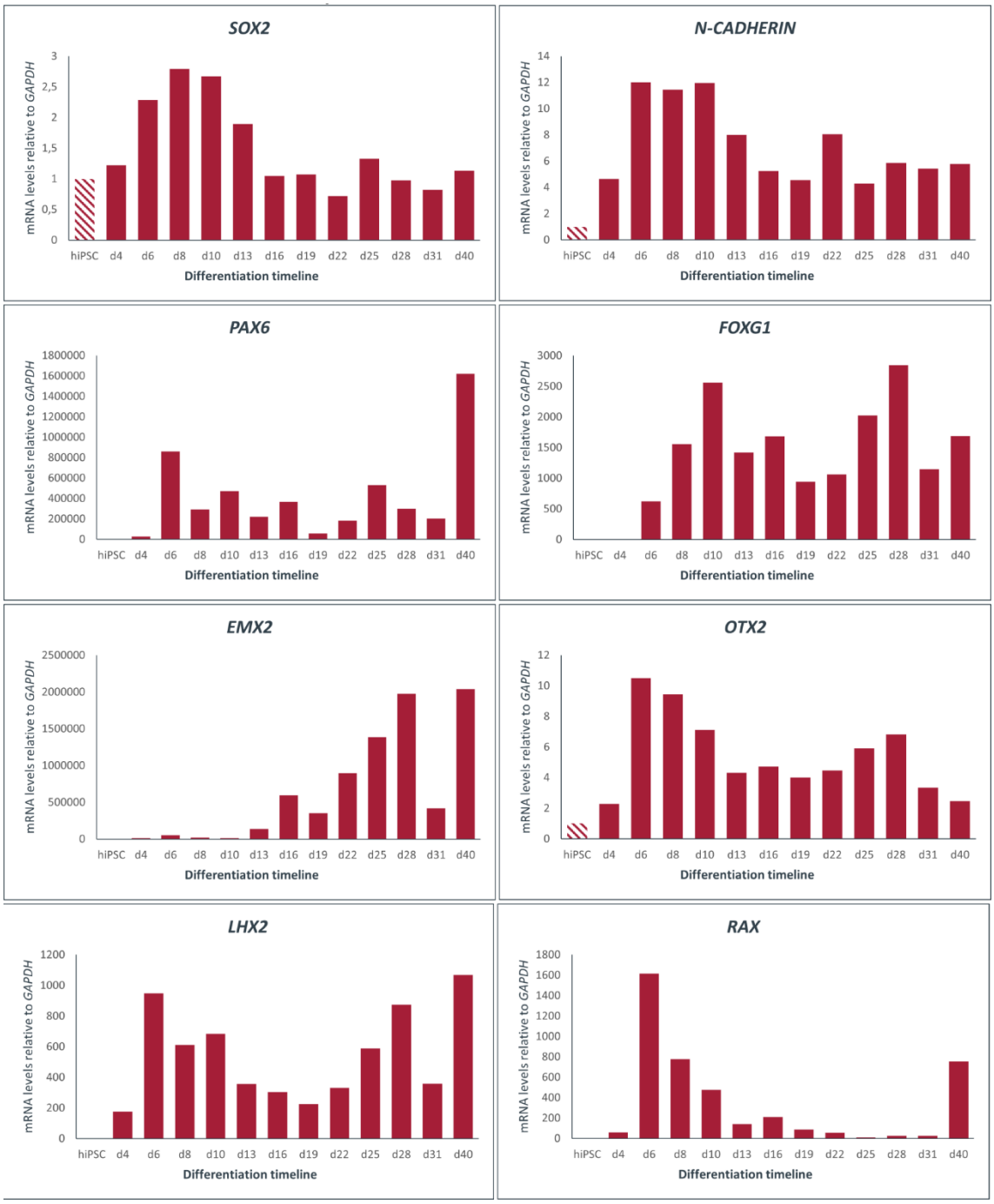

Figure 36: DOPEoids RNA expression timeline – forebrain markers

Relative mRNA expression to *GAPDH*, normalized to hiPSC expression on days 4 to 40 of the DOPEoid differentiation.

SOX2, being highly expressed in hiPSC as well as other stem cells like neural progenitor cells, shows a peak expression at day 8 of the differentiation. From day 16 onwards, a sustained expression can be observed.

The expression pattern of neural cell-adhesion component *N-CADHERIN* is similar to the one of *SOX2*, although it is not as highly expressed in hiPSC. *N-CADHERIN* expression also peaks between day 6 and day 10 and decreases afterwards but shows a sustained high expression from day 16 onwards.

Elevated expression of the early neural / forebrain marker *PAX6* starts on day 4 and rises on day 6. Form here, the *PAX6* expression stays high, although with some fluctuations.

FOXG1, an important marker of the anterior telencephalon, but also neurogenic placodes, shows increased expression from day 4. A sustained, high expression can be observed from day 6 onwards, with some fluctuations.

The expression of the dorsal telencephalic marker *EMX2*, which can also be found in the OP, shows an increased expression starting on day 4 but then increases from day 13 onwards with a late peak at day 40.

OTX2, an important marker for the posterior forebrain / ventral telencephalon, shows a peak in its expression on day 6. *OTX2*, also being a marker for the neurogenic placodes / OP, shows a relatively steady elevated expression from day 13 onwards. Here, the expression shows some fluctuations and is slightly down trending.

The expression of *LHX2*, also an important dorsal telencephalic marker, shows an early peak in expression at day 6. From day 16 to day 22, a steady and high expression can be observed. From day 25, *LHX2* expression rises again to a 2nd peak on day 40.

RAX, a ventral forebrain marker shows a peak in expression on day 6, but afterwards, its expression drastically decreases. On day 40, the expression of *RAX* shows jump in expression with a smaller 2nd peak.

6.4.4 DOPEoids RNA expression timeline – placodal & mesenchymal markers

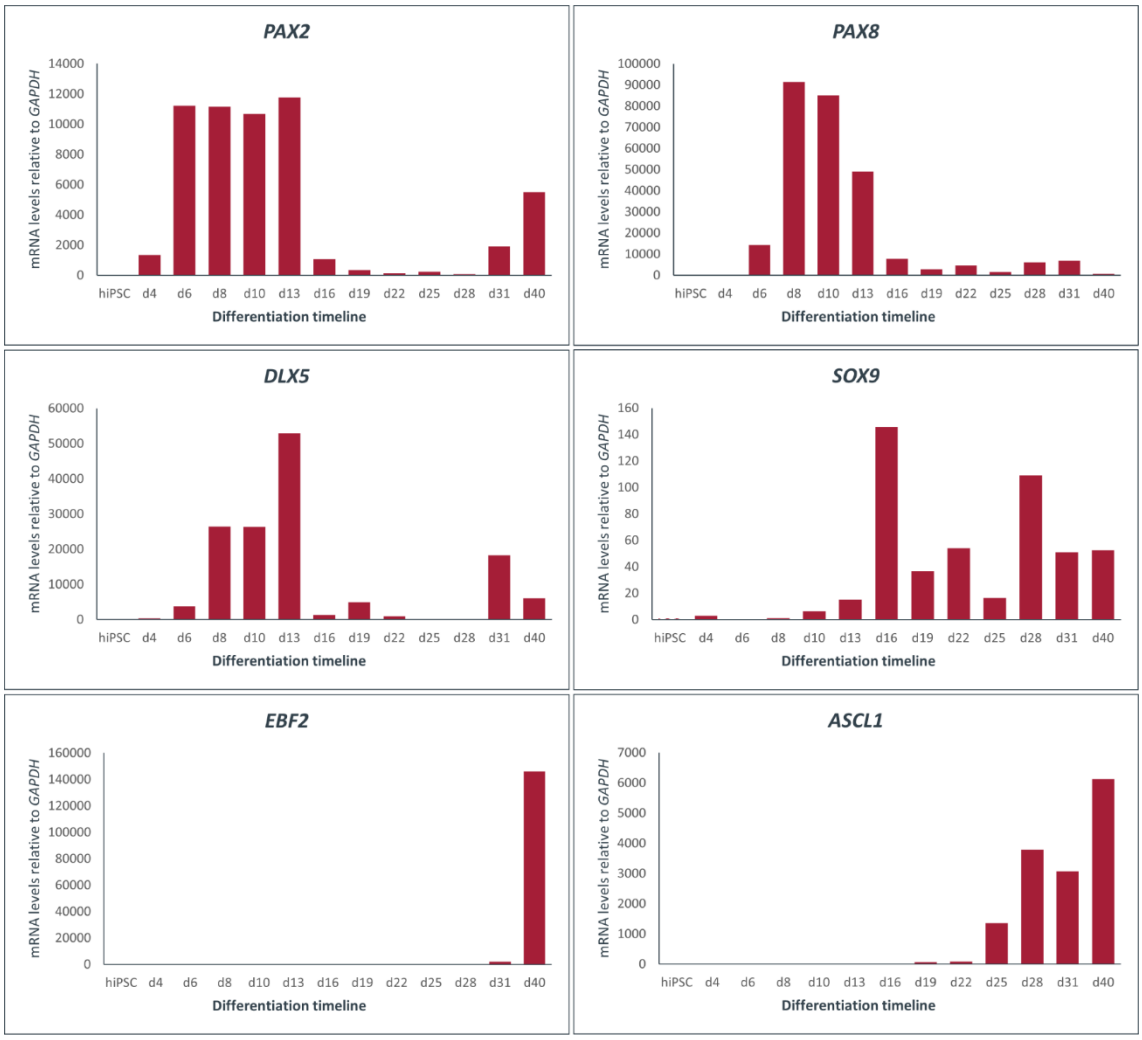

Figure 37: DOPEoids RNA expression timeline – placodal & mesenchymal markers

Relative mRNA expression to *GAPDH*, normalized to hiPSC expression on days 4 to 40 of the DOPEoid differentiation. Exception: *EBF2* expression normalized to day 19 since no expression was detected before.

PAX2, an important marker of the posterior placodal region and otic placode, shows high expression from day 6 to day 13 of the differentiation. From day 16 onwards, PAX2 is not highly expressed anymore, although with a 2nd peak of expression on day 40.

Likewise, *PAX8*, also an important posterior placodal and otic marker, shows a peak in expression on day 6 with a steep decrease in expression to day 16 and low expression hereon after.

The expression of *DLX5*, a marker of the early NNE and NB shows a high expression on day 8 to day 13 but is not generally highly expressed afterwards.

SOX9, a marker for head mesenchyme and the OP, shows a slight increase in expression from day 4 to day 10. From day 13 onward, the expression of *SOX9* is rising and shows clearly elevated expression, although with some fluctuations.

EBF2 mRNA can be first detected on day 19, and its expression is rising continually with a steep rise in expression on days 31 and 40.

ASCL1, also a neural progenitor marker of the OP, shows a steep rise in expression from day 19 onward with a peak expression on day 40.

6.5 DOPEoids protocol adaption – outlook

As shown above, DOPEoids are complex organoids, which integrate at least four different tissues within one aggregate. Since organoid development is largely dependent on tissue cross talk, which relies on healthy components with optimal growth conditions, the standard protocol was adapted to promote neural grown. The culture conditions were adapted from day 21 onwards based on brain organoid technology, as described in section **5.4.2.2**. On day 40, the DOPEoids from this modified protocol are analyzed for morphological maturation, mesenchyme, and surface epithelium markers, as well as definite olfactory marker EBF2 expression.

6.5.1 DOPEoids outlook – maturation & mesenchyme

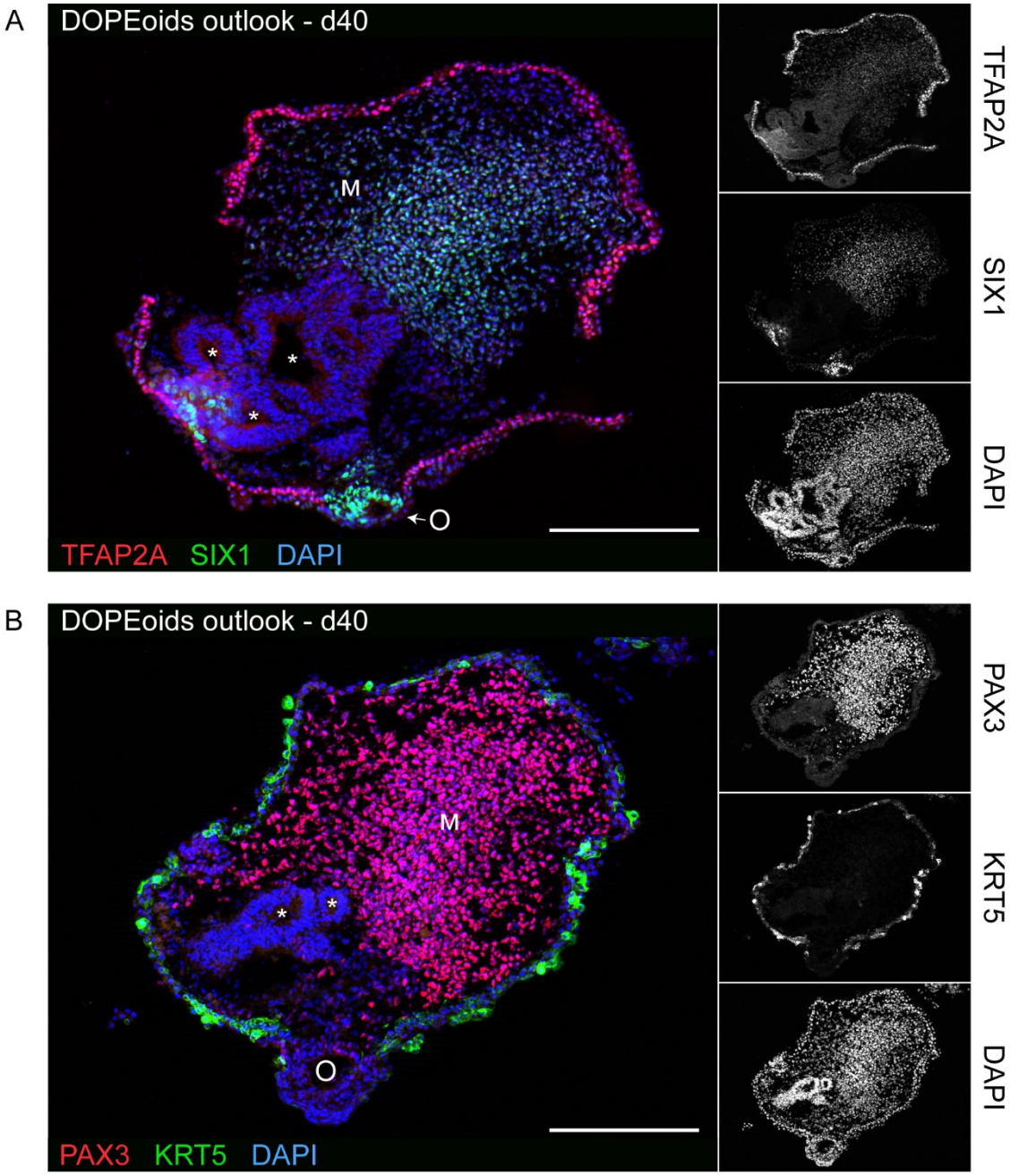

Figure 38: DOPEoids outlook: maturation & mesenchyme – d40

(A) organoid stained for TFAP2A (red) and SIX1 (green). (B) serial section of organoid from (A) stained for PAX3 (red) and KRT5 (green). Nuclei counterstaining with DAPI (blue). O marking invaginated placodal patch, asterisks marking neural tubuli, M marking head-like mesenchyme. Scalebars: 200 µm. **(A)** TFAP2A, SIX1 & DAPI. **(B)** PAX3, KRT5 & DAPI.

The neural tubuli inside the DOPEoids (lumen marked by asterisks) are thicker and show a more folded morphology compared to the standard protocol on day 31. The stratified cuboid surface epithelium shows a high expression of TFAP2A in basal cell layers and weaker expression in higher cell layers. Additionally, a prominent signal for KRT5, a basal cell marker of the developing skin, can be observed. A large compartment of $TFAP2A^{+}/SIX1^{+}/PAX3^{+}$ head mesenchyme-like cells can be observed between the neural tubuli and the surface epithelium (M). At 6 o´clock of the organoid, a surface epithelium covered vesicle can be observed, which is most likely product of the complete invagination of a pseudo-stratified placodal patch, similar to the formation of the nasal sac *in vivo* (O). This olfactory-like vesicle shows expression of olfactory placodal marker SIX1 but not TFAP2A. Also, some $PAX3^{+}$ cells can be observed in the olfactory-like vesicle. Furthermore, strong expression of neurogenic placodal marker FOXG1 (data not shown) and anterior placodal region marker SIX3 can be observed in this vesicle, as well as in the neural tubuli (**Supp. Fig. S3**).

6.5.2 DOPEoids outlook – definite olfactory progenitors

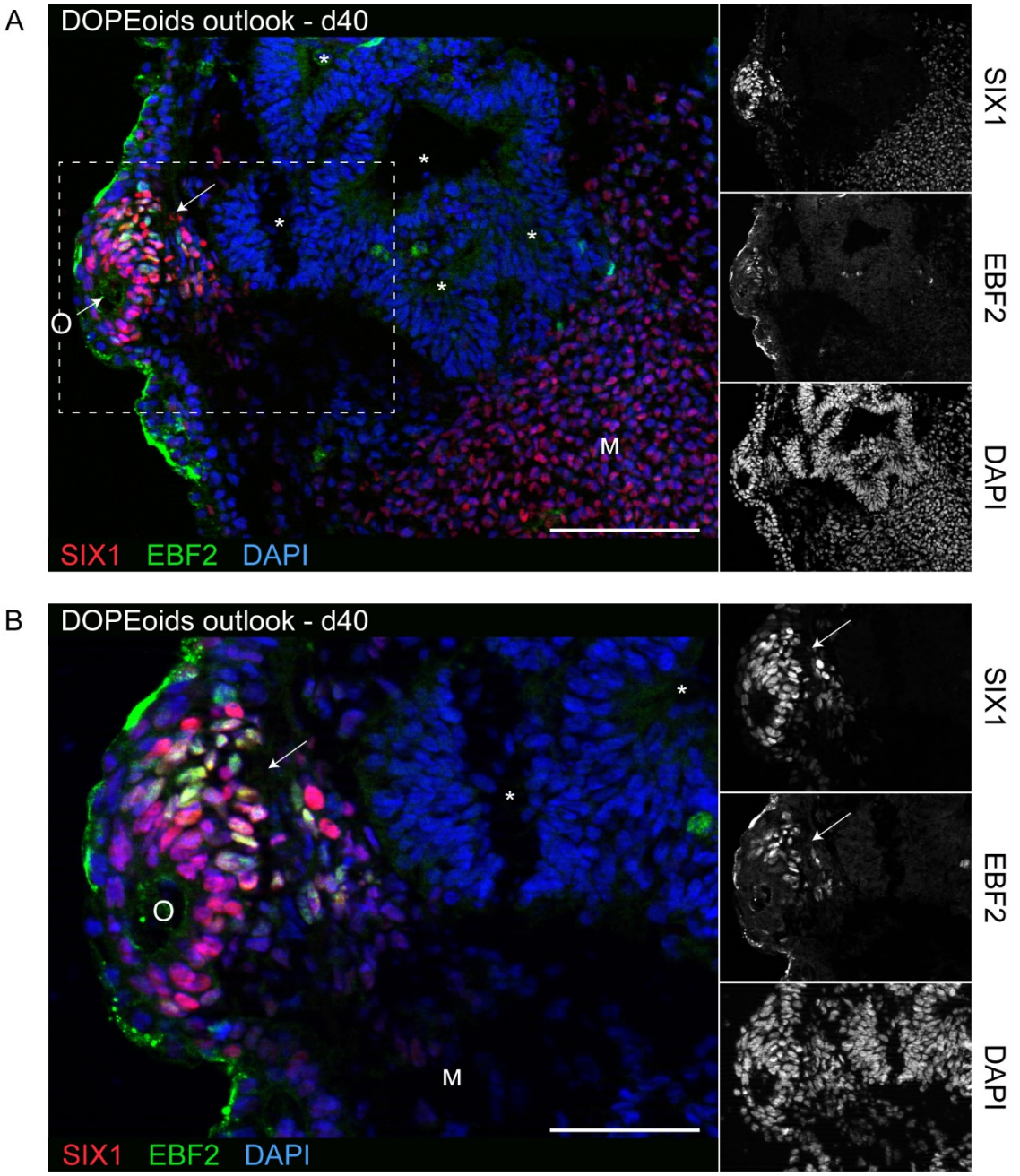

Figure 39: DOPEoids outlook: definite olfactory progenitors – d40

Same section as shown in **(Fig. 31 A)** stained for SIX1 (red) and EBF2 (green). Nuclei counter-staining with DAPI (blue). Dotted rectangle in (A) indicates area of higher magnification shown in (B). O marking invaginated placodal patch, arrow marking co-expression of SIX1 and EBF2, marking definite olfactory progenitors, asterisks marking neural tubuli, M marking head-like mesenchyme. Scalebars: (A) 100 µm, (B) 50 µm. **(A+B)** SIX1, EBF2 & DAPI.

The cells making up the pseudostratified olfactory-like vesicle are expressing olfactory placodal marker SIX1 (O). Some cells of the olfactory-like vesicle are co-expressing SIX1 and EBF2, a distinct marker for olfactory progenitors of neural lineage (arrows). EBF2 is also a marker of the developing brain, but here no expression can be found in the neural tubuli (lumen marked by asterisks). The thickness and increased folding of the neural tubuli inside the organoids becomes even more evident than in **Figure 38**. The head-like mesenchyme is made up of polygonal cells expressing SIX1 (M).

7 Discussion

7.1 Culture methods

7.1.1 Starting media

As starting media, the gfCDM as described for anterior pituitary organoids is used (89). Using the E1 cell line, the concentration of 5 % KOSR is sufficient to generate DOPEoids, although the group also describes possible cell line specific variations ranging from 5 % to 20 % KOSR requirement (154). For the otic organoids, a similar starting medium is used, although without KOSR but with insulin and transferrin supplementation. Nevertheless, KOSR may be crucial for DOPEoid development with some possible WNT and BMP agonists contained in this semi-defined supplement (see below) (95). To create a standardized and fully reproducible DOPEoid protocol, further efforts will need to be made to replace semi- and undefined products like BSA and KOSR.

7.1.2 Starting conditions

For the generation of DOPEoids, hiPSC are first dissociated into single cells and ~ 10 000 cells then plated into each well of an ultra-low attachment v-bottom 96-well plate in gfCDM. Unlike other PPR organoid protocols utilizing this SFEBq protocol, the EB formation is aided by centrifugation at 1000 rpm (188 g) for 5 min (80,89,96). The medium on day 0 is also supplemented with the small molecules Y-27632 (10 µM), a ROCK inhibitor, and Blebbistatin (10 µM), a non-muscle myosin II inhibitor. Both substances inhibit apoptosis after dissociation of hPSC into single cells and increase survival (173,176).

7.1.3 Early TGFβ & WNT inhibition

From day 0 to day 8 the medium is supplemented with SB431542, a small molecule inhibitor of the TGFβ pathway, and IWP2, a small molecule WNT pathway inhibitor, to create a forebrain and later telencephalic core in the organoids. Inhibition of TGFβ leads to a loss of pluripotency and blocks mesodermal and endodermal differentiation, whilst promoting ectodermal fate (82). WNT inhibition in combination with TGFβ disruption has been used by others to create telencephalic precursors and cortical organoids (83,158). For this study, the combination

of WNT inhibition and TGFβ inhibition was chosen over the dual SMAD inhibition (BMP inhibition + TGFβ inhibition) since BMP signaling is important for NNE formation and prolonged WNT inhibition is also necessary to promote $PAX6^+$ anterior placodal fates and block intermediate and posterior placodal fates (94). In accordance, the generation of $PAX2^+$/$PAX8^+$ otic organoids – being a derivative of the posterior placodal region – is reliant on WNT agonists (96).

Nevertheless, WNT signals are important for the formation of the NC and therefore the cranial mesenchyme, also found in the DOPEoids. The presence of the head-like mesenchyme can most likely be explained by the choice of IWP2 as an indirect WNT inhibitor and possible WNT agonist contained in the used KOSR (95,177). Since IWP2 inhibits PORCUPINE and hence the production of WNT agonists for para- or autocrine secretion, WNT agonists from the culture media can still promote NC formation. The formation and maturation of telencephalic-like structures in this environment might be enhanced by the expression of endogenous WNT inhibitors as DKK1 like *in vivo*, although this must be further elucidated (38). Interestingly, when IWP2 is substituted with IWR1e, another small molecule inhibitor of WNT, the differentiation fails to produce DOPEoids / any organoids with a $TFAP2A^+$/E-$CADHERIN^+$ surface epithelium (n=6, 2 different cell lines; data not shown). In contrast to IWP2, IWR1e is a TANKYRASE inhibitor, which leads to the intracellular destabilization of β-CATENIN and hence intracellular WNT signal disruption (177). It follows, that extracellular signals from the KOSR supplement would likewise be blocked by IWR1e. Instead of DOPEoids, either non-DOPEoids or cortical-like organoids are created under those conditions, highlighting the importance of some remnant WNT signaling for DOPEoid and NC formation.

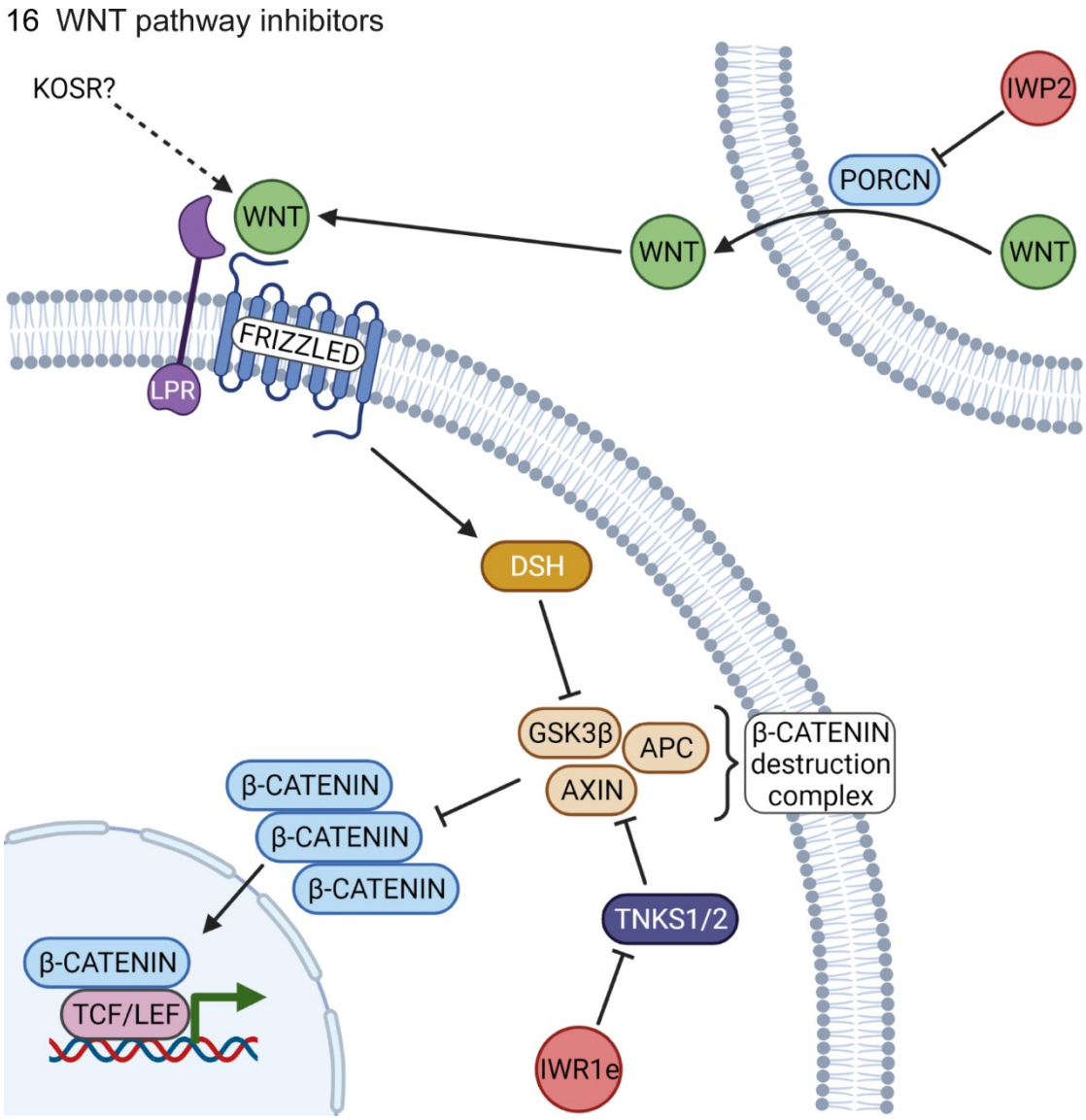

Figure 40: Canonical WNT pathway inhibitors

Schematic pathway cascade of the canonical WNT pathway with IWP2 and IWR1e (red) as inhibitors. WNT (from auto- paracrine secretion and possibly the KOSR) binding to FRIZZLED and LPR as co-receptor, activating DSH, which destabilizes the β-CATENIN destruction complex, allowing for the built-up β-CATENIN and its translocation to the nucleus, co-activating gene expression of target genes. IWP2 as PORCUPINE inhibitor, hindering the palmitoylation and therefore transmembrane transport of WNT, inhibiting autocrine and paracrine signaling. IWR1e as TANKYRASE inhibitor, disinhibiting the β-CATENIN destruction complex and leading to increased β-CATENIN destabilization. Figure created with BioRender.com.

7.1.4 BMP4 and Phenanthroline

On day 3 of the differentiation, a high and short pulse of BMP4 (65 ng/ml) is used to induce an NNE-like surface ectoderm over the developing forebrain / telencephalic core and induce a NB within this ectoderm (91). From day 5 to day 8, BMP signaling was blocked using the small molecule LDN193189 (100 nM), since the

formation of the PPR is dependent in low BMP signaling after an initial BMP4 exposure (91). The BMP4 concentration to induce a NNE used here is significantly higher than given in the literature (ranging from 2.5 to 10 ng/ml) (94–96,156). Higher BMP4 requirements can be explained to some extent by line specific BMP4 intrinsic activity (156), but these levels may be supratherapeutic and their re-titration more economic. The formation and maturation of a TFAP2A$^+$/E-CADHERIN$^+$ surface epithelium on the DOPEoids in the absence of exogenous BMP signaling at later timepoints might be explained by possible expression in the DOPEoids and / or BMP agonist in the KOSR used (95).

On day 3 to day 5 Phenanthroline (10 µM), a small molecule that has been shown to enhance SIX1$^+$ CP-like cells, is added (95).

7.1.5 Maturation

The prolonged addition of SB431542 (10 µM) until day 26 in combination with FGF2 (20 ng/ml) exposure is used to promote PPR / CP fate, as described before in 2D conditions (95). Extended exposure to FGF2 is also known to promote forebrain fates (178) and FGF2 signaling is inhibiting lens fates (92). The addition of FGF8 (100 ng/ml) from day 9 to day 26 together with FGF2 and SB431542 can be contradicting. Although there are some implications that FGF8 can act as a caudalizing factor in CNS development (178), it is also known to be an important morphogen for the adaption of olfactory placodal fate in the anterior placodal region (47,179). Some caudalizing effects on the forebrain / telencephalic core could explain the co-expression of posterior forebrain / diencephalic marker OTX2 with anterior forebrain / telencephalic maker FOXG1 and dorsal forebrain marker PAX6 (see below).

From day 27 to day 40, GDNF, BDNF, cAMP and Vitamin C are added to promote neural maturation and differentiation (157,178).

7.1.6 Hypoxia and ECM – key differences to other protocols

The DOPEoid differentiation protocol utilizes incubation at 37 °C with 5 % CO_2 under hypoxic conditions (5 % O_2), whilst other placodal or ectodermal organoid protocols generally use normoxic conditions (20 % O_2) (89,96,156). Interestingly, these hypoxic conditions are necessary to generate a TFAP2A$^+$/E-CADHERIN$^+$

surface epithelium around the telencephalic core. When cultured under normoxic conditions from the start of the differentiation, the generated organoids show a non-DOPEoid or a brain organoid character with a thick, pseudostratified columnar epithelium expressing neural markers on the outside of the organoids (n=6, 2 different cell lines; data not shown). Although hypoxia is not directly implicated in NNE formation and other groups have induced NNE under normoxic conditions, hypoxia may be necessary to closely mimic the embryonic conditions *in vivo*, since mammalian development occurs under hypoxic conditions (180,181). In accordance to that, hypoxia induced factors (HIFs) have been shown to play a role in embryonic development (181). For example, the production and migration of cranial NC cells is heavily dependent on hypoxic conditions, as normoxia limits their production and migration *in vivo* (182). Also, early mammalian embryos grown in normoxic conditions showed severe craniofacial impairments and faithful culture in normoxia was only possible at later timepoints, highlighting the importance of hypoxia for craniofacial induction (182,183). With the generation of four tissue types within the DOPEoids, they are likely closer to the situation of the developing head than pituitary or otic organoids, since pituitary organoids do not incorporate a mesenchyme and otic organoids are oriented inside-out (89,96). Although necessary for initial induction of a four-tissue DOPEoid with an outside-out orientation, a later increase in oxygen concentration may be necessary to improve maturation, similar to the situation *in vivo* (182).

In contrast to other organoid protocols, the DOPEoid protocol does not require the use of exogenous ECM components like embedding organoids in Matrigel® or adding Matrigel® to the culture media. This synthetic extracellular scaffold is sometimes needed for brain organoids, since they do not include basement membrane building mesenchymal cells, which hinders faithful cellular organization (184,185). Otic organoids also utilize ECM components for stabilization and maturation, since their NNE is oriented towards the inside (96). The use of added ECM components is not necessary for DOPEoid formation since the DOPEoids exhibit a *in vivo*-like outside-out orientation and a NC derived head mesenchyme building two stable basement membranes – one for the neural tubuli and one for the surface ectoderm. This renders the DOPEoids closer to the situation *in vivo*

and simplifies their culture whilst also reducing semi-defined substances as Matrigel®.

7.1.7 Summary – pushing towards an OP

The DOPEoid differentiation protocol is based on two major principals: First, morphogenic cues for cell differentiation towards OP, telencephalic and NC fates are bath administered in a temporal fashion. Second, the embryonic concept of self-organization is utilized, after the initial induction of four different tissues within one DOPEoid.

This morphogen-based approach pushes placodal cells towards olfactory fate and not other placodes. Using BMP4 signaling with subsequent BMP inhibition and FGF signaling, cells are pushed towards a CP fate. With WNT antagonism, anterior placodal region identity is induced, whilst intermediate and posterior placodal identity is inhibited. Inside the anterior placodal region, using FGF2 the formation of a lens placode is inhibited, whilst FGF8 is inducing an OP. Finally, the organoids are not treated with SHH agonists, which are crucial factors for pituitary differentiation, inhibiting anterior pituitary differentiation (89).

7.2 NNE-like surface epithelium, PPR & Placodal patches

7.2.1 Surface epithelium – induction

A TFAP2A$^+$/E-CADHERIN$^+$ surface epithelium can be first observed as a simple squamous epithelium on day 8 and then as a simple cuboid epithelium by day 10. This NNE-like surface epithelium becomes stratified by day 13 and increases in thickness until day 31.

A strong argument for the NNE character of this epithelium can be made by the co-expression of TFAP2A$^+$/E-CADHERIN$^+$, which has also been used by others to define NNE in organoid culture (96). TFAP2A is a key transcriptional regulator in the early NNE as well as the PPR (39). E-Cadherin is a cell-adhesion molecule, which can be found exclusively in the NNE by late gastrula stages (186). The low-level expression of PAX6 in the surface epithelium on day 31 can be explained by possible PAX6 expression in the NNE in closer proximity to the eye anlage (187) or could be unspecific background. Likewise, the N-CADHERIN signal in

the surface epithelium is most likely background signal. The NNE-like surface ectoderm also expresses DLX3 and GATA3 (data not shown), which are also important markers for the developing NNE and later the PPR *in vivo* (39,46).

The timepoint at which the suspected NNE appears is later than in otic organoids (day 4 – 6) but earlier as in pituitary organoids (~ day 24) (89,96). This can be explained by a different induction strategy. Whilst in otic organoids, the NNE is directly induced and the otic placodes differentiated from this NNE, DOPEoids as well as pituitary organoids induce a NNE around a pre-induced CNS-like core (89,96). This explains the later appearance of the NNE in DOPEoids as well as pituitary organoids. The NNE appears earlier in DOPEoids compared to pituitary organoids, since in DOPEoids the cues for NNE induction are administered during forebrain induction, whilst in pituitary organoids, the oral ectoderm induction takes place after the hypothalamic tissue is induced (89). These different induction strategies may limit temporal comparisons between the different protocol.

During development, the future skin ectoderm is protected by a layer of squamous cells called “periderm”, which can also be recapitulated in skin organoids (156,188). Although no cells with a flat morphology can be observed in DOPEoids, it might be too early for periderm definition in the NNE, since in skin organoids it arises after ~ 50 days in culture (156). Since peridermal cells in DOPEoids could also have a more cuboidal morphology, it will take more extensive characterization of the NNE-like surface ectoderm in terms of keratin expression profiles.

7.2.2 Surface epithelium – PPR-like cells

On day 10 of the differentiation, the first cells co-expressing E-CADHERIN, TFAP2A and SIX1 appear in the surface epithelium, indicating NB or PPR-like cells. This is in accordance with the co-expression of SIX1 and TFAP2A in the early PPR, since the NB specifying gene TFAP2A induces the PPR marker SIX1 (46). These PPR like cells also show expression of placodal markers EYA 1 & 2, as well as NNE genes DLX3 and GATA3 (data not shown). DLX3 and GATA3 play important roles in the induction of the PPR and are later restricted to NNE fates (39,189). This combinational code makes a strong argument for these cuboidal surface epithelium cells to represent the NB and early PPR. This induction

of PPR-like cells in a NNE-like surface epithelium in the DOPEoids argues for the induction of the PPR in the NNE in humans, which has been suggested in other species (9).

On day 13 and day 16, most cells can be characterized as TFAP2A^{+}/SIX1^{+} PPR-like cells, but their percentage decreases on day 25 and they cannot be observed anymore by day 31. The reason for this could be, that initially – also under the influence of Phenanthroline – a lot of PPR like cells are induced in the NNE which lose SIX1 expression and return to their NNE origin after the first placodal patches emerge on day 16 (95). Another explanation could be sampling errors, that by chance a higher percentage of PPR-like cells was present in the sections than in the whole organoids, and that in fact most cells on days 13 and 16 are in fact still of non-PPR NNE character. This seems unlikely since the data can be reproduced in multiple differentiations and DOPEoids.

The emergence of clusters of SIX1^{+}/TFAP2A$^{-/low}$ cells on day 13 in the surface epithelium most likely marks the late PPR, since TFAP2A is down regulated in the PPR after initial PPR induction and specification (39). The transition of these SIX1^{+}/TFAP2A$^{-/low}$ cell clusters to the thickened placodal patches representing the anterior placodal region / CP is most likely fluid (see section below).

7.2.3 Placodal patches

By day 16 the first thickened placodal patches occur in the surface epithelium and become more thickened and pseudostratified from there on. These patches show a strong expression of PPR and CP marker SIX1. SIX1 is also an important marker of the OP and its development, with maintained expression in tissue stem cells of the adult OE in mice, which explains its constant expression in the placodal patches (190). These patches are negative for TFAP2A, which further strengthens the argument for placodal character, since Tfap2a is downregulated in the late PPR and CP (46).

As mentioned earlier, the transitions of late PPR to anterior placodal region and later CP / OP are most likely fluid and can´t easily be distinguished in DOPEoids, since the thickened pseudostratified patches mostly share their morphology and SIX1^{+}/TFAP2A^{-} expression pattern. During DOPEoid development, some

patches become concave and partially invaginate into the underlying mesenchyme. This process, which occurs in all anterior placodal region derived CP, but not in the intermediate placodal region derived trigeminal placode, provide a strong argument for anterior / olfactory character (9). As mentioned above, this invagination is a key hallmark of olfactory development as the nasal pit forms (63). The otic placode – a product of the posterior placodal region – also invaginates, although the WNT inhibition used in this protocol makes otic induction highly unlikely. One must note that not all placodal patches of the DOPEoids show signs of invagination. A possible reason for this may be different maturation stages, or varying signals from the underlying mesenchyme since invaginations are mostly observed in DOPEoids with a very prominent mesenchyme. Although invagination is an important step *in vivo*, it is not necessarily a hallmark in organoid-based CP formation. This has been demonstrated by Ozone and co-workers, who demonstrated functional anterior pituitary formation in hPSC derived organoids with the possibility but not necessity for invagination of these tissues into the underlying CNS tissue. (89). Likewise, DOPEoids can incorporate invaginating as well as not invagination OP-like structures.

7.2.3.1 Anterior placodal region

Other than the invagination of placodal patches and the sustained SIX1 expression also the expression of PAX6 on day 19 and SIX3 and OTX2 on day 22 in the patches indicate anterior placodal origin. As mentioned earlier the *PAX* genes are key factors in defining the A-P identity of the placodal ectoderm (45). The expression of PAX6 clearly identifies the placodal patches in the DOPEoids as of anterior placodal region origin since it is not expressed in the intermediate and posterior placodal fields (39). Furthermore, OTX2 and SIX3 are also important markers of the anterior placodal region and their expression in the placodal patches suggests anterior placodal fate (39,46). Since most of these transcription factors are expressed not only in the anterior placodal region, but also in the olfactory placode (see below) a clear discrimination between an anterior placodal field and a committed OP is hard. The only marker mentioned here not expressed in the OP is PAX6, since it is down regulated as soon as the OP is induced from the anterior placodal region (47). This being said, there appear to be some

interspecies variations since Pax6 expression can be observed in the OP of mice (191). Similarly, PAX6 is expressed in the developing human OE at later stages (192). In the DOPEoids, PAX6 expression can be observed in the placodal patches on day 19 but is lost on day 31. This argues that, mimicking the situation *in vivo* – at least in some species – PAX6 is downregulated during OP development *in vitro* but may be upregulated again later in DOPEoid development when the OP matures to an OE. Concluding, day 19 most likely represents a state resembling the anterior placodal region, whilst day 31 marks the OP. Further studies are needed to characterize the PAX6 expression pattern in DOPEoids and assess, if PAX6 is upregulated again at a later timepoint in OE-like tissue.

Since an invaginating patch can be observed on day 21 – representing a hallmark of olfactory development and therefore possible OP – it is possible that the margins between the anterior placodal region and the OP are fluid and that some variations in the developmental timeline (+/- some days) can be observed across DOPEoids. To further elucidate this switch and clarify the timeline, a more detailed temporal characterization of marker expression across DOPEoids is needed.

7.2.3.2 Olfactory placode

When the marker expression of the DOPEoid placodal patches is analyzed, not only their anterior placodal origin, but also their olfactory fate becomes evident. The OP is the only neurogenic placode in the anterior placodal region and hence transcription factors for neural determination are of great importance for its development (9).

The expression of SIX1 and SOX2 is very prominent in the placodal patches. It is generally accepted, that under the influence of an underlying nasal mesenchyme these two factors are key for the ability to generate neurons (45). Given the fact, that the OP is the only neurogenic placode from the established anterior placodal field, these cells most likely indicate olfactory character. Although Six1 is broadly expressed in placodal tissues, as well as meso- and endoderm, its expression is lost in the prospective lens placode (9,45,81,193). The expression of both, Six1 and Sox2 is retained throughout olfactory development and can be

found in the stem cell population of the adult OE in mice (190). Likewise, the trigeminal placode also co-expresses Six1 and Sox2 in some but not all species, although not derived from a $Pax6^+$ anterior placodal region and without invagination (39,44).

Whilst Sox2 expression can also be found in the lens placode, the co-expression of SIX1 and SOX2 in a $PAX6^+$ anterior placodal region derived patch indicates olfactory fate (57,191).

Also the expression of SIX3 in the patches points not only towards anterior placodal fate, but also to olfactory fate, since Six3 is also expressed in the OP of mice as well as the neighboring forebrain (194). Similar, the expression of OTX2 in the placodal patches also points in the direction of the OP, since Otx2 is not only expressed in the anterior and intermediate CNS regions, but later also in the invaginating OP and developing OE (9,78). Six3 and Otx2 expression can also be found in the lens placode, but the combinational code of transcription factors makes olfactory fate much more likely (9,194).

The expression of FOXG1 in the placodal patches is also evidence for olfactory fate, since FoxG1 is known to be expressed in the OP and important for olfactory neurogenesis (9,57). Later in development, FoxG1 expression is maintained in the OE and marks GBC and HBC in adult mice (190). In model organisms, FoxG1 is expressed in the anterior placodal region and later lost in the prospective lens placode, whilst the OP remains expressing high levels of FoxG1(9). FoxG1 also plays an important role in the development of the inner ear (39).

The expression of neuronal marker TUBB3 in the placodal patches clearly indicates the character of a neurogenic placode on day 31 in the DOPEoids. Since the OP is the only neurogenic placode derived from the anterior placodal field, this evidence points towards olfactory fate of these placodal patches. TUBB3 can be found in the OP of mice and in the OE, TUBB3 is a marker of immature OSN in humans (25,195). Likewise, the bipolar character of these cells, which is shared with mature and immature OSN, indicates a sensory neuronal identity, indicative of an immature OE / OP (28).

The expression of E-CADHERIN and N-CADHERIN can also be observed in the placodal patches of the DOPEoids. This could be attributed to an unfaithful switch from surface E-CADHERIN expression to N-CADHERIN expression in some cells, or – more likely – the co-expression of E-CADHERIN and N-CADHERIN in the placodal patches, as seen in the developing CP, especially the OP (186,196–198). The different morphology can be explained by difference in morphology compared to the stratified cuboidal surface epithelium and possibly by the redundancy of N-CADHERIN and E-CADHERIN as cell-adhesion molecules, allowing the relative down regulation compared to the non-N-CADHERIN expressing NNE-like surface epithelium.

Taken together, although no feature (patch morphology, invagination, timeline or expression of a sole marker) can define the placodal patches in the DOPEoids as OP-like patches, their combination makes a strong argument for olfactory fate. Specifically, the appearance of invaginating patches most likely originating from an anterior placodal area-like patch expressing PAX6, together with the expression of an OP-specific marker combination, gives strong evidence for the olfactory fate of the DOPEoids.

7.2.4 RNA level – surface epithelium, PPR & placodal patches

As mentioned before, the DOPEoids RNA data until day 28 originate from 4 pooled pre-selected DOPEoids from one differentiation (n=1), whilst day 31 and day 40 originate from three and two differentiations, respectively (n=3; n=2). This means, that the data discussed here and in the following sections on RNA data does not hold up to statistical interpretation and can only be regarded as “hints”. The interpretation of this RNA data should be seen with caution, as true effects might be masked and more data must be gathered in order to make firm claims, supported by statistical analysis.

Furthermore, the RNA was isolated from whole DOPEoids and hence conclusions about the expression of a certain cell population have to be made with caution. Nevertheless, the RNA data does give some interesting clues about the character of the DOPEoids and is generally in line with the protein level-based insights about DOPEoids and their olfactory fate.

The relatively low expression of *E-CADHERIN* during the DOPEoid differentiation can be explained by the high expression of *E-CADHERIN* in hiPSC, whilst in DOPEoids it is only expressed in the surface epithelium (199). The *E-CADHERIN* expression on day 4 is most likely due to remnant *E-CADHERIN* expression after the loss of pluripotency, matching the observations on a protein level. From day 8 – when an NNE-like surface epithelium starts to form – the *E-CADHERIN* expression starts to increase and reaches a peak on day 16, as the epithelium becomes stratified. Although the surface epithelium grows in thickness until day 31, the relative *E-CADHERIN* expression decreases (with a spike on day 28, which is most likely an outlier). This general decrease in surface epithelial signal can be explained by the decrease in surface-area-to-volume ratio (A/V) as the DOPEoids grow. Since the DOPEoids can be idealized as a mathematical ball, their surface area, volume, and A/V ratio can be calculated using the following equations:

Surface area (A): $A = 4\pi r^2$

Volume (V): $V = \frac{4}{3}\pi r^3$

Surface-area-to-volume ratio (A/V): $\frac{4\pi r^2}{\frac{4}{3}\pi r^3} = \frac{3}{r}$

Estimating the radius of a DOPEoid on day 8 as 150 µm and on day 31 as 300 µm, the A/V ratio halves from 20 000 m^{-1} to 10 000 m^{-1}. This means that since the surface area of a DOPEoid is expanding by the power of 2 and the volume is expanding by the power of 3, the RNA signal originating in the surface epithelium is being "diluted" by the cells in the core. The result of this is the decrease in relative RNA expression in the bulk, even though the expression is not necessarily decreasing in the surface epithelium.

Similar results can be seen with the expression of the other epithelial markers *TFAP2A*, *DLX3* and *GATA3*, which play also an important role in PPR commitment (39). All of them are very highly expressed in the DOPEoids compared to hiPSC, which is due to low expression rates in the hiPSC and high expression rates in the DOPEoids.

TFAP2A and *GATA3* show a steep increase in expression on day 13 and peak at day 16, similar to the expression of *E-CADHERIN*. This also underlines their importance in PPR specification, since PPR-like cells are especially prominent in staining on days 13 and 16. From day 16 the expression is generally down trending due to the mentioned change in A/V ratio, although with some fluctuations, which can be explained by variability across the DOPEoids. The relatively slow downtrend and high expression of *TFAP2A* later in the DOPEoids can also be explained by its expression not only in the surface epithelium but also in the head mesenchyme-like compartment, since TFAP2A is also expressed in the nasal mesenchyme during human development (192). This also matches the observations of a high TFAP2A expressions in the mesenchyme compartment found in the staining of DOPEoids.

The expression of *DLX3* is similar, although with an increase in expression starting on day 4 and peaking again at the PPR stage around day 13 and day 16, followed by a downtrend. The early rise in *DLX3* may be explained by a possible early role on NNE induction. Furthermore *DLX3* is also a marker for the OP, which might explain its relatively high expression from day 25 to day 40 (200).

The relatively low expression of the epithelial markers *E-CADHERIN*, *TFAP2A*, *DLX3* and *GATA3* on day 10 is most likely the result of an outlier bulk / DOPEoid with low epithelial proportion.

DLX5 is also a gene of great importance in early NNE commitment and PPR formation, which explains its high and early expression during days 8 – 13 (9). Later in development, *DLX5* is upregulated in the olfactory and otic CP, which can explain the rise in expression in the DOPEoids on day 31 and 40 (9) (201,202).

KRT5, which is an important marker for basal cells of the developing epidermis and OE, can be first detected on day 19 and rises to peak on day 40, which can be explained by the maturation of the surface NNE in the DOPEoids to an immature, stratified epidermis expressing *KRT5*. Roughly in the same timeframe, KRT5 expression can be seen in skin organoids on day 55 (156).

Other than *TFAP2A*, *DLX3/5* and *GATA3*, the *SIX*, *EYA* and *DACH* genes are also of great importance in PPR development (45). The expression of *SIX1* and *EYA2* drastically increases on day 13 and 16, implicating upregulation during PPR induction. *EYA1*, *EYA4* and *DACH1* are already highly expressed at an earlier timepoint (day 4 and day 6), suggesting some role in NNE commitment. Interestingly, *SIX1*, *EYA1/2/4* and *DACH1* show a relatively steady expression or even a rise in expression (with some fluctuations), even though they are markers for the PPR which is generated in the surface epithelium. This can be explained by the fact that Six1, Eya2 and Dach1 can also be found in the nasal mesenchyme, and Dach1 protein expression can also be found in the developing forebrain (194,203). Possibly, the expression of *EYA2* and *EYA4* can also be explained by expression in the nasal mesenchyme, although this must be further elucidated. Furthermore, the sustained and / or increasing expression of these markers also points towards an increase in expression not only in the nasal mesenchyme, but also in the surface epithelium / placodal patches, since Six1 and Eya1 are also important markers for the OP and other neurogenic placodes (45).

The sustained expression of *PAX6* can be interpreted as evidence for an anterior placodal region, matching the data on a protein level, although it is also highly expressed in CNS tissue and therefore the neural tubuli of the DOPEoids.

Besides the sustained expression of *SIX1*, *EYA1/2/4*, *DACH1*, and *DLX5*, other marker genes can be used to argue for OP-fate in the DOPEoids. As mentioned earlier, *FoxG1*, *Otx2*, *N-cadherin* and *Sox2* are also important markers for the OP and high expression of these genes can be found in the placodal patches of DOPEoids (57,78,191,196,198). As neural markers, this high expression can be largely led back to expression in the neural tubuli, but since they can be found in the placodal patches of DOPEoids on a protein level, these genes are likely also expressed on an RNA level in the placodal patches, indicating OP. Future studies, investigating the expression patterns in different tissues of the DOPEoids will be needed to prove and characterize the expression of these neural / OP genes in the placodal patches.

Emx2 and *Lhx2* are generally highly expressed in the developing forebrain, which largely explains their human ortholog expression in the DOPEoids, but they are also later markers for the OP (190,204,205). *Lhx2* expression is even maintained in the murine adult OE (190). Hence, the expression of *LHX2* and *EMX2* can in part be a result of expression in placodal patches of the DOPEoids, although LHX2 was not detected in the placodal patches and *EMX2* was not analyzed on a protein level. *Emx2* is not only expressed in the OP / OE, but also in the otic placode, although the combinational signature with other markers makes the OP far more likely (205). To make clear statements about the expression of *EMX2* and *LHX2* in the placodal patches of the DOPEoids, they must be examined more thoroughly on a protein level and the RNA expression of isolated patches must be analyzed.

From day 13 onwards the expression of *SOX9* – a marker of NC derived head mesenchyme, the otic placode and the OP – is also rising with some fluctuations (206). This can be due to a growing nasal mesenchyme in the DOPEoids, but also expression in OP patches can play a role. Since the DOPEoids were not stained for SOX9, further studies have to characterize the *SOX9* expression in the placodal patches and mesenchyme compartment of the DOPEoids.

Ebf2 and *Ascl1* are two transcription markers specific for the OP and OE, since they play a key role in the lineage commitment of ORN (25,45,207–209). In the DOPEoids, *EBF2* expression increases on days 31 and 40 after *ASCL1* shows a steep rise in expression from day 19 onward. This matches data, indicating *Ebf2* as a downstream target of *Ascl1* in neuronal development (210). *Ebf2* and *Ascl1* are also markers of the developing CNS, but the outlook data with the modified DOPEoid protocol shows EBF2 expression in the OP-like vesicle but not in the neural tubuli, making the case for OP origin of this RNA signal (210). *EBF2* and *ASCL1* have to be further assessed in the future.

7.2.5 Exclusion of other placodes

Most of the markers described above can also be found in the otic placode. A strong case against the presence of the otic placode can be made by the RNA expression profile of *PAX2* and *PAX8*, both important markers of the otic placode

(96). *PAX2* and *PAX8* are highly expressed early before the induction of the placodal patches in the DOPEoids, but downregulated afterwards, implying the absence of posterior placodal region and otic placode like cells. Although *PAX2* shows a peak in expression on day 40, the absence of highly expressed *PAX8* makes the otic placode rather unlikely. Likewise, PAX2 and PAX8 staining did not show expression in the placodal patches (data not shown).

The other placodes can be excluded by the combinational code of transcription factor expression which is specific for the OP: The lens placode can be excluded by the expression of SIX1 in the placodal patches of the DOPEoids and the non-neurogenic anterior pituitary placode can be excluded by the expression of TUBB3 (39,193). The trigeminal placode can be excluded by the invagination tendency of the placodal patches and the transitory PAX6 expression, marking anterior placodal ectoderm (39).

The expression of *ASCL1* and *EBF2* as OP specific markers resembles a strong 2nd line of evidence for the presence of an OP and excludes other placodes. Nevertheless, arguments for the OP against other placodes are mostly based upon the expression of a marker combination specific for the olfactory region in the absence of an otic placode. In the future, the exclusion of other placodal structures by a broader marker study, as well as the identification and analysis of more OP specific markers seems intriguing to further strengthen this evidence.

7.2.6 Surface epithelium, PPR & placodal patches – conclusion

The timeline, morphology and marker expression indicate that the surface epithelium on the DOPEoids resembles the NNE in an *in vitro* model. In this epithelium – closely mimicking the developmental timeline *in vivo* – a PPR and later an anterior placodal region arises, as indicated by anterior PPR specific marker combinations. From this anterior placodal region in the DOPEoids a partly invaginating OP arises which will presumably give rise to a human OE if cultivated and matured further. The marker combination specific to the OP as well as the exclusion of other placodes indicates the induction of cells of olfactory fate, which develop similar to the situation *in vivo*.

To my knowledge, this is the first recapitulation of the (human) olfactory development with a faithful induction of a (human) OP in a 3D organoid model. The DOPEoids are a major milestone on the way to a fully functional olfactory organoid model system and will be the foundation for further research. In the future, efforts to mature the DOPEoids with their OP and analyze the character of its cells will bring more insight on the human olfactory development and greatly enhance neurobiological research possibilities *in vitro*.

7.3 Neural tubuli

7.3.1 Neural tubuli - morphology

On day 16 the first neural tubuli with a flat / cuboid cell shape emerge, which then mature to columnar / pseudostratified neural tubuli with an increased wall thickness. The thickness further increases to reach a maximum on day 31. This appearance of radially oriented, neural tube-like tubuli which increase in thickness with dominant pseudostratification somewhat resembles the CNS maturation *in vivo* and has likewise been demonstrated in several brain organoid models (72,76,157,158). Nevertheless, the DOPEoids neural tubuli are significantly less dense and thick than their brain organoid counterparts. This is due to the fact that the maximum age of DOPEoids was 31 or 40 days for protein and RNA level, respectively. In contrast to that, some brain organoid protocols cultivate organoids for > 2 months to reach full development (72). Nevertheless, some brain organoid protocols also generate significantly thicker tubuli by day 20, which can be explained by cell culture conditions, specifically adapted to CNS organoid formation (76). As mentioned earlier, one major contrast is the normoxic / hyperoxic condition used in brain organoid cultivation, whilst the DOPEoid protocol relies on hypoxic conditions to induce an NNE-like surface epithelium. The modified DOPEoid protocol which gives rise to more mature DOPEoids as presented in the outlook data, has an increased oxygen concentration (20 % O_2) from day 21 onward and its protocol is adapted after brain organoid protocols (72,157). This led to an increased thickness of the neural tubuli, indicating a more mature neural tissue under these circumstances. Other brain organoid protocols also make use

of agitation to increase the nutrient and oxygen supply to the center of the organoids (72).

The circular appearance of the neural tubuli may imply an anterior / dorsal CNS character, since ventral hypothalamic-like tubuli are more elongated (76). Nevertheless, this can also be caused by the absence of a spinning bioreactor in cell culture, since dorsal forebrain-like tissues also show an elongated morphology if cultured using a spinning bioreactor (72).

Taken together, the DOPEoids show the development of neural tubuli as seen in brain organoids, although their maturation is still inferior compared to pure brain organoid protocols. In the future, further modifications like agitation, normoxic conditions and neural media will be useful to further increase the maturation of the neural tubuli and hence the whole DOPEoid, as indicated by the outlook data.

7.3.2 Neural tubuli – protein data

The marker expression on a protein level in the immunofluorescence staining also indicates the neural fate of the tubuli in the core of the DOPEoids. Prior to the emergence of the tubuli on day 16, the core already expresses the neural / forebrain markers SOX2, SIX3, PAX6, OTX2 and FOXG1, all of which are important markers for neural progenitors and the developing forebrain (72,76,78).

Later, when the pseudostratified neural tubuli arise and thicken, SOX2 is still expressed, indicating the neural progenitor character similar to the cells in the *in vivo* SVZ (211). The expression of SIX3 in the tubuli can also be explained by telencephalic fate, since Six3 is upregulated in various telencephalic structures like the developing cortex and the ventral *telencephalon* (212).

Later in development, PAX6 and FOXG1 are both markers of the anterior and dorsal telencephalic neocortex and expressed in the neural tubuli of the DOPEoids (74,76). In contrast to that OTX2, although being an early forebrain marker is later restricted to the *diencephalon* and ventral *telencephalon* (72,78). Nevertheless, the neural tubuli co-express OTX2 together with PAX6 and FOXG1. One possible explanation would be the incomplete maturation of the neural tubuli in the DOPEoids with retained OTX2 expression in telencephalic tissues or lacking

forebrain sub-specification, since the DOPEoid protocol is not optimized for CNS tissue maturation. Nonetheless, the more likely reason for this co-expression is the induction of a dorsal LGE-like character in the neural tubuli of the DOPEoids which has close ties to the olfactory system as it gives rise to the interneurons of the OB (79). In this dorsal LGE, the dorsal cortical marker Pax6, the anterior marker FoxG1 and the ventral telencephalic marker Otx2 overlap, defining a unique progenitor population (57,76–78,213). To show the identity of the neural tubuli as of dorsal LGE character, GSH2, a key marker of the LGE and other ventral markers like NKX2.1 must be examined in the future (76,77).

LHX2 expression can also be found in the neural tubuli of the DOPEoids. Lhx2 plays an important role in the generation of the dorsal neocortex and is expressed in its SVZ (214). Although Lhx2 is directly interacting with Pax6 and FoxG1 in neural development, its expression cannot be found in the dorsal LGE and is restricted pallially in mice (214,215). The co-expression of these markers could be explained by a possible cross species difference between humans and mice or incomplete maturation in the DOPEoid model.

The neural tubuli of the DOPEoids also show expression of the neural cell-adhesion molecule N-CADHERIN and exhibit polarity, with the apical side expressing ZO1 faced towards the lumen (186). Both features are a major hallmark of the CNS structures in brain organoids, making the neural character of the tubuli in the DOPEoids with a polarity similar to the situation *in vivo* and *in vitro* highly likely (72,76). The VIMENTIN expression – a marker of RG as progenitor cells in the SVZ – also indicates a neural character of the tubuli with a prominent progenitor cell population, also indicated by SOX2 and PAX6 (216).

This strong expression of VIMENTIN together with a lack of expression of the later neuronal marker TUBB3 makes a strong case for the developing CNS character of the tubuli without later stages of maturation. This is most likely due to the culture conditions, since TUBB3 expression can be found in brain organoids (72,76).

7.3.3 Neural tubuli – morphology & protein data: summary

The morphological and protein data from the immunofluorescence staining indicates the induction of radially organized neural tubuli, expressing telencephalic markers, at least in part indicative of the generation of a dorsal LGE, although pallial and less matured tissues are also likely to be present. Further characterization of these neural tubuli and protocol adaptions to improve their maturation will help to further elucidate their identity and generate DOPEoids closely resembling the *in vivo* development.

7.3.4 Neural tubuli – RNA data

As shown in the staining, the majority of the cells in the DOPEoids can be found in the core forming the neural tubuli. As a result, the RNA of these cells makes up most of the signal in the bulk analysis and therefore the expression of neural markers can be traced back to the core. The expression of *SOX2*, *PAX6*, *FOXG1*, *OTX2*, *LHX2* and *N-CADHERIN* on an RNA level matches the observations on a morphological / protein level:

The stem cell marker *SOX2* is highly expressed in hiPSC and shows a high expression throughout the differentiation, indicating the presence of neural progenitor cells (72). The expression of *SOX2* peaks early in the differentiation before the appearance of tubuli, which can be explained by the role of *Sox2* in the early commitment of the neural plate towards neural fate (46). A similar expression pattern can be observed for *N-CADHERIN* , although at a higher relative expression, since the Cadherin expression switches from *E-Cadherin* to *N-Cadherin* during early neural commitment (196).

As mentioned above, *PAX6* and *OTX2* are also markers of early neural commitment and hence a peak in expression can be observed prior to the appearance of the first neural tubuli (72,73). *PAX6* constantly shows a very high expression with fluctuations which are probably due to variabilities in the DOPEoids, although the expression level is always very high compared to hiPSC. Relative to hiPSC, *OTX2* is not as highly expressed but still shows a high expression throughout the differentiation, although with an overall downtrend. A possible reason for this might be the restriction of *Otx2* to the diencephalon and the dorsal LGE within

the ventral telencephalon, whereas it is expressed more broadly in the forebrain before it becomes regionally restricted (73,78). This would explain the early peak during neural induction as well as the following downtrend in expression since its expression level in these structures is less pronounced.

FOXG1 is also highly expressed before the first neural tubuli can be observed, indicating a role in neural induction. Later *FOXG1* is strongly expressed throughout the differentiation, matching the protein data, indicating anterior telencephalic character of the structures found in the DOPEoids.

Likewise, *LHX2* expression also shows an early peak during neural commitment and then shows a rise in expression from day 19 onwards, indicating a growing population of dorsal telencephalic fate (214).

EMX2 and *RAX* have not been analyzed on a protein level. The increase in *EMX2* expression in the 2nd half of the differentiation timeline can be explained by the expression of *Emx2* in dorsal telencephalic progenitors as the forebrain becomes more sub-regionalized (205). The ventral forebrain marker *RAX* shows a peak in expression early during the differentiation whilst neural commitment occurs. This matches *in vivo* data, showing strong *Rax* expression in the anterior neural fold (217). Later in the differentiation, the expression decreases drastically, whilst the dorsal and telencephalic markers (e.g. *EMX2*) increase, indicating commitment to dorsal and telencephalic fates in the DOPEoids. This is in accordance *in vivo* data, where *Rax* is restricted to the ventral diencephalon – especially the hypothalamus – later during development (217,218).

7.3.5 Neural tubuli – summary

The marker expression in the neural tubuli, both on a protein and indirectly on an RNA level indicates, that these tubuli are in fact of neural origin and that cells resembling the dorsal LGE and the dorsal telencephalon are induced inside of the DOPEoids. This close proximity of these telencephalic structures to the surface ectoderm and the placodal patches with a nasal mesenchyme in between matches observations of the development of the human olfactory system *in vivo* close to the forebrain (63). To further mature the DOPEoids and hopefully

generate a functioning OE *in vitro*, further efforts to mature and characterize the forebrain structures inside the organoids must be undertaken.

7.4 Mesenchyme

7.4.1 Mesenchyme – morphology & protein data

On day 16 the first scattered TFAP2A^{+}/E-CADHERIN^{-} cells can be observed between the surface epithelium and the neural tubuli. This cell population further propagates, forming a distinct compartment by day 25, which resembles the developing NC-derived nasal-like mesenchyme. The expression of TFAP2A in the absence of E-CADHERIN can be used to define this population as nasal-like mesenchyme, because Tfap2a expression is maintained in the NC – which gives rise to the nasal mesenchyme *in vivo* – after it is down regulated in the late PPR / CP (46). TFAP2A expression can also be observed in the nasal mesenchyme of the human fetus (192). The loss of E-CADHERIN expression can be explained by its down regulation during EMT, which also occurs *in vivo* (219). Also, the nasal mesenchyme *in vivo* as well as in the DOPEoids does not express N-CADHERIN or T (data not shown), both important markers for mesoderm derived mesenchyme, which excludes the mesodermal lineage (220,221). Furthermore, the cells of this nasal mesenchyme also express SIX1, similar to the Six1 expression in the NC derived head mesenchyme *in vivo* (222). PAX3, also a marker for the nasal mesenchyme is also expressed in this compartment (data not shown for classical DOPEoids, only for outlook data) (223).

These nasal mesenchymal cells not only express transcription factors, but also the intermediate filament protein VIMENTIN, a marker for mesenchymal cells (224). The compartment of this nasal mesenchyme in the DOPEoids contains two concentrated lines of basement membrane proteins COLLAGEN IV and LAMININ, indicating the presence of two separate basement membranes for the surface epithelium and the neural tubuli, respectively (225). Because those basement membranes are located at the borders of the mesenchymal compartment in the DOPEoids, their construction or at least their maintenance can be attributed to the mesenchymal-like cells. This is because, the diffuse expression of

COLLAGEN IV and LAMININ in the nasal mesenchyme of the DOPEoids increases over time and resembles the processes *in vivo* (226).

This architectural makeup of the DOPEoids is unique compared to other organoid models. Their structure closely resembles the structure of an embryonic head, since an apical-out surface epithelium and apical-in NT-like structures are both sitting back-to-back on a mesenchyme derived basement membrane (63). As mentioned earlier, other PPR based protocols are faced outside-in and require Matrigel® embedding (96), or lack a mesenchymal compartment and tubuli like structures (89). Since most brain organoids lack the ECM support found in the DOPEoids, they rely partly on Matrigel®, making the DOPEoids an intriguing approach to further study brain development and improve other organoid protocols.

7.4.2 Mesenchyme – RNA data

The RNA expression also supports the case for a NC-derived head-like mesenchyme, although some RNA expression also originates in other tissues. As mentioned before, Dach1 and Eya1 are also expressed in the nasal mesenchyme, explaining the sustained and growing expression of *DACH1* and *EYA1* in the DOPEoids (194). Likewise, the prolonged expression of *TFAP2A* and *SIX1* in the DOPEoids at rather high expression rates matches the *in vivo* expression.

SOX9 is a NC and OP marker not analyzed on a protein level but only on a RNA level (206,222). *SOX9* expression in the DOPEoids shows a growing expression from day 13 onwards (with some fluctuations due to variabilities in the DOPEoids), which can be explained by the expression in the NC-derived head-like mesenchyme, but some signal from the OP is highly likely.

7.4.3 Mesenchyme – summary

The protein and RNA data, together with the presence of basement membranes and elongated polygonal cell shape as distinct morphological features, indicate the presence of a nasal mesenchyme-like compartment inside the DOPEoids. To further characterize this mesenchymal compartment, more markers of the NC and head mesenchyme like SOX10 and PDGFRα have to be analyzed (156,175).

7.5 DOPEoids – a functional organoid model?

The DOPEoids described in this study can be regarded as a partly functioning organoid model, based on the organoid definition proposed by Lancaster et al. (149). As a stem cell-based model, four distinct cellular compartments with specific cell types can be observed, which are organized similarly to the embryonic head. They also show a great level of self-organization and mirror the *in vivo* development. The DOPEoids are resembling the development of the human nasal region, but future maturation efforts will need to be made to generate a functional OE *in vitro*. Also, the exact mechanisms of self-organization and tissue interactions in the DOPEoids have not yet been elucidated and call for further in-depth analyses. Therefore, DOPEoids already show key features of a functional organoid model but are not yet resembling the functionality of the maturing olfactory system.

7.6 Outlook data

As mentioned before, DOPEoids from a modified differentiation protocol show more maturation compared to the classical protocol (day 40 data not shown on protein level for classical protocol). These results are promising, but have to be interpreted with caution, since this experiment was only performed once (n=1). Further repetitions and analyses are needed to obtain a reliable data foundation.

To improve the maturation of the DOPEoids, day 21 was picked as a timepoint to change protocol conditions, since all major tissues have been induced in the DOPEoids by then. The organoids are selected for DOPEoids and 4-5 per well are transferred to an ultra-low adhesion 12 well plate, to allow for paracrine interaction between DOPEoids and ensure a sufficient nutrient supply as DOPEoids grow in size. The starting media with its supplement was adapted after several major brain organoid protocols and the otic organoid protocol in order to enhance organoid maturation (72,96,154,157). N2 and B27 (w/o Vitamin A) supplement are used together with increased concentrations of GDNF and BDNF and sustained FGF2 exposure to enhance neural growth (96,157). For incubation, normoxic conditions are used instead of hypoxia to mature the induced tissues, as being standard practice in the publications mentioned above.

Compared to the classical condition, the DOPEoids from the modified differentiation protocol are a lot bigger, which can largely be attributed to a dominant nasal mesenchyme-like compartment made up of TFAP2A$^+$/SIX1$^+$/PAX3$^+$ cells. As mentioned earlier, these cells represent the NC-derived nasal mesenchyme, which seems to be positively influenced by the modified culture conditions. Similarly, the NNE-like surface epithelium shows a more continuous expression of KRT5 on a protein level compared to the classical condition (data not shown). Also, the different layers of the epithelium show different characteristics, namely a reduced TFAP2A expression in the upper layers, possibly indicating periderm-like cells (156). Furthermore, the neural tubuli show a higher cell density and wall thickness, indicating enhanced maturation. Taken together, the epithelium, the mesenchyme and especially the neural tubuli seem to benefit from the modified culture condition, emphasizing the advantages of further protocol adaptations.

The most promising maturation, however, can be observed when looking at the placodal patches of the DOPEoids derived from the modified protocol. They retain a marker expression which can be clearly linked to the olfactory fate (as mentioned above) and some show the formation of a nasal sac like structure, as it can be observed *in vivo* (63). The cells of this olfactory-like vesicle co-express SIX1, SIX3, OTX2 and FOXG1 (SIX3 see **Supplemental Figure S3**, data not shown for OTX2 and FOXG1) and some cells even show the co-expression of PAX3. In this case, PAX3 expression most likely does not implicate intermediate placodal origin, but may be evidence that some cells of the developing OE are of NC origin, as shown previously by others *in vivo* (62). To further show the contributions of different tissues to the OE in humans, the DOPEoids seem to be a suitable model system. EBF2, being an important and specific marker of the OP, can also be observed in the cells of this olfactory-like vesicle co-expressed with SIX1, suggesting the commitment of these cells to an olfactory neuronal lineage.

In conclusion, the modification of the DOPEoids protocol seems to enhance the maturation and modeling capacities of this organoid system, even with the integration of cells of different origin into the OP. These results are promising for further analyses and maturation efforts.

7.7 Conclusion & prospects

This work shows for the first time the generation of hiPSC derived 3D organoids of olfactory fate on the level of an OP. The developmental timeline of the DOPEoids recapitulates key steps found *in vivo* and further characterization reveals the presence of key tissues of the developing embryo head. Besides the presence of an OP, the morphological architecture of the DOPEoids with an outside-out orientation and two separate basement membranes built by a head-like mesenchyme are major novelties of this work.

In order to generate a functioning OE *in vitro*, the maturation efforts from this work have to be intensified. Longer cultivation and in a more maturation promoting culture environment will generate more mature DOPEoids, which will most likely also exhibit cellular functions of the developing OE. The examination of functional olfactory processes as odorant signaling must be undertaken in order to fulfill the organoid definitions in full.

To strengthen the evidence for olfactory character of the DOPEoids, as well as to further characterize all tissues of the DOPEoids, the expression of a much broader marker set has to be examined over an extended time course. Furthermore, the generation of reporter lines co-expressing fluorescent proteins with key markers of the development promise exciting new data. These reporter line derived DOPEoids will be more suitable for live cell analysis and cell type specific analysis, aided by FACS sorting. Ultimately, single cell RNA sequencing is a promising tool for the characterization of different cell types in the DOPEoids, as well as to uncover more marker genes for the human olfactory development and establish a more detailed timeline.

The differentiation protocol described here as well as its modifications are a major milestone in the generation of such a model, but many hurdles will have to be met. Especially the batch-to-batch and organoid-to-organoid variability – two major drawbacks of organoid technology – must be improved to generate more reliable data and a standardized model system. Here, the culture conditions – which include undefined and animal-based products such as KOSR or BSA – will have to be optimized towards a fully defined and xenofree standard. However, since

the induction of several tissues in the DOPEoids seems to be dependent on signals from these products, the mechanisms of their induction on a signal / morphogen level must be elucidated first.

In the future, efforts to further mature the DOPEoids and to hopefully generate a functioning OE *in vitro* will lead to a better understanding of human olfactory development and its pathologies. Such a model system will enable basic research on the pathogenesis and possible prevention and even therapy of neurodegenerative disorders as well as adult neurogenesis – the holy grail of neuroscience.

8 Supplemental information

8.1 DOPEoids vs. non-DOPEoids

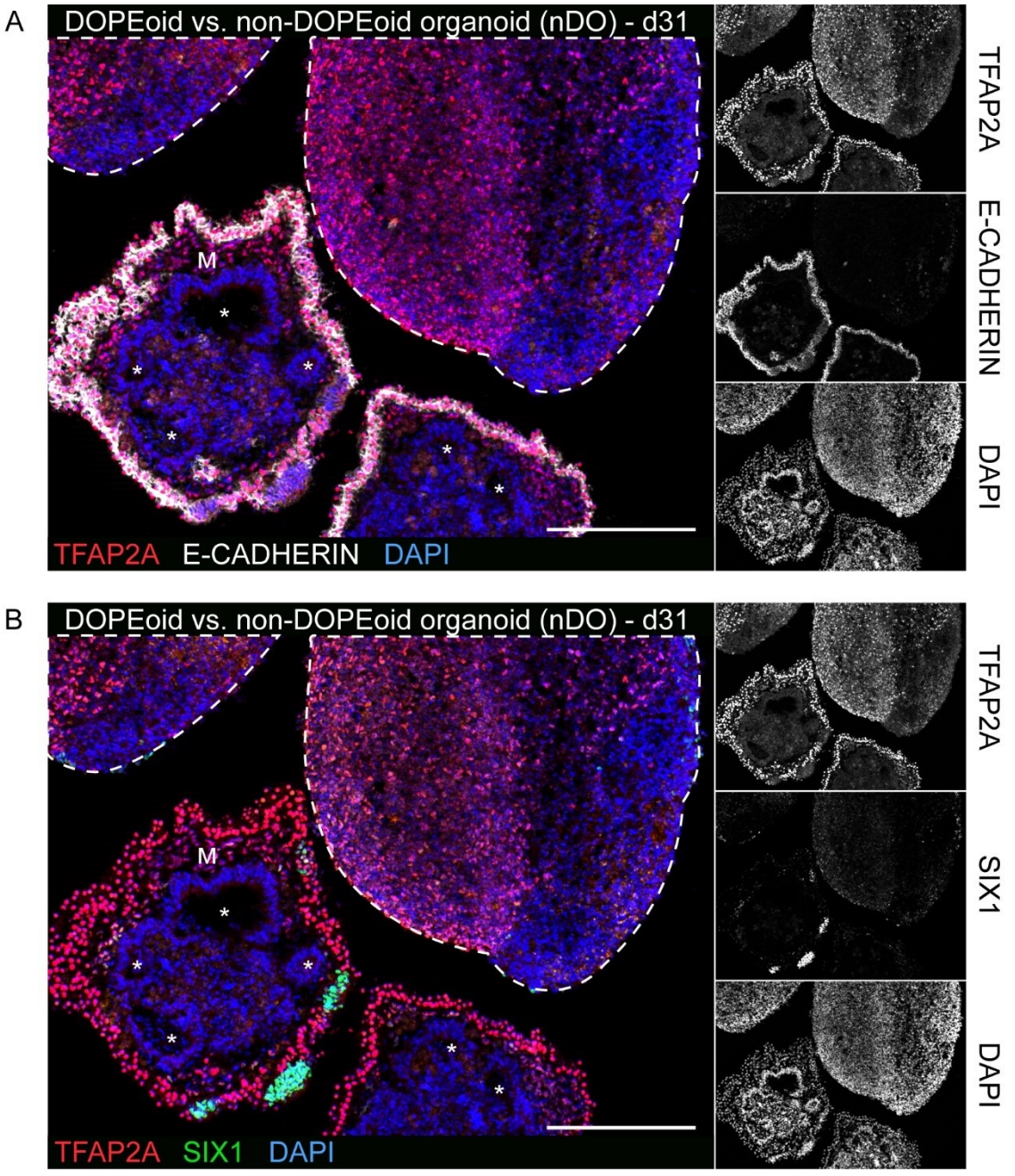

Supplemental Figure S1: DOPEoids vs. non-DOPEoids – morphology & protein data

Organoids stained for TFAP2A (red), SIX1 (green) and E-CADHERIN (white). Nuclei counter-staining with DAPI (blue). Same staining as **(Fig. 22/23)** in lower magnification. Dotted outline marks non-DOPEoids, asterisks marking neural tubuli, M marking head-like mesenchyme. Scale-bars: 200 µm. **(A)** TFAP2A, E-CADHERIN & DAPI **(B)** TFAP2A, SIX1 & DAPI.

In **Supplemental Figure S1**, the same staining as in **Figures 22 / 23** is shown with a lower magnification, highlighting the differences between DOPEoids and non-DOPEoids as described in section **6.1**. The non-DOPEoids (top two organoids, dashed outline) do not show a TFAP2A^{+}/E-CADHERIN^{+} surface epithelium but exhibit a rather uniform, scattered expression of TFAP2A. They do not exhibit E-CADHERIN expression or morphological features like the neural tubuli (asterisks) or a mesenchyme-like compartment (M), as found in the DOPEoids (two bottom organoids). The non-DOPEoids are significantly larger and sometimes show central cell death (data not shown) compared to the DOPEoids. The SIX1 expression found in the non-DOPEoids is weak and diffusely scattered.

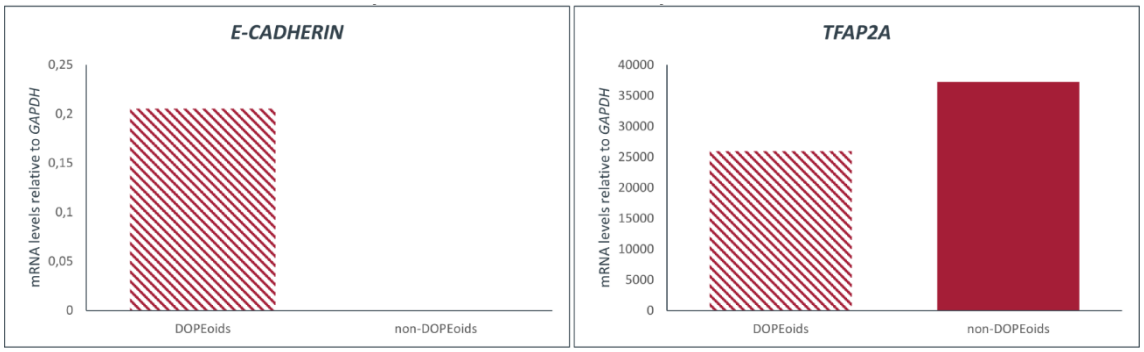

Supplemental Figure S2: DOPEoids vs. non-DOPEoids – gene expression

Relative mRNA expression to *GAPDH* (normalized to hiPSC) of DOPEoids (left) compared to non-DOPEoids (right) on day 31 of the DOPEoid differentiation.

In **Supplemental Figure S2**, the gene expression of *E-CADHERIN* and *TFAP2A* is compared between DOPEoids and non-DOPEoids on day 31 of the differentiation. In accordance with **Supplemental Figure S1**, the *E-CADHERIN* expression is almost not detectable in non-DOPEoids. The *TFAP2A* expression is higher than in the DOPEoids, indicating large scale diffuse expression.

.

8.2 DOPEoids outlook – basement membrane & SIX3 expression

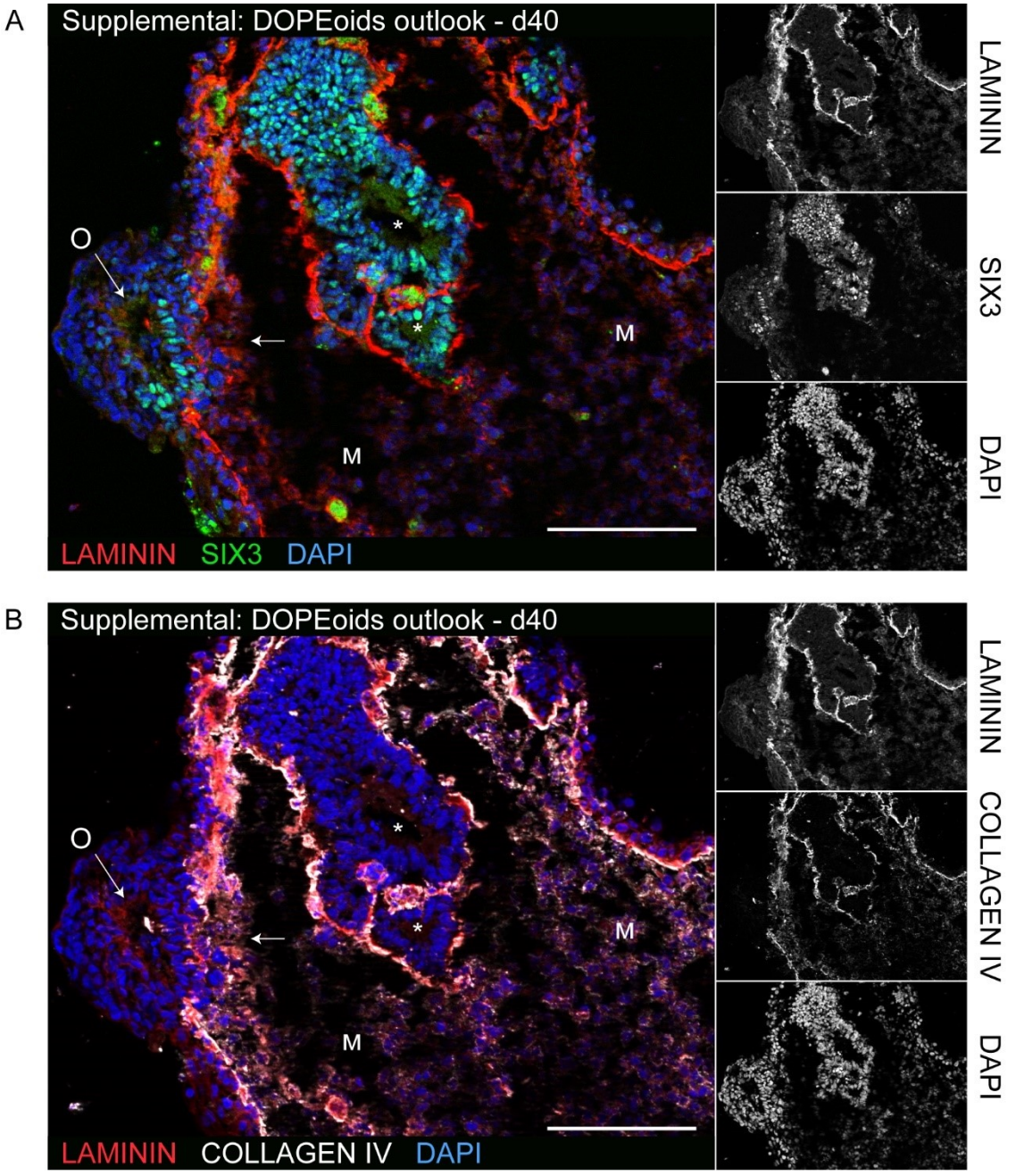

Supplemental Figure S3: DOPEoids outlook: basement membrane & SIX3 expression

Organoids stained for LAMININ (red), SIX3 (green) and COLLAGEN IV (white). Nuclei counter-staining with DAPI (blue). O marking invaginated placodal patch, asterisks marking neural tubuli, arrow marking SIX3⁺ cells of invaginated placodal patch, M marking head-like mesenchyme. Scalebars: 100 µm. **(A)** LAMININ, SIX3 & DAPI **(B)** LAMININ, COLLAGEN IV & DAPI.

49 Spadina Ave. Suite 200
Toronto ON M5V 2J1 Canada
www.biorender.com

Confirmation of Publication and Licensing Rights

May 27th, 2022
Science Suite Inc.

Subscription: *Student Plan*
Agreement number: *WY23YV6W9N*
Journal name: *Dissertation at the University of Tuebingen, Medical Faculty*

To whom this may concern,

This document is to confirm that Georg Frey has been granted a license to use the BioRender content, including icons, templates and other original artwork, appearing in the attached completed graphic pursuant to BioRender's Academic License Terms. This license permits BioRender content to be sublicensed for use in journal publications.

All rights and ownership of BioRender content are reserved by BioRender. All completed graphics must be accompanied by the following citation: "Created with BioRender.com".

BioRender content included in the completed graphic is not licensed for any commercial uses beyond publication in a journal. For any commercial use of this figure, users may, if allowed, recreate it in BioRender under an Industry BioRender Plan.

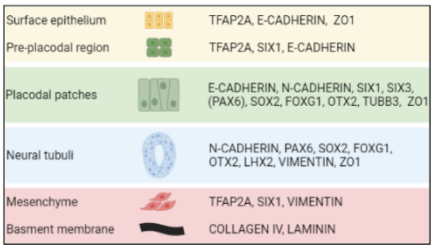

For any questions regarding this document, or other questions about publishing with BioRender refer to our BioRender Publication Guide, or contact BioRender Support at support@biorender.com.

49 Spadina Ave. Suite 200
Toronto ON M5V 2J1 Canada
www.biorender.com

Confirmation of Publication and Licensing Rights

May 27th, 2022
Science Suite Inc.

Subscription: *Student Plan*
Agreement number: *ZK23YV71DG*
Journal name: *Dissertation at the Univserity of Tuebingen, Medical Faculty*

To whom this may concern,

This document is to confirm that Georg Frey has been granted a license to use the BioRender content, including icons, templates and other original artwork, appearing in the attached completed graphic pursuant to BioRender's Academic License Terms. This license permits BioRender content to be sublicensed for use in journal publications.

All rights and ownership of BioRender content are reserved by BioRender. All completed graphics must be accompanied by the following citation: "Created with BioRender.com".

BioRender content included in the completed graphic is not licensed for any commercial uses beyond publication in a journal. For any commercial use of this figure, users may, if allowed, recreate it in BioRender under an Industry BioRender Plan.

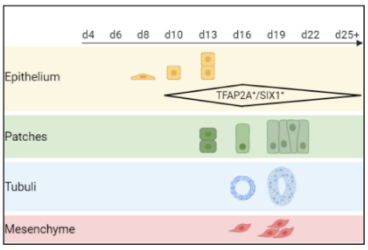

For any questions regarding this document, or other questions about publishing with BioRender refer to our BioRender Publication Guide, or contact BioRender Support at support@biorender.com.

49 Spadina Ave. Suite 200
Toronto ON M5V 2J1 Canada
www.biorender.com

Confirmation of Publication and Licensing Rights

May 27th, 2022
Science Suite Inc.

Subscription: *Student Plan*
Agreement number: *SB23YV743E*
Journal name: *Dissertation University of Tuebingen, Medical Faculty*

To whom this may concern,

This document is to confirm that Georg Frey has been granted a license to use the BioRender content, including icons, templates and other original artwork, appearing in the attached completed graphic pursuant to BioRender's Academic License Terms. This license permits BioRender content to be sublicensed for use in journal publications.

All rights and ownership of BioRender content are reserved by BioRender. All completed graphics must be accompanied by the following citation: "Created with BioRender.com".

BioRender content included in the completed graphic is not licensed for any commercial uses beyond publication in a journal. For any commercial use of this figure, users may, if allowed, recreate it in BioRender under an Industry BioRender Plan.

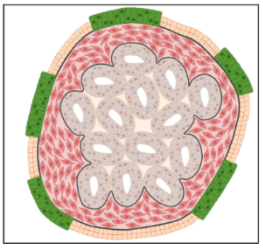

For any questions regarding this document, or other questions about publishing with BioRender refer to our BioRender Publication Guide, or contact BioRender Support at support@biorender.com.

49 Spadina Ave. Suite 200
Toronto ON M5V 2J1 Canada
www.biorender.com

Confirmation of Publication and Licensing Rights

May 27th, 2022
Science Suite Inc.

Subscription: *Student Plan*
Agreement number: *MZ23YV76DX*
Journal name: *Dissertation University of Tuebingen, Medical Faculty*

To whom this may concern,

This document is to confirm that Georg Frey has been granted a license to use the BioRender content, including icons, templates and other original artwork, appearing in the attached completed graphic pursuant to BioRender's Academic License Terms. This license permits BioRender content to be sublicensed for use in journal publications.

All rights and ownership of BioRender content are reserved by BioRender. All completed graphics must be accompanied by the following citation: "Created with BioRender.com".

BioRender content included in the completed graphic is not licensed for any commercial uses beyond publication in a journal. For any commercial use of this figure, users may, if allowed, recreate it in BioRender under an Industry BioRender Plan.

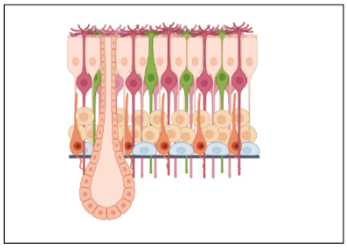

For any questions regarding this document, or other questions about publishing with BioRender refer to our BioRender Publication Guide, or contact BioRender Support at support@biorender.com.

Supplemental Figure S4: BioRender.com – publication licenses #1

49 Spadina Ave. Suite 200
Toronto ON M5V 2J1 Canada
www.biorender.com

Confirmation of Publication and Licensing Rights

May 27th, 2022
Science Suite Inc.

Subscription: *Student Plan*
Agreement number: *LV23YV787L*
Journal name: *Dissertation University of Tuebingen, Medical Faculty*

To whom this may concern,

This document is to confirm that Georg Frey has been granted a license to use the BioRender content, including icons, templates and other original artwork, appearing in the attached completed graphic pursuant to BioRender's Academic License Terms. This license permits BioRender content to be sublicensed for use in journal publications.

All rights and ownership of BioRender content are reserved by BioRender. All completed graphics must be accompanied by the following citation: "Created with BioRender.com".

BioRender content included in the completed graphic is not licensed for any commercial uses beyond publication in a journal. For any commercial use of this figure, users may, if allowed, recreate it in BioRender under an Industry BioRender Plan.

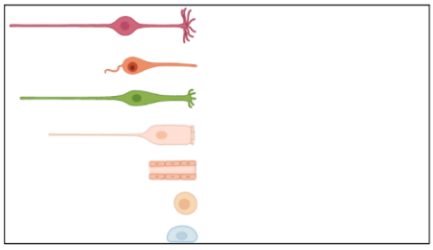

For any questions regarding this document, or other questions about publishing with BioRender refer to our BioRender Publication Guide, or contact BioRender Support at support@biorender.com.

49 Spadina Ave. Suite 200
Toronto ON M5V 2J1 Canada
www.biorender.com

Confirmation of Publication and Licensing Rights

May 27th, 2022
Science Suite Inc.

Subscription: *Student Plan*
Agreement number: *VB23YV7A4V*
Journal name: *Dissertation University of Tuebingen, Medical Faculty*

To whom this may concern,

This document is to confirm that Georg Frey has been granted a license to use the BioRender content, including icons, templates and other original artwork, appearing in the attached completed graphic pursuant to BioRender's Academic License Terms. This license permits BioRender content to be sublicensed for use in journal publications.

All rights and ownership of BioRender content are reserved by BioRender. All completed graphics must be accompanied by the following citation: "Created with BioRender.com".

BioRender content included in the completed graphic is not licensed for any commercial uses beyond publication in a journal. For any commercial use of this figure, users may, if allowed, recreate it in BioRender under an Industry BioRender Plan.

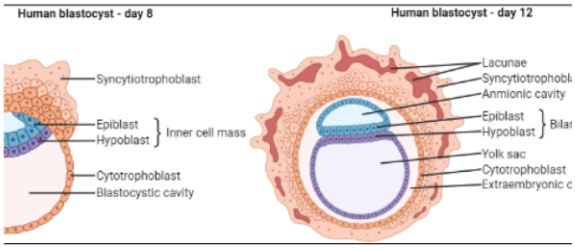

For any questions regarding this document, or other questions about publishing with BioRender refer to our BioRender Publication Guide, or contact BioRender Support at support@biorender.com.

49 Spadina Ave. Suite 200
Toronto ON M5V 2J1 Canada
www.biorender.com

Confirmation of Publication and Licensing Rights

May 27th, 2022
Science Suite Inc.

Subscription: *Student Plan*
Agreement number: *PI23YV7BZI*
Journal name: *Dissertation University of Tuebingen, Medical Faculty*

To whom this may concern,

This document is to confirm that Georg Frey has been granted a license to use the BioRender content, including icons, templates and other original artwork, appearing in the attached completed graphic pursuant to BioRender's Academic License Terms. This license permits BioRender content to be sublicensed for use in journal publications.

All rights and ownership of BioRender content are reserved by BioRender. All completed graphics must be accompanied by the following citation: "Created with BioRender.com".

BioRender content included in the completed graphic is not licensed for any commercial uses beyond publication in a journal. For any commercial use of this figure, users may, if allowed, recreate it in BioRender under an Industry BioRender Plan.

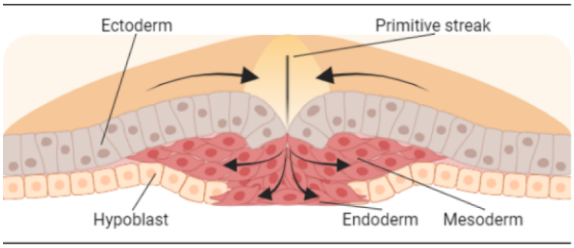

For any questions regarding this document, or other questions about publishing with BioRender refer to our BioRender Publication Guide, or contact BioRender Support at support@biorender.com.

49 Spadina Ave. Suite 200
Toronto ON M5V 2J1 Canada
www.biorender.com

Confirmation of Publication and Licensing Rights

May 27th, 2022
Science Suite Inc.

Subscription: *Student Plan*
Agreement number: *YR23YV7G3S*
Journal name: *Dissertation University of Tuebingen, Medical Faculty*

To whom this may concern,

This document is to confirm that Georg Frey has been granted a license to use the BioRender content, including icons, templates and other original artwork, appearing in the attached completed graphic pursuant to BioRender's Academic License Terms. This license permits BioRender content to be sublicensed for use in journal publications.

All rights and ownership of BioRender content are reserved by BioRender. All completed graphics must be accompanied by the following citation: "Created with BioRender.com".

BioRender content included in the completed graphic is not licensed for any commercial uses beyond publication in a journal. For any commercial use of this figure, users may, if allowed, recreate it in BioRender under an Industry BioRender Plan.

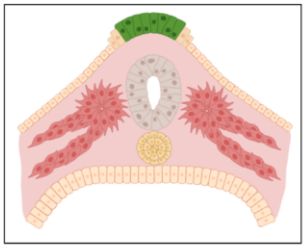

For any questions regarding this document, or other questions about publishing with BioRender refer to our BioRender Publication Guide, or contact BioRender Support at support@biorender.com.

Supplemental Figure S5: BioRender.com – publication licenses #2

bio RENDER

49 Spadina Ave. Suite 200
Toronto ON M5V 2J1 Canada
www.biorender.com

Confirmation of Publication and Licensing Rights

May 27th, 2022
Science Suite Inc.

Subscription:	*Student Plan*
Agreement number:	*KU23YV7HJT*
Journal name:	*Dissertation University of Tuebingen, Medical Faculty*

To whom this may concern,

This document is to confirm that Georg Frey has been granted a license to use the BioRender content, including icons, templates and other original artwork, appearing in the attached completed graphic pursuant to BioRender's Academic License Terms. This license permits BioRender content to be sublicensed for use in journal publications.

All rights and ownership of BioRender content are reserved by BioRender. All completed graphics must be accompanied by the following citation: "Created with BioRender.com".

BioRender content included in the completed graphic is not licensed for any commercial uses beyond publication in a journal. For any commercial use of this figure, users may, if allowed, recreate it in BioRender under an Industry BioRender Plan.

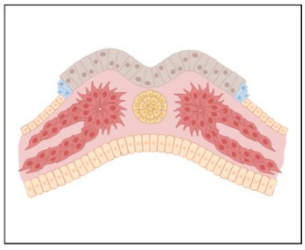

For any questions regarding this document, or other questions about publishing with BioRender refer to our BioRender Publication Guide, or contact BioRender Support at support@biorender.com.

bio RENDER

49 Spadina Ave. Suite 200
Toronto ON M5V 2J1 Canada
www.biorender.com

Confirmation of Publication and Licensing Rights

May 27th, 2022
Science Suite Inc.

Subscription:	*Student Plan*
Agreement number:	*WL23YV7JCL*
Journal name:	*Dissertation University of Tuebingen, Medical Faculty*

To whom this may concern,

This document is to confirm that Georg Frey has been granted a license to use the BioRender content, including icons, templates and other original artwork, appearing in the attached completed graphic pursuant to BioRender's Academic License Terms. This license permits BioRender content to be sublicensed for use in journal publications.

All rights and ownership of BioRender content are reserved by BioRender. All completed graphics must be accompanied by the following citation: "Created with BioRender.com".

BioRender content included in the completed graphic is not licensed for any commercial uses beyond publication in a journal. For any commercial use of this figure, users may, if allowed, recreate it in BioRender under an Industry BioRender Plan.

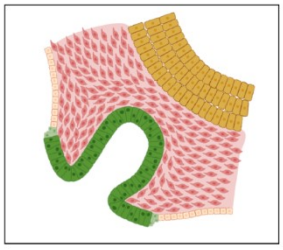

For any questions regarding this document, or other questions about publishing with BioRender refer to our BioRender Publication Guide, or contact BioRender Support at support@biorender.com.

bio RENDER

49 Spadina Ave. Suite 200
Toronto ON M5V 2J1 Canada
www.biorender.com

Confirmation of Publication and Licensing Rights

May 27th, 2022
Science Suite Inc.

Subscription:	*Student Plan*
Agreement number:	*NJ23YV7LB5*
Journal name:	*Dissertation University of Tuebingen, Medical Faculty*

To whom this may concern,

This document is to confirm that Georg Frey has been granted a license to use the BioRender content, including icons, templates and other original artwork, appearing in the attached completed graphic pursuant to BioRender's Academic License Terms. This license permits BioRender content to be sublicensed for use in journal publications.

All rights and ownership of BioRender content are reserved by BioRender. All completed graphics must be accompanied by the following citation: "Created with BioRender.com".

BioRender content included in the completed graphic is not licensed for any commercial uses beyond publication in a journal. For any commercial use of this figure, users may, if allowed, recreate it in BioRender under an Industry BioRender Plan.

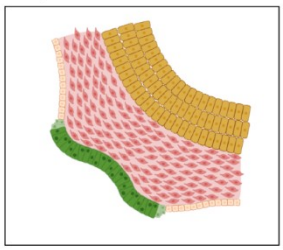

For any questions regarding this document, or other questions about publishing with BioRender refer to our BioRender Publication Guide, or contact BioRender Support at support@biorender.com.

bio RENDER

49 Spadina Ave. Suite 200
Toronto ON M5V 2J1 Canada
www.biorender.com

Confirmation of Publication and Licensing Rights

May 27th, 2022
Science Suite Inc.

Subscription:	*Student Plan*
Agreement number:	*AY23YV7MWG*
Journal name:	*Dissertation University of Tuebingen, Medical Faculty*

To whom this may concern,

This document is to confirm that Georg Frey has been granted a license to use the BioRender content, including icons, templates and other original artwork, appearing in the attached completed graphic pursuant to BioRender's Academic License Terms. This license permits BioRender content to be sublicensed for use in journal publications.

All rights and ownership of BioRender content are reserved by BioRender. All completed graphics must be accompanied by the following citation: "Created with BioRender.com".

BioRender content included in the completed graphic is not licensed for any commercial uses beyond publication in a journal. For any commercial use of this figure, users may, if allowed, recreate it in BioRender under an Industry BioRender Plan.

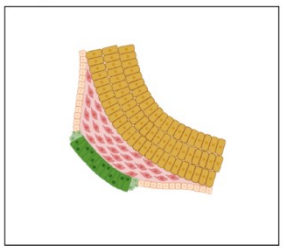

For any questions regarding this document, or other questions about publishing with BioRender refer to our BioRender Publication Guide, or contact BioRender Support at support@biorender.com.

Supplemental Figure S6: BioRender.com – publication licenses #3

49 Spadina Ave. Suite 200
Toronto ON M5V 2J1 Canada
www.biorender.com

Confirmation of Publication and Licensing Rights

May 27th, 2022
Science Suite Inc.

Subscription: *Student Plan*
Agreement number: *DQ23YV7ONW*
Journal name: *Dissertation University of Tuebingen, Medical Faculty*

To whom this may concern,

This document is to confirm that Georg Frey has been granted a license to use the BioRender content, including icons, templates and other original artwork, appearing in the attached completed graphic pursuant to BioRender's Academic License Terms. This license permits BioRender content to be sublicensed for use in journal publications.

All rights and ownership of BioRender content are reserved by BioRender. All completed graphics must be accompanied by the following citation: "Created with BioRender.com".

BioRender content included in the completed graphic is not licensed for any commercial uses beyond publication in a journal. For any commercial use of this figure, users may, if allowed, recreate it in BioRender under an Industry BioRender Plan.

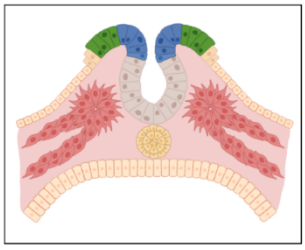

For any questions regarding this document, or other questions about publishing with BioRender refer to our BioRender Publication Guide, or contact BioRender Support at support@biorender.com.

49 Spadina Ave. Suite 200
Toronto ON M5V 2J1 Canada
www.biorender.com

Confirmation of Publication and Licensing Rights

May 27th, 2022
Science Suite Inc.

Subscription: *Student Plan*
Agreement number: *GO23YV7Q4F*
Journal name: *Dissertation University of Tuebingen, Medical Faculty*

To whom this may concern,

This document is to confirm that Georg Frey has been granted a license to use the BioRender content, including icons, templates and other original artwork, appearing in the attached completed graphic pursuant to BioRender's Academic License Terms. This license permits BioRender content to be sublicensed for use in journal publications.

All rights and ownership of BioRender content are reserved by BioRender. All completed graphics must be accompanied by the following citation: "Created with BioRender.com".

BioRender content included in the completed graphic is not licensed for any commercial uses beyond publication in a journal. For any commercial use of this figure, users may, if allowed, recreate it in BioRender under an Industry BioRender Plan.

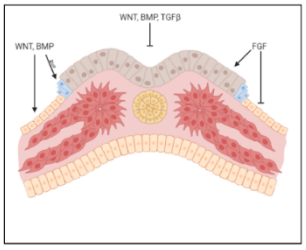

For any questions regarding this document, or other questions about publishing with BioRender refer to our BioRender Publication Guide, or contact BioRender Support at support@biorender.com.

49 Spadina Ave. Suite 200
Toronto ON M5V 2J1 Canada
www.biorender.com

Confirmation of Publication and Licensing Rights

May 27th, 2022
Science Suite Inc.

Subscription: *Student Plan*
Agreement number: *PB23YV7S76*
Journal name: *Dissertation University of Tuebingen, Medical Faculty*

To whom this may concern,

This document is to confirm that Georg Frey has been granted a license to use the BioRender content, including icons, templates and other original artwork, appearing in the attached completed graphic pursuant to BioRender's Academic License Terms. This license permits BioRender content to be sublicensed for use in journal publications.

All rights and ownership of BioRender content are reserved by BioRender. All completed graphics must be accompanied by the following citation: "Created with BioRender.com".

BioRender content included in the completed graphic is not licensed for any commercial uses beyond publication in a journal. For any commercial use of this figure, users may, if allowed, recreate it in BioRender under an Industry BioRender Plan.

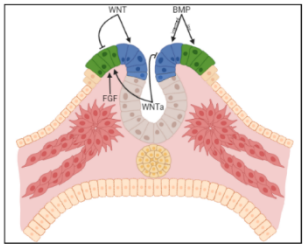

For any questions regarding this document, or other questions about publishing with BioRender refer to our BioRender Publication Guide, or contact BioRender Support at support@biorender.com.

49 Spadina Ave. Suite 200
Toronto ON M5V 2J1 Canada
www.biorender.com

Confirmation of Publication and Licensing Rights

May 27th, 2022
Science Suite Inc.

Subscription: *Student Plan*
Agreement number: *YB23YV7UIQ*
Journal name: *Dissertation University of Tuebingen, Medical Faculty*

To whom this may concern,

This document is to confirm that Georg Frey has been granted a license to use the BioRender content, including icons, templates and other original artwork, appearing in the attached completed graphic pursuant to BioRender's Academic License Terms. This license permits BioRender content to be sublicensed for use in journal publications.

All rights and ownership of BioRender content are reserved by BioRender. All completed graphics must be accompanied by the following citation: "Created with BioRender.com".

BioRender content included in the completed graphic is not licensed for any commercial uses beyond publication in a journal. For any commercial use of this figure, users may, if allowed, recreate it in BioRender under an Industry BioRender Plan.

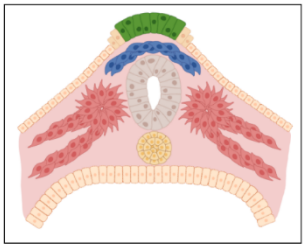

For any questions regarding this document, or other questions about publishing with BioRender refer to our BioRender Publication Guide, or contact BioRender Support at support@biorender.com.

Supplemental Figure S7: BioRender.com – publication licenses #4

49 Spadina Ave. Suite 200
Toronto ON M5V 2J1 Canada
www.biorender.com

Confirmation of Publication and Licensing Rights

May 27th, 2022
Science Suite Inc.

Subscription: *Student Plan*
Agreement number: *KR23YV6LNB*
Journal name: *Dissertation University of Tuebingen, Medical Faculty*

To whom this may concern,

This document is to confirm that Georg Frey has been granted a license to use the BioRender content, including icons, templates and other original artwork, appearing in the attached completed graphic pursuant to BioRender's Academic License Terms. This license permits BioRender content to be sublicensed for use in journal publications.

All rights and ownership of BioRender content are reserved by BioRender. All completed graphics must be accompanied by the following citation: "Created with BioRender.com".

BioRender content included in the completed graphic is not licensed for any commercial uses beyond publication in a journal. For any commercial use of this figure, users may, if allowed, recreate it in BioRender under an Industry BioRender Plan.

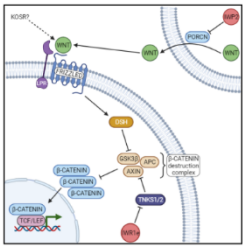

For any questions regarding this document, or other questions about publishing with BioRender refer to our BioRender Publication Guide, or contact BioRender Support at support@biorender.com

Supplemental Figure S8: BioRender.com – publication licenses #5

9 References

Aumüller, Gerhard et al. (2014): *Duale Reihe Anatomie*, 3rd Edition, Stuttgart: Georg Thieme Verlag – see consecutive reference no. 14

Doty, Richard L. (ed.) (2015): *Handbook of Olfaction and Gustation*, 3rd Edition, New York: John Wiley & Sons Ltd. – see consecutive reference no. 10

Pape, Hans-Christian and Kurzt, Armin and Silbernagl, Stefan (2014): *Physiologie*, 7th Edition, Stuttgart: Georg Thieme Verlag – see consecutive reference no. 18

Standring, Susan et al. (eds.) (2016): Gray´s Anatomy, 41st Edition, Churchill Livingstone: Elsevier – see consecutive reference no. 66

1. **Bjornevik K, Cortese M, Healy BC, Kuhle J, Mina MJ, Leng Y, et al.** Longitudinal analysis reveals high prevalence of Epstein-Barr virus associated with multiple sclerosis. Science (80-). 2022 Jan 21;375(6578):296–301.
2. **Hawkes CH, Del Tredici K, Braak H**. Parkinson's disease: a dual-hit hypothesis. Neuropathol Appl Neurobiol. 2007 Dec 1;33(6):599–614.
3. **Braak H, Del Tredici K, Rüb U, De Vos RAI, Jansen Steur ENH, Braak E**. Staging of brain pathology related to sporadic Parkinson's disease. Neurobiol Aging. 2003 Mar 1;24(2):197–211.
4. **Rietdijk CD, Perez-Pardo P, Garssen J, van Wezel RJA, Kraneveld AD**. Exploring Braak's hypothesis of parkinson's disease. Front Neurol. 2017 Feb 13;8(FEB):37.
5. **Alves J, Petrosyan A, Magalhães R**. Olfactory dysfunction in dementia. World J Clin Cases WJCC. 2014;2(11):661.
6. **Miller DB, O'Callaghan JP**. Biomarkers of Parkinson's disease: Present and future. Metabolism. 2015 Mar 1;64(3):S40–6.
7. **Saito Y, Shioya A, Sano T, Sumikura H, Murata M, Murayama S**. Lewy body pathology involves the olfactory cells in Parkinson's disease and related disorders. Mov Disord. 2016 Jan 1;31(1):135–8.
8. **Rey NL, Wesson DW, Brundin P**. The olfactory bulb as the entry site for prion-like propagation in neurodegenerative diseases. Neurobiol Dis. 2018 Jan 1;109:226–48.
9. **Schlosser G**. Induction and specification of cranial placodes. Dev Biol. 2006 Jun 15;294(2):303–51.
10. **Doty RL, editor**. Handbook of Olfaction and Gustation. 3rd Editio. John Wiley & Sons, Ltd; 2015.
11. **Shepherd GM**. Perception without a Thalamus: How Does Olfaction Do It? Neuron. 2005 Apr 21;46(2):166–8.
12. **Stevenson RJ**. An initial evaluation of the functions of human olfaction. Chem Senses. 2010 Nov 25;35(1):3–20.
13. **Willander J, Larsson M**. Olfaction and emotion: the case of autobiographical memory. Mem Cognit. 2007;35(7):1659–63.

14. **Aumüller G, Aust G, Engele J, Kirsch J, Maio G, Mayerhofer A, et al.** Duale Reihe Anatomie. 3rd ed. Stuttgart: Georg Thieme Verlag; 2014.
15. **Hahn I, Scherer PW, Mozell MM**. Velocity profiles measured for airflow through a large-scale model of the human nasal cavity. 1993.
16. **Mackay-Sim A, St John JA**. Olfactory ensheathing cells from the nose: Clinical application in human spinal cord injuries [Internet]. Vol. 229, Experimental Neurology. Exp Neurol; 2011. p. 174–80.
17. **Matthews HR, Reisert J**. Calcium, the two-faced messenger of olfactory transduction and adaptation. Curr Opin Neurobiol. 2003 Aug 1;13(4):469–75.
18. **Pape HC, Kurtz A, Silbernagl S**. Physiologie. 7th Editio. Physiologie. Stuttgart: Georg Thieme Verlag; 2014. 583–670 p.
19. **Verbeurgt C, Wilkin F, Tarabichi M, Gregoire F, Dumont JE, Chatelain P**. Profiling of Olfactory Receptor Gene Expression in Whole Human Olfactory Mucosa. PLoS One. 2014 May 6;9(5):e96333.
20. **Malnic B, Godfrey PA, Buck LB**. The human olfactory receptor gene family. Proc Natl Acad Sci. 2004 Feb 24;101(8):2584–9.
21. **Zhang X, de la Cruz O, Pinto JM, Nicolae D, Firestein S, Gilad Y**. Characterizing the expression of the human olfactory receptor gene family using a novel DNA microarray. Genome Biol. 2007 May 17;8(5):1–10.
22. **Buck L, Axel R**. A novel multigene family may encode odorant receptors: A molecular basis for odor recognition. Cell. 1991 Apr 5;65(1):175–87.
23. **Hanchate NK, Kondoh K, Lu Z, Kuang D, Ye X, Qiu X, et al.** Single-cell transcriptomics reveals receptor transformations during olfactory neurogenesis. Science (80-). 2015 Dec 4;350(6265):1251–5.
24. **Holbrook EH, Wu E, Curry WT, Lin DT, Schwob JE**. Immunohistochemical characterization of human olfactory tissue. Laryngoscope. 2011 Aug 1;121(8):1687–701.
25. **Durante MA, Kurtenbach S, Sargi ZB, Harbour JW, Choi R, Kurtenbach S, et al.** Single-cell analysis of olfactory neurogenesis and differentiation in adult humans. Nat Neurosci. 2020 Mar 1;23(3):323–6.
26. **Montani G, Tonelli S, Elsaesser R, Paysan J, Tirindelli R**. Neuropeptide Y in the olfactory microvillar cells. Eur J Neurosci. 2006 Jul 1;24(1):20–4.
27. **Schwob JE, Jang W, Holbrook EH, Lin B, Herrick DB, Peterson JN, et al.** Stem and progenitor cells of the mammalian olfactory epithelium: Taking poietic license. J Comp Neurol. 2017 Mar 1;525(4):1034–54.
28. **Hahn CG, Han LY, Rawson NE, Mirza N, Borgmann-Winter K, Lenox RH, et al.** In vivo and in vitro neurogenesis in human olfactory epithelium. J Comp Neurol. 2005 Mar 7;483(2):154–63.
29. **Cho HJ, Shan Y, Whittington NC, Wray S**. Nasal Placode Development, GnRH Neuronal Migration and Kallmann Syndrome. Front Cell Dev Biol. 2019 Jul 11;7:121.
30. **Hahn C, Han L, Rawson NE, Mirza N, Borgmann-Winter K, Lenox RH, et al.** In vivo and in vitro neurogenesis in human olfactory epithelium. J Comp Neurol. 2005;483(2):154–63.
31. **O'Rahilly R, Müller F**. Human Embryology and Teratology. 3rd ed. New York: Wiley-Liss, Inc; 2001.
32. **Nakaya Y, Sheng G**. Epithelial to mesenchymal transition during

gastrulation: An embryological view. Dev Growth Differ. 2008 Dec 1;50(9):755–66.
33. **Schlosser G, Patthey C, Shimeld SM**. The evolutionary history of vertebrate cranial placodes II: Evolution of ectodermal patterning. Dev Biol. 2014 May 1;389(1):98–119.
34. **Sasai Y, De Robertis EM**. Ectodermal Patterning in Vertebrate Embryos. Dev Biol. 1997 Feb 1;182(1):5–20.
35. **Beddington RSP**. Induction of a second neural axis by the mouse node. Development. 1994 Mar 1;120(3):613–20.
36. **Gaulden J, Reiter JF**. Neur-ons and neur-offs: regulators of neural induction in vertebrate embryos and embryonic stem cells. Hum Mol Genet. 2008 Apr 15;17(R1):R60–6.
37. **Smith WC, Harland RM**. Expression cloning of noggin, a new dorsalizing factor localized to the Spemann organizer in Xenopus embryos. Cell. 1992 Sep 4;70(5):829–40.
38. **Mukhopadhyay M, Shtrom S, Rodriguez-Esteban C, Chen L, Tsukui T, Gomer L, et al.** Dickkopf1 Is Required for Embryonic Head Induction and Limb Morphogenesis in the Mouse. Dev Cell. 2001 Sep 1;1(3):423–34.
39. **Moody SA, LaMantia AS**. Transcriptional regulation of cranial sensory placode development. Curr Top Dev Biol. 2015;111:301.
40. **Schlosser G**. Early embryonic specification of vertebrate cranial placodes. Wiley Interdiscip Rev Dev Biol. 2014 Sep 1;3(5):349–63.
41. **Schlosser G, Glenn Northcutt R**. Development of Neurogenic Placodes in Xenopus laevis. J Comp Neurol. 2000;418:121–46.
42. **Winklbauer R**. Development of the lateral line system in Xenopus. Prog Neurobiol. 1989 Jan 1;32(3):181–206.
43. **Huang X, Saint-Jeannet JP**. Induction of the neural crest and the opportunities of life on the edge. Dev Biol. 2004 Nov 1;275(1):1–11.
44. **Schlosser G, Ahrens K**. Molecular anatomy of placode development in Xenopus laevis. Dev Biol. 2004 Jul 15;271(2):439–66.
45. **Saint-Jeannet JP, Moody SA**. Establishing the pre-placodal region and breaking it into placodes with distinct identities. Dev Biol. 2014 May 1;389(1):13–27.
46. **Grocott T, Tambalo M, Streit A**. The peripheral sensory nervous system in the vertebrate head: A gene regulatory perspective. Vol. 370, Developmental Biology. Academic Press Inc.; 2012. p. 3–23.
47. **Bailey AP, Bhattacharyya S, Bronner-Fraser M, Streit A**. Lens Specification Is the Ground State of All Sensory Placodes, from which FGF Promotes Olfactory Identity. Dev Cell. 2006 Oct 1;11(4):505–17.
48. **Jacobson AG**. THE DETERMINATION AND POSITIONING OF THE NOSE, LENS AND EAR. III. EFFECTS OF REVERSING THE ANTERO-POSTERIOR AXIS OF EPIDERMIS, NEURAL PLATE AND NEURAL FOLD. J Exp Zool. 1963;154(3):293–303.
49. **Martin K, Groves AK**. Competence of cranial ectoderm to respond to Fgf signaling suggests a two-step model of otic placode induction. Development. 2006 Mar 1;133(5):877–87.
50. **Leung AW, Kent Morest D, Li JYH**. Differential BMP signaling controls formation and differentiation of multipotent preplacodal ectoderm

progenitors from human embryonic stem cells. Dev Biol. 2013 Jul 15;379(2):208–20.
51. **Klingenstein M**. Charakterisierung von in vitro differenzierten olfaktorischen. 2017;
52. **Singh S, Groves AK**. The molecular basis of craniofacial placode development. Wiley Interdiscip Rev Dev Biol. 2016 May 7;5(3):363–76.
53. **Ohto H, Kamada S, Tago K, Tominaga SI, Ozaki H, Sato S, et al.** Cooperation of Six and Eya in Activation of Their Target Genes through Nuclear Translocation of Eya. Mol Cell Biol. 1999 Oct;19(10):6815.
54. **Li X, Oghi KA, Zhang J, Krones A, Bush KT, Glass CK, et al.** Eya protein phosphatase activity regulates Six1-Dach-Eya transcriptional effects in mammalian organogenesis. Nature. 2003 Nov 20;426(6964):247–54.
55. **Tavares ALP, Jourdeuil K, Neilson KM, Majumdar HD, Moody SA**. Sobp modulates the transcriptional activation of Six1 target genes and is required during craniofacial development. Dev. 2021 Sep 1;148(17).
56. **Wakamatsu Y**. Mutual repression between Pax3 and Pax6 is involved in the positioning of ophthalmic trigeminal placode in avian embryo. Dev Growth Differ. 2011 Dec;53(9):994–1003.
57. **Duggan CD, DeMaria S, Baudhuin A, Stafford D, Ngai J**. Foxg1 Is Required for Development of the Vertebrate Olfactory System. J Neurosci. 2008 May 14;28(20):5229.
58. **Schwanzel-Fukuda M, Pfaff DW**. Origin of luteinizing hormone-releasing hormone neurons. Nature. 1989;338(6211):161–4.
59. **Wray S, Grant P, Gainer H**. Evidence that cells expressing luteinizing hormone-releasing hormone mRNA in the mouse are derived from progenitor cells in the olfactory placode. Proc Natl Acad Sci U S A. 1989 Oct 1;86(20):8132–6.
60. **Muske LE**. Evolution of gonadotropin-releasing hormone (GnRH) neuronal systems. [Internet]. Vol. 42, Brain, behavior and evolution. Karger Publishers; 1993. p. 215–30.
61. **Baker C V, Bronner-Fraser M**. Vertebrate cranial placodes I. Embryonic induction. Dev Biol. 2001 Apr 1;232(1):1–61.
62. **Forni PE, Taylor-Burds C, Melvin VS, Williams T, Wray S**. Neural crest and ectodermal cells intermix in the nasal placode to give rise to GnRH-1 neurons, sensory neurons, and olfactory ensheathing cells. J Neurosci. 2011 May 4;31(18):6915–27.
63. **Müller F, O'Rahilly R**. Olfactory Structures in Staged Human Embryos. Cells Tissues Organs. 2004;178(2):93–116.
64. **Xue L, Yi H, Huang Z, Shi YB, Li WX**. Global gene expression during the human organogenesis: From tran-scription profiles to function predictions. Int J Biol Sci. 2011;7(7):1068–76.
65. **Taroc EZM, Prasad A, Lin JM, Forni PE**. The terminal nerve plays a prominent role in GnRH-1 neuronal migration independent from proper olfactory and vomeronasal connections to the olfactory bulbs. Biol Open. 2017 Oct 15;6(10):1552–68.
66. **Standring S, editor**. Gray´s Anatomy. 41st ed. Churchill Livingstone: Elsevier; 2016.
67. **Götz M, Huttner WB**. The cell biology of neurogenesis. Nat Rev Mol Cell

Biol 2005 610. 2005 Nov;6(10):777–88.
68. **Zecevic N, Chen Y, Filipovic R**. Contributions of cortical subventricular zone to the development of the human cerebral cortex. J Comp Neurol. 2005 Oct 17;491(2):109–22.
69. **Lui JH, Hansen D V., Kriegstein AR**. Development and evolution of the human neocortex. Cell. 2011 Jul 8;146(1):18–36.
70. **Hansen D V., Lui JH, Parker PRL, Kriegstein AR**. Neurogenic radial glia in the outer subventricular zone of human neocortex. Nat 2010 4647288. 2010 Mar 25;464(7288):554–61.
71. **Fietz SA, Kelava I, Vogt J, Wilsch-Bräuninger M, Stenzel D, Fish JL, et al.** OSVZ progenitors of human and ferret neocortex are epithelial-like and expand by integrin signaling. Nat Neurosci. 2010 Jun;13(6):690–9.
72. **Lancaster MA, Renner M, Martin CA, Wenzel D, Bicknell LS, Hurles ME, et al.** Cerebral organoids model human brain development and microcephaly. Nature. 2013 Aug 28;501(7467):373–9.
73. **Larsen KB, Lutterodt MC, Møllgård K, Møller M**. Expression of the homeobox genes OTX2 and OTX1 in the early developing human brain. J Histochem Cytochem. 2010 Jul 30;58(7):669–78.
74. **Tao W, Lai E**. Telencephalon-restricted expression of BF-1, a new member of the HNF-3/fork head gene family, in the developing rat brain. Neuron. 1992;8(5):957–66.
75. **Sloan SA, Andersen J, Paşca AM, Birey F, Paşca SP**. Generation and assembly of human brain region–specific three-dimensional cultures. Nat Protoc. 2018 Sep 1;13(9):2062–85.
76. **Cederquist GY, Asciolla JJ, Tchieu J, Walsh RM, Cornacchia D, Resh MD, et al.** Specification of positional identity in forebrain organoids. Vol. 37, Nature Biotechnology. Nature Publishing Group; 2019. p. 436–44.
77. **Puelles L, Kuwana E, Puelles E, Bulfone A, Shimamura K, Keleher J, et al.** Pallial and Subpallial Derivatives in the Embryonic Chick and Mouse Telencephalon, Traced by the Expression of the Genes Dlx-2, Emx-1, Nkx-2.1, Pax-6, and Tbr-1 THE JOURNAL OF COMPARATIVE NEUROLOGY 424:409-438 (2000). J Comp Neurol. 2000;424:409–38.
78. **Hoch R V., Lindtner S, Price JD, Rubenstein JLR**. OTX2 Transcription Factor Controls Regional Patterning Within The Medial Ganglionic Eminence (MGE) And Regional Identity Of The Septum. Cell Rep. 2015 Jul 21;12(3):482.
79. **Rubenstein JLR, Campbell K**. Neurogenesis in the Basal Ganglia. Compr Dev Neurosci Patterning Cell Type Specif Dev CNS PNS. 2013 Jan 1;455–73.
80. **Eiraku M, Watanabe K, Matsuo-Takasaki M, Kawada M, Yonemura S, Matsumura M, et al.** Self-Organized Formation of Polarized Cortical Tissues from ESCs and Its Active Manipulation by Extrinsic Signals. Cell Stem Cell. 2008 Nov 6;3(5):519–32.
81. **Litsiou A, Hanson S, Streit A**. A balance of FGF, BMP and WNT signalling positions the future placode territory in the head. Development. 2005 Sep 15;132(18):4051–62.
82. **Chambers SM, Fasano CA, Papapetrou EP, Tomishima M, Sadelain M, Studer L**. Highly efficient neural conversion of human ES and iPS cells by

dual inhibition of SMAD signaling. Nat Biotechnol. 2009 Mar;27(3):275–80.
83. **Watanabe K, Kamiya D, Nishiyama A, Katayama T, Nozaki S, Kawasaki H, et al.** Directed differentiation of telencephalic precursors from embryonic stem cells. Nat Neurosci. 2005 Mar;8(3):288–96.
84. **Nieuwkoop PD**. Activation and organization of the central nervous system in amphibians. Part III. Synthesis of a new working hypothesis. J Exp Zool. 1952 Jun 1;120(1):83–108.
85. **Blumberg B, Bolado J, Moreno TA, Kintner C, Evans RM, Papalopulu N**. An essential role for retinoid signaling in anteroposterior neural patterning. Development. 1997 Jan 15;124(2):373–9.
86. **Yoshihara SI, Omichi K, Yanazawa M, Kitamura K, Yoshihara Y**. Arx homeobox gene is essential for development of mouse olfactory system. Development. 2005 Feb;132(4):751–62.
87. **Storm EE, Garel S, Borello U, Hebert JM, Martinez S, McConnel SK, et al.** Dose-dependent functions of Fgf8 in regulating telencephalic patterning centers. Development. 2006 May 1;133(9):1831–44.
88. **Lupo G, Harris WA, Lewis KE**. Mechanisms of ventral patterning in the vertebrate nervous system. Nat Rev Neurosci 2006 72. 2006 Feb;7(2):103–14.
89. **Ozone C, Suga H, Eiraku M, Kadoshima T, Yonemura S, Takata N, et al.** Functional anterior pituitary generated in self-organizing culture of human embryonic stem cells. Nat Commun. 2016 Jan 14;7(1):1–10.
90. **Patthey C, Edlund T, Gunhaga L**. Wnt-regulated temporal control of BMP exposure directs the choice between neural plate border and epidermal fate. Development. 2009 Jan 1;136(1):73–83.
91. **Kwon HJ, Bhat N, Sweet EM, Cornell RA, Riley BB**. Identification of Early Requirements for Preplacodal Ectoderm and Sensory Organ Development. PLOS Genet. 2010 Sep;6(9):e1001133.
92. **Sjödal M, Edlund T, Gunhaga L**. Time of Exposure to BMP Signals Plays a Key Role in the Specification of the Olfactory and Lens Placodes Ex Vivo. Dev Cell. 2007 Jul 1;13(1):141–9.
93. **Pera EM, De Robertis EM**. A direct screen for secreted proteins in Xenopus embryos identifies distinct activities for the Wnt antagonists Crescent and Frzb-1. Mech Dev. 2000 Sep 1;96(2):183–95.
94. **Dincer Z, Piao J, Niu L, Ganat Y, Kriks S, Zimmer B, et al.** Specification of functional cranial placode derivatives from human pluripotent stem cells. Cell Rep. 2013 Dec 12;5(5):1387–402.
95. **Tchieu J, Zimmer B, Fattahi F, Amin S, Zeltner N, Chen S, et al.** A Modular Platform for Differentiation of Human PSCs into All Major Ectodermal Lineages. Cell Stem Cell. 2017 Sep 7;21(3):399-410.e7.
96. **Koehler KR, Nie J, Longworth-Mills E, Liu XP, Lee J, Holt JR, et al.** Generation of inner ear organoids containing functional hair cells from human pluripotent stem cells. Nat Biotechnol. 2017;35(6):583–9.
97. **Park BY, Saint-Jeannet JP**. Hindbrain-derived Wnt and Fgf signals cooperate to specify the otic placode in Xenopus. Dev Biol. 2008 Dec 1;324(1):108–21.
98. **Lassiter RNT, Dude CM, Reynolds SB, Winters NI, Baker CVH, Stark MR**. Canonical Wnt signaling is required for ophthalmic trigeminal placode

cell fate determination and maintenance. Dev Biol. 2007 Aug 15;308(2):392–406.
99. **Janesick A, Shiotsugu J, Taketani M, Blumberg B**. RIPPLY3 is a retinoic acid-inducible repressor required for setting the borders of the pre-placodal ectoderm. Development. 2012 Mar 15;139(6):1213–24.
100. **Wang Y, Martin JF, Bai CB**. Direct and indirect requirements of Shh/Gli signaling in early pituitary development. Dev Biol. 2010 Dec 15;348(2):199–209.
101. **Karlstrom RO, Talbot WS, Schier AF**. Comparative synteny cloning of zebrafish you-too: mutations in the Hedgehog target gli2 affect ventral forebrain patterning. Genes Dev. 1999 Feb 15;13(4):388–93.
102. **Martin GR**. Isolation of a pluripotent cell line from early mouse embryos cultured in medium conditioned by teratocarcinoma stem cells (embryonic stem cells/inner cell masses/differentiation in vsitro/embryonal carcinoma cells/growth factors). Vol. 78, Developmental Biology. 1981.
103. **Evans MJ, Kaufman MH**. Establishment in culture of pluripotential cells from mouse embryos. Nature. 1981;292(5819):154–6.
104. **Liu G, David BT, Trawczynski M, Fessler RG**. Advances in Pluripotent Stem Cells: History, Mechanisms, Technologies, and Applications [Internet]. Vol. 16, Stem Cell Reviews and Reports. Springer; 2020. p. 3–32.
105. **Bragança J, Lopes JA, Mendes-Silva L, Santos JMA**. Induced pluripotent stem cells, a giant leap for mankind therapeutic applications [Internet]. Vol. 11, World Journal of Stem Cells. Baishideng Publishing Group Co; 2019. p. 421–30.
106. **Reubinoff BE, Pera MF, Fong CY, Trounson A, Bongso A**. Embryonic stem cell lines from human blastocysts: Somatic differentiation in vitro. Nat Biotechnol. 2000;18(4):399–404.
107. **Brickman JM, Serup P**. Properties of embryoid bodies. Wiley Interdiscip Rev Dev Biol. 2017 Mar 1;6(2):259.
108. **Takahashi K, Tanabe K, Ohnuki M, Narita M, Ichisaka T, Tomoda K, et al.** Induction of Pluripotent Stem Cells from Adult Human Fibroblasts by Defined Factors. Cell. 2007 Nov 30;131(5):861–72.
109. **Thomson JA**. Embryonic stem cell lines derived from human blastocysts. Science (80-). 1998 Nov 6;282(5391):1145–7.
110. **Yu J, Thomson JA**. Pluripotent stem cell lines [Internet]. Vol. 22, Genes and Development. Cold Spring Harbor Laboratory Press; 2008. p. 1987–97.
111. **Niwa H, Burdon T, Chambers I, Smith A**. Self-renewal of pluripotent embryonic stem cells is mediated via activation of STAT3. Genes Dev. 1998 Jul 1;12(13):2048–60.
112. **Silva SS, Rowntree RK, Mekhoubad S, Lee JT**. X-chromosome inactivation and epigenetic fluidity in human embryonic stem cells. Proc Natl Acad Sci U S A. 2008 Mar 25;105(12):4820–5.
113. **Kee K, Angeles VT, Flores M, Nguyen HN, Reijo Pera RA**. Human DAZL, DAZ and BOULE genes modulate primordial germ-cell and haploid gamete formation. Nature. 2009 Nov 12;462(7270):222–5.
114. **Tesar PJ, Chenoweth JG, Brook FA, Davies TJ, Evans EP, Mack DL,**

et al. New cell lines from mouse epiblast share defining features with human embryonic stem cells. Nature. 2007 Jul 12;448(7150):196–9.
115. **Brons IGM, Smithers LE, Trotter MWB, Rugg-Gunn P, Sun B, Chuva De Sousa Lopes SM, et al.** Derivation of pluripotent epiblast stem cells from mammalian embryos. Nature. 2007 Jul 12;448(7150):191–5.
116. **Nichols J, Smith A**. Naive and Primed Pluripotent States. Vol. 4, Cell Stem Cell. Cell Press; 2009. p. 487–92.
117. **Hanna J, Cheng AW, Saha K, Kim J, Lengner CJ, Soldner F, et al.** Human embryonic stem cells with biological and epigenetic characteristics similar to those of mouse ESCs. Proc Natl Acad Sci U S A. 2010 May 18;107(20):9222–7.
118. **Wilmut I, Schnieke AE, McWhir J, Kind AJ, Campbell KHS**. Viable offspring derived from fetal and adult mammalian cells. Nature. 1997 Feb 27;385(6619):810–3.
119. **Tachibana M, Amato P, Sparman M, Gutierrez NM, Tippner-Hedges R, Ma H, et al.** Human embryonic stem cells derived by somatic cell nuclear transfer. Cell. 2013 Jun 6;153(6):1228–38.
120. **Campbell KHS, McWhir J, Ritchie WA, Wilmut I**. Sheep cloned by nuclear transfer from a cultured cell line. Nature. 1996 Mar 7;380(6569):64–6.
121. **Cowan CA, Atienza J, Melton DA, Eggan K**. Developmental Biology: Nuclear reprogramming of somatic cells after fusion with human embryonic stem cells. Science (80-). 2005 Aug 26;309(5739):1369–73.
122. **Tada M, Takahama Y, Abe K, Nakatsuji N, Tada T**. Nuclear reprogramming of somatic cells by in vitro hybridization with ES cells. Curr Biol. 2001 Oct 2;11(19):1553–8.
123. **Takahashi K, Yamanaka S**. Induction of Pluripotent Stem Cells from Mouse Embryonic and Adult Fibroblast Cultures by Defined Factors. Cell. 2006 Aug 25;126(4):663–76.
124. **Engels EM**. Human embryonic stem cells - The German debate [Internet]. Vol. 3, Nature Reviews Genetics. European Association for Cardio-Thoracic Surgery; 2002. p. 636–41.
125. **Raab S, Klingenstein M, Liebau S, Linta L**. A Comparative View on Human Somatic Cell Sources for iPSC Generation. Vol. 2014, Stem Cells International. Hindawi Limited; 2014.
126. **Rowe RG, Daley GQ**. Induced pluripotent stem cells in disease modelling and drug discovery [Internet]. Vol. 20, Nature Reviews Genetics. Nature Publishing Group; 2019. p. 377–88.
127. **Ou Z, Niu X, He W, Chen Y, Song B, Xian Y, et al.** The Combination of CRISPR/Cas9 and iPSC Technologies in the Gene Therapy of Human β-thalassemia in Mice. Sci Rep. 2016 Sep 1;6(1):1–13.
128. **Koci B, Luerman G, Duenbostell A, Kettenhofen R, Bohlen H, Coyle L, et al.** An impedance-based approach using human iPSC-derived cardiomyocytes significantly improves in vitro prediction of in vivo cardiotox liabilities. Toxicol Appl Pharmacol. 2017 Aug 15;329:121–7.
129. **Fusaki N, Ban H, Nishiyama A, Saeki K, Hasegawa M**. Efficient induction of transgene-free human pluripotent stem cells using a vector based on Sendai virus, an RNA virus that does not integrate into the host genome.

Proc Japan Acad Ser B Phys Biol Sci. 2009 Oct;85(8):348–62.
130. **Warren L, Manos PD, Ahfeldt T, Loh YH, Li H, Lau F, et al.** Highly efficient reprogramming to pluripotency and directed differentiation of human cells with synthetic modified mRNA. Cell Stem Cell. 2010 Nov 5;7(5):618–30.
131. **Junying Y, Kejin H, Kim SO, Shulan T, Stewart R, Slukvin II, et al.** Human induced pluripotent stem cells free of vector and transgene sequences. Science (80-). 2009 May 8;324(5928):797–801.
132. **Kaji K, Norrby K, Paca A, Mileikovsky M, Mohseni P, Woltjen K**. Virus-free induction of pluripotency and subsequent excision of reprogramming factors. Nature. 2009 Apr 9;458(7239):771–5.
133. **Okita K, Nakagawa M, Hyenjong H, Ichisaka T, Yamanaka S**. Generation of mouse induced pluripotent stem cells without viral vectors. Science (80-). 2008 Nov 7;322(5903):949–53.
134. **Huangfu D, Maehr R, Guo W, Eijkelenboom A, Snitow M, Chen AE, et al.** Induction of pluripotent stem cells by defined factors is greatly improved by small-molecule compounds. Nat Biotechnol. 2008 Jul 22;26(7):795–7.
135. **Shi Y, Desponts C, Do JT, Hahm HS, Schöler HR, Ding S**. Induction of Pluripotent Stem Cells from Mouse Embryonic Fibroblasts by Oct4 and Klf4 with Small-Molecule Compounds. Cell Stem Cell. 2008 Nov 6;3(5):568–74.
136. **Weltner J, Balboa D, Katayama S, Bespalov M, Krjutškov K, Jouhilahti EM, et al.** Human pluripotent reprogramming with CRISPR activators. Nat Commun. 2018 Dec 1;9(1):1–12.
137. **Loh YH, Agarwal S, Park IH, Urbach A, Huo H, Heffner GC, et al.** Generation of induced pluripotent stem cells from human blood. Blood. 2009 May 28;113(22):5476–9.
138. **Zhou T, Benda C, Duzinger S, Huang Y, Li X, Li Y, et al.** Generation of induced pluripotent stem cells from urine. J Am Soc Nephrol. 2011 Jul 1;22(7):1221–8.
139. **Aasen T, Raya A, Barrero MJ, Garreta E, Consiglio A, Gonzalez F, et al.** Efficient and rapid generation of induced pluripotent stem cells from human keratinocytes. Nat Biotechnol. 2008 Nov 17;26(11):1276–84.
140. **Tabar V, Studer L**. Pluripotent stem cells in regenerative medicine: Challenges and recent progress [Internet]. Vol. 15, Nature Reviews Genetics. Nature Publishing Group; 2014. p. 82–92.
141. **Gurdon JB, Bourillot PY**. Morphogen gradient interpretation [Internet]. Vol. 413, Nature. Nature Publishing Group; 2001. p. 797–803.
142. **Li W, Ding S**. Small molecules that modulate embryonic stem cell fate and somatic cell reprogramming. Vol. 31, Trends in Pharmacological Sciences. Elsevier Current Trends; 2010. p. 36–45.
143. **Reubinoff BE, Itsykson P, Turetsky T, Pera MF, Reinhartz E, Itzik A, et al.** Neural progenitors from human embryonic stem cells. Nat Biotechnol. 2001 Dec 1;19(12):1134–40.
144. **Zhang SC, Wernig M, Duncan ID, Brüstle O, Thomson JA**. In vitro differentiation of transplantable neural precursors from human embryonic stem cells. Nat Biotechnol. 2001 Dec 1;19(12):1129–33.
145. **Kaufman DS, Hanson ET, Lewis RL, Auerbach R, Thomson JA**. Hematopoietic colony-forming cells derived from human embryonic stem

cells. Proc Natl Acad Sci U S A. 2001 Sep 11;98(19):10716–21.
146. **Kehat I, Kenyagin-Karsenti D, Snir M, Segev H, Amit M, Gepstein A, et al.** Human embryonic stem cells can differentiate into myocytes with structural and functional properties of cardiomyocytes. J Clin Invest. 2001 Aug 1;108(3):407–14.
147. **Torrent R, De Angelis Rigotti F, Dell'Era P, Memo M, Raya A, Consiglio A**. Using iPS Cells toward the Understanding of Parkinson's Disease. J Clin Med. 2015 Mar 30;4(4):548–66.
148. **Liu C, Oikonomopoulos A, Sayed N, Wu JC**. Modeling human diseases with induced pluripotent stem cells: From 2D to 3D and beyond. Dev. 2018 Mar 1;145(5).
149. **Lancaster MA, Knoblich JA**. Organogenesisin a dish: Modeling development and disease using organoid technologies [Internet]. Vol. 345, Science. American Association for the Advancement of Science; 2014.
150. **Wu SM, Hochedlinger K**. Harnessing the potential of induced pluripotent stem cells for regenerative medicine [Internet]. Vol. 13, Nature Cell Biology. Nature Publishing Group; 2011. p. 497–505.
151. **ten Berge D, Koole W, Fuerer C, Fish M, Eroglu E, Nusse R**. Wnt Signaling Mediates Self-Organization and Axis Formation in Embryoid Bodies. Cell Stem Cell. 2008 Nov 6;3(5):508–18.
152. **Van Den Brink SC, Baillie-Johnson P, Balayo T, Hadjantonakis AK, Nowotschin S, Turner DA, et al.** Symmetry breaking, germ layer specification and axial organisation in aggregates of mouse embryonic stem cells. Dev. 2014 Nov 1;141(22):4231–42.
153. **Elkabetz Y, Panagiotakos G, Al Shamy G, Socci ND, Tabar V, Studer L**. Human ES cell-derived neural rosettes reveal a functionally distinct early neural stem cell stage. Genes Dev. 2008 Jan 15;22(2):152–65.
154. **Kasai T, Suga H, Sakakibara M, Ozone C, Matsumoto R, Kano M, et al.** Hypothalamic Contribution to Pituitary Functions Is Recapitulated In Vitro Using 3D-Cultured Human iPS Cells. Cell Rep. 2020 Jan 7;30(1):18-24.e5.
155. **Li ML, Aggeler J, Farson DA, Hatier C, Hassell J, Bissell MJ**. Influence of a reconstituted basement membrane and its components on casein gene expression and secretion in mouse mammary epithelial cells. Proc Natl Acad Sci U S A. 1987 Jan 1;84(1):136–40.
156. **Lee J, Rabbani CC, Gao H, Steinhart MR, Woodruff BM, Pflum ZE, et al.** Hair-bearing human skin generated entirely from pluripotent stem cells. Nature. 2020 Jun 18;582(7812):399–404.
157. **Pasca AM, Sloan SA, Clarke LE, Tian Y, Makinson CD, Huber N, et al.** Functional cortical neurons and astrocytes from human pluripotent stem cells in 3D culture. Nat Methods. 2015 Jun 30;12(7):671–8.
158. **Kadoshima T, Sakaguchi H, Nakano T, Soen M, Ando S, Eiraku M, et al.** Correction Correction for "Self-organization of axial polarity, inside-out layer pattern, and species-specific progenitor dynamics in human ES cell-derived neocortex," by. Proc Natl Acad Sci. 2013;110:20284–9.
159. **Nakano T, Ando S, Takata N, Kawada M, Muguruma K, Sekiguchi K, et al.** Self-formation of optic cups and storable stratified neural retina from human ESCs. Cell Stem Cell. 2012 Jun 14;10(6):771–85.
160. **Lee GY, Kenny PA, Lee EH, Bissell MJ**. Three-dimensional culture

models of normal and malignant breast epithelial cells. Nat Methods. 2007 Apr 29;4(4):359–65.
161. **Kale S, Biermann S, Edwards C, Tarnowski C, Morris M, Long MW**. Three-dimensional cellular development is essential for ex vivo formation of human bone. Nat Biotechnol. 2000;18(9):954–8.
162. **Stevens KR, Kreutziger KL, Dupras SK, Korte FS, Regnier M, Muskheli V, et al.** Physiological function and transplantation of scaffold-free and vascularized human cardiac muscle tissue. Proc Natl Acad Sci U S A. 2009 Sep 29;106(39):16568–73.
163. **Chiron S, Tomczak C, Duperray A, Lainé J, Bonne G, Eder A, et al.** Complex interactions between human myoblasts and the surrounding 3D fibrin-based matrix. PLoS One. 2012 Apr 27;7(4).
164. **Takasato M, Er PX, Becroft M, Vanslambrouck JM, Stanley EG, Elefanty AG, et al.** Directing human embryonic stem cell differentiation towards a renal lineage generates a self-organizing kidney. Nat Cell Biol. 2014 Jan 15;16(1):118–26.
165. **Spence JR, Mayhew CN, Rankin SA, Kuhar MF, Vallance JE, Tolle K, et al.** Directed differentiation of human pluripotent stem cells into intestinal tissue in vitro. Nature. 2011 Feb 3;470(7332):105–10.
166. **Takebe T, Sekine K, Enomura M, Koike H, Kimura M, Ogaeri T, et al.** Vascularized and functional human liver from an iPSC-derived organ bud transplant. Nature. 2013 Jul 3;499(7459):481–4.
167. **Dye BR, Hill DR, Ferguson MA, Tsai YH, Nagy MS, Dyal R, et al.** In vitro generation of human pluripotent stem cell derived lung organoids. Elife. 2015 Mar 24;2015(4):1–25.
168. **McCracken KW, Catá EM, Crawford CM, Sinagoga KL, Schumacher M, Rockich BE, et al.** Modelling human development and disease in pluripotent stem-cell-derived gastric organoids. Nature. 2014 Dec 18;516(7531):400–4.
169. **Hohwieler M, Illing A, Hermann PC, Mayer T, Stockmann M, Perkhofer L, et al.** Human pluripotent stem cell-derived acinar/ductal organoids generate human pancreas upon orthotopic transplantation and allow disease modelling. Gut. 2017 Mar 1;66(3):473–86.
170. **Wimmer RA, Leopoldi A, Aichinger M, Wick N, Hantusch B, Novatchkova M, et al.** Human blood vessel organoids as a model of diabetic vasculopathy. Nature. 2019 Jan 24;565(7740):505–10.
171. **Chua CW, Shibata M, Lei M, Toivanen R, Barlow LJ, Bergren SK, et al.** Single luminal epithelial progenitors can generate prostate organoids in culture. Nat Cell Biol. 2014 Oct 1;16(10):951–61.
172. **Boretto M, Cox B, Noben M, Hendriks N, Fassbender A, Roose H, et al.** Development of organoids from mouse and human endometrium showing endometrial epithelium physiology and long-term expandability. Dev. 2017 May 15;144(10):1775–86.
173. **Watanabe K, Ueno M, Kamiya D, Nishiyama A, Matsumura M, Wataya T, et al.** A ROCK inhibitor permits survival of dissociated human embryonic stem cells. Nat Biotechnol. 2007 Jun 27;25(6):681–6.
174. **Suga H, Kadoshima T, Minaguchi M, Ohgushi M, Soen M, Nakano T, et al.** Self-formation of functional adenohypophysis in three-dimensional

culture. Nature. 2011 Dec 1;480(7375):57–62.
175. **Koehler KR, Mikosz AM, Molosh AI, Patel D, Hashino E**. Generation of inner ear sensory epithelia from pluripotent stem cells in 3D culture. Nature. 2013 Aug 8;500(7461):217–21.
176. **Ohgushi M, Matsumura M, Eiraku M, Murakami K, Aramaki T, Nishiyama A, et al.** Molecular Pathway and Cell State Responsible for Dissociation-Induced Apoptosis in Human Pluripotent Stem Cells. Cell Stem Cell. 2010 Aug 6;7(2):225–39.
177. **Chen B, Dodge ME, Tang W, Lu J, Ma Z, Fan CW, et al.** Small molecule-mediated disruption of Wnt-dependent signaling in tissue regeneration and cancer. Nat Chem Biol. 2009 Feb 6;5(2):100–7.
178. **Perrier AL, Tabar V, Barberi T, Rubio ME, Bruses J, Topf N, et al.** Derivation of midbrain dopamine neurons from human embryonic stem cells. Proc Natl Acad Sci U S A. 2004 Aug 24;101(34):12543–8.
179. **Balmer CW, LaMantia AS**. Noses and neurons: Induction, morphogenesis, and neuronal differentiation in the peripheral olfactory pathway. Vol. 234, Developmental Dynamics. 2005. p. 464–81.
180. **Okazaki K, Maltepe E**. Oxygen, epigenetics and stem cell fate. http://dx.doi.org/102217/174607511171. 2005 Dec 23;1(1):71–83.
181. **Dunwoodie SL**. The Role of Hypoxia in Development of the Mammalian Embryo. Dev Cell. 2009 Dec 15;17(6):755–73.
182. **Scully D, Keane E, Batt E, Karunakaran P, Higgins DF, Itasaki N**. Hypoxia promotes production of neural crest cells in the embryonic head. Development. 2016 May 15;143(10):1742–52.
183. **Morriss G, New D**. Effect of oxygen concentration on morphogenesis of cranial neural folds and neural crest in cultured rat embryos. Embryol Exp Morphol. 1979;Dec(54):17–35.
184. **Sievers J, Pehlemann FW, Gude S, Berry M**. Meningeal cells organize the superficial glia limitans of the cerebellum and produce components of both the interstitial matrix and the basement membrane. J Neurocytol. 1994 Feb;23(2):135–49.
185. **Lancaster MA, Corsini NS, Wolfinger S, Gustafson EH, Phillips AW, Burkard TR, et al.** Guided self-organization and cortical plate formation in human brain organoids. Nat Biotechnol. 2017;35.
186. **Nandadasa S, Tao Q, Menon NR, Heasman J, Wylie C**. N- and E-cadherins in Xenopus are specifically required in the neural and non-neural ectoderm, respectively, for F-actin assembly and morphogenetic movements. Development. 2009 Apr 15;136(8):1327–38.
187. **Nishina S, Kohsaka S, Yamaguchi Y, Handa H, Kawakami A, Fujisawa H, et al.** PAX6 expression in the developing human eye. Br J Ophthalmol. 1999 Jun 1;83(6):723–7.
188. **Fuchs E**. Scratching the surface of skin development. Nat 2007 4457130. 2007 Feb 21;445(7130):834–42.
189. **Pieper M, Ahrens K, Rink E, Peter A, Schlosser G**. Differential distribution of competence for panplacodal and neural crest induction to non-neural and neural ectoderm. Development. 2012 Mar 15;139(6):1175–87.
190. **Sokpor G, Abbas E, Rosenbusch J, Staiger JF, Tuoc T**. Transcriptional

and Epigenetic Control of Mammalian Olfactory Epithelium Development. Vol. 55, Molecular Neurobiology. Humana Press Inc.; 2018. p. 8306–27.
191. **Donner AL, Episkopou V, Maas RL**. Sox2 and Pou2f1 interact to control lens and olfactory placode development. Dev Biol. 2007 Mar 15;303(2):784.
192. **Casoni F, Malone SA, Belle M, Luzzati F, Collier F, Allet C, et al.** Development of the neurons controlling fertility in humans: New insights from 3D imaging and transparent fetal brains. Dev. 2016 Nov 1;143(21):3969–81.
193. **Sato S, Ikeda K, Shioi G, Ochi H, Ogino H, Yajima H, et al.** Conserved expression of mouse Six1 in the pre-placodal region (PPR) and identification of an enhancer for the rostral PPR. Dev Biol. 2010 Aug 1;344(1):158–71.
194. **Purcell P, Oliver G, Mardon G, Donner AL, Maas RL**. Pax6-dependence of Six3, Eya1 and Dach1 expression during lens and nasal placode induction. Gene Expr Patterns. 2005 Dec 1;6(1):110–8.
195. **Panaliappan TK, Wittmann W, Jidigam VK, Mercurio S, Bertolini JA, Sghari S, et al.** Sox2 is required for olfactory pit formation and olfactory neurogenesis through BMP restriction and Hes5 upregulation. Dev. 2018 Jan 15;145(2).
196. **Liu Q, Marrs JA, Azodi E, Kerstetter AE, Babb SG, Hashmi L**. Differential expression of cadherins in the developing and adult zebrafish olfactory system. J Comp Neurol. 2004 Oct 18;478(3):269–81.
197. **Matsumata M, Uchikawa M, Kamachi Y, Kondoh H**. Multiple N-cadherin enhancers identified by systematic functional screening indicate its Group B1 SOX-dependent regulation in neural and placodal development. Dev Biol. 2005 Oct 15;286(2):601–17.
198. **Akins MR, Benson DL, Greer CA**. Cadherin expression in the developing mouse olfactory system. J Comp Neurol. 2007 Apr 1;501(4):483–97.
199. **Redmer T, Diecke S, Grigoryan T, Quiroga-Negreira A, Birchmeier W, Besser D**. E-cadherin is crucial for embryonic stem cell pluripotency and can replace OCT4 during somatic cell reprogramming. EMBO Rep. 2011 Jul;12(7):720.
200. **Beanan MJ, Sargent TD**. A PEER REVIEWED FORUM Regulation and Function of Dlx3 in Vertebrate. Dev Dyn. 2000;553(June):545–53.
201. **Riley BB, Phillips BT**. Ringing in the new ear: resolution of cell interactions in otic development. Dev Biol. 2003 Sep 15;261(2):289–312.
202. **McLarren KW, Litsiou A, Streit A**. DLX5 positions the neural crest and preplacode region at the border of the neural plate. Dev Biol. 2003 Jul 1;259(1):34–47.
203. **Chen B, Kim EH, Xu PX**. Initiation of olfactory placode development and neurogenesis is blocked in mice lacking both Six1 and Six4. Dev Biol. 2009 Feb 1;326(1):75–85.
204. **Palaniappan TK, Slekiene L, Gunhaga L, Patthey C**. Extensive apoptosis during the formation of the terminal nerve ganglion by olfactory placode-derived cells with distinct molecular markers. Differentiation. 2019 Nov 1;110:8–16.
205. **Pannese M, Lupo G, Kablar B, Boncinelli E, Barsacchi G, Vignali R**.

The Xenopus Emx genes identify presumptive dorsal telencephalon and are induced by head organizer signals. Mech Dev. 1998;73(1):73–83.
206. **Spokony RF, Aoki Y, Saint-Germain N, Magner-Fink E, Saint-Jeannet JP**. The transcription factor Sox9 is required for cranial neural crest development in Xenopus. Development. 2002 Jan 15;129(2):421–32.
207. **Cau E, Gradwohl G, Fode C, Guillemot F**. Mash1 activates a cascade of bHLH regulators in olfactory neuron progenitors. Development. 1997 Apr 15;124(8):1611–21.
208. **Burns CJ, Vetter ML**. Xath5 regulates neurogenesis in the Xenopus olfactory placode. Dev Dyn. 2002 Dec 1;225(4):536–43.
209. **Garel S, Mari´n F, Mari´n M, Genevie` MG, Matté G, Vesque C, et al.** Family of Ebf/Olf-1-Related Genes Potentially Involved in Neuronal Differentiation and Regional Specification in the Central Nervous System. Dev Dyn. 1997;210:191–205.
210. **Aydin B, Kakumanu A, Rossillo M, Moreno-Estellés M, Garipler G, Ringstad N, et al.** Proneural factors Ascl1 and Neurog2 contribute to neuronal subtype identities by establishing distinct chromatin landscapes. Nat Neurosci 2019 226. 2019 May 13;22(6):897–908.
211. **Hutton SR, Pevny LH**. SOX2 expression levels distinguish between neural progenitor populations of the developing dorsal telencephalon. Dev Biol. 2011 Apr 1;352(1):40–7.
212. **Conte I, Morcillo J, Bovolenta P**. Comparative analysis of Six3 and Six6 distribution in the developing and adult mouse brain. Dev Dyn. 2005 Nov 1;234(3):718–25.
213. **Kohwi M, Osumi N, Rubenstein JLR, Alvarez-Buylla A**. Pax6 Is Required for Making Specific Subpopulations of Granule and Periglomerular Neurons in the Olfactory Bulb. J Neurosci. 2005 Jul 27;25(30):6997.
214. **Chou SJ, Tole S**. Lhx2, an evolutionarily conserved, multifunctional regulator of forebrain development. Brain Res. 2019 Feb 15;1705:1–14.
215. **Tole S, Remedios R, Saha B, Stoykova A**. Selective Requirement of Pax6, But Not Emx2, in the Specification and Development of Several Nuclei of the Amygdaloid Complex. J Neurosci. 2005 Mar 9;25(10):2753.
216. **Kamei Y, Inagaki N, Nishizawa M, Tsutsumi O, Taketani Y, Inagaki M**. Visualization of Mitotic Radial Glial Lineage Cells in the Developing Rat Brain by Cdc2 Kinase-Phosphorylated Vimentin. Glia. 1998;23:191–9.
217. **Furukawa T, Kozak CA, Cepko CL**. rax, a novel paired-type homeobox gene, shows expression in the anterior neural fold and developing retina. Proc Natl Acad Sci U S A. 1997 Apr 1;94(7):3088–93.
218. **Orquera DP, Nasif S, Low MJ, Rubinstein M, de Souza FSJ**. Essential function of the transcription factor Rax in the early patterning of the mammalian hypothalamus. Dev Biol. 2016 Aug 1;416(1):212.
219. **Cano A, Pérez-Moreno MA, Rodrigo I, Locascio A, Blanco MJ, Del Barrio MG, et al.** The transcription factor Snail controls epithelial–mesenchymal transitions by repressing E-cadherin expression. Nat Cell Biol 2000 22. 2000 Jan 13;2(2):76–83.
220. **Herrmann BG, Labeit S, Poustka A, King TR, Lehrach H**. Cloning of the T gene required in mesoderm formation in the mouse. Nat 1990 3436259.

1990;343(6259):617–22.
221. **Hatta K, Takagi S, Fujisawa H, Takeichi M**. Spatial and temporal expression pattern of N-cadherin cell adhesion molecules correlated with morphogenetic processes of chicken embryos. Dev Biol. 1987 Mar 1;120(1):215–27.
222. **Fonseca BF, Couly G, Dupin E**. Respective contribution of the cephalic neural crest and mesoderm to SIX1-expressing head territories in the avian embryo. BMC Dev Biol. 2017 Oct 10;17(1):1–15.
223. **Mansouri A, Stoykova A, Torres M, Gruss P**. Dysgenesis of cephalic neural crest derivatives in Pax7−/− mutant mice. Development. 1996 Mar 1;122(3):831–8.
224. **Hay ED**. The mesenchymal cell, its role in the embryo, and the remarkable signaling mechanisms that create it. Dev Dyn. 2005 Jul 1;233(3):706–20.
225. **Pierce G, Nakane P**. Antigens of epithelial basement membranes of mouse, rat, and man, a study utilizing enzyme-labeled antibody. Subj Strain Bibliogr 1967. 1967 Jan 1;
226. **Marinkovich MP, Keene DR, Rimberg CS, Burgeson RE**. Cellular origin of the dermal-epidermal basement membrane. Dev Dyn. 1993 Aug 1;197(4):255–67.

Erklärung zum Eigenanteil

Die Arbeit wurde am Institut für Neuroanatomie und Entwicklungsbiologie unter Betreuung von Prof. Dr. Stefan Liebau durchgeführt.

Die Konzeption der Studie erfolgte durch und in Zusammenarbeit mit Dr. Moritz Klingenstein, Postdoc und Dr. Stefanie Klingenstein, Postdoc.

Die Versuche wurden nach Einarbeitung durch Dr. Moritz Klingenstein, Dr. Stefanie Klingenstein und Sabine Conrad von mir eigenständig durchgeführt. Erhebung der RT-qPCR Daten mittels Biomark™ Fludigm wurde durch Sabine Conrad durchgeführt.

Die statistische Auswertung erfolgte nach Beratung durch Dr. Stefanie Klingenstein durch mich.

Ich versichere, das Manuskript selbständig verfasst zu haben und keine weiteren als die von mir angegebenen Quellen verwendet zu haben.

Tübingen, den 27.07.2022

[Karl Georg Simon Frey]

Acknowledgements

First and foremost, I want to thank Stefan Liebau for giving me the opportunity to write this thesis. He not only supported me with expert guidance, but also gave me the opportunity and freedom to develop and progress my own ideas. Through many discussions and coffee sessions he formed my understanding of science and set an example of what being a fair, honest & humble scientist should be.

I also want to thank Moritz & Stefanie Klingenstein who supported and encouraged me to pursue different and challenging projects, giving me the freedom and trusting me with the responsibility to do so. The fruitful discussions in the institute and on many national and international meetings are the foundation of this thesis.

Furthermore, I want to thank Meltem Avci-Adali for evaluating this thesis.

I owe special thanks to Sabine Conrad, who taught me everything about cell culture and laboratory work. Her spirited help and support made this project possible.

I also want to thank all the past and current members of the INDB group in Tübingen, who have been good friends and wonderful colleagues. The discussions, feedback & input from them often inspired and motivated my efforts.

Without my family and friends, this thesis would not have been possible. I want to thank them for all their support, honest interest, motivation & patience.

Finally, I owe gratitude to my partner Anne, who has been the greatest motivation, inspiration & muse. She supported me through the ups and downs of this journey, stood by my side & always saw a way, even if I didn’t.